Karlsruhe Institute of Technology

Statistics of energy dissipation of a driven two-level system

Zur Erlangung des akademischen Grades eines
DOKTORS DER NATURWISSENSCHAFTEN
von der Fakultät für Physik
des Karlsruher Instituts für Technologie

genehmigte

DISSERTATION
von

Dipl.-Phys. Philip Wollfarth

aus Karlsruhe

Institut für Theorie
der Kondensierten Materie

Tag der mündlichen Prüfung:	25. 11. 2016
Referent:	Prof. Dr. Alexander Shnirman
Korreferent:	PD Dr. Boris Narozhny

Für meinen Papa.

Contents

1. Introduction

Within the last decade tremendous progress in designing, controlling and measuring mesoscopic systems has been achieved. For example, in the context of quantum information the design of superconducting qubits enabled the improvement of their coherence times up to 100 μs. Such coherence times are achieved in three-dimensional transmon qubits [1] in which a Josephson junction is embedded in a three-dimensional cavity. Similar coherence times are nowadays possible in xmon qubits [2], which are constructed on a planar chip. This results in a comparatively simpler production and control of such qubits. At the same time the ability to control and manipulate mesoscopic electronic systems has considerably progressed.

All these experimental advances have opened up an avenue to study a quite different field of research: thermodynamics in the quantum regime. In a classical picture, thermodynamics provides universal relations between macroscopic physical quantities such as temperature heat or work. Microscopically these relations arise from statistical mechanics. The dynamics of isolated microscopic systems is symmetric with respect to time reversal as their respective microscopic equations of motions obey this symmetry. The irreversibility paradox exists within this context. At first glance the time-reversible dynamics of the particles seem to contradict the fact that macroscopic processes in principle are irreversible. However, from a statistical point of view, this paradox is easily resolved. Considering a macroscopic closed system consisting of a huge number of particles $N \sim 10^{23}$, whose individual dynamics are time-reversible, it is very unlikely that the system will return to its initial phase space volume.

In thermodynamics everything is well defined and understood considering equilibrium situations. From a microscopic point of view, even in equilibrium, matter is in a state of motion undergoing random fluctuations. In the beginning of the last century it was discovered that these equilibrium fluctuations determine the dynamics of a system in linear response as it is driven out from equilibrium. These early results are known as Einstein-relation [3, 4] derived in the context of brownian motion, and as Johnson-Nyquist noise relation associated to the thermal noise of an electronic resistor [5, 6]. These relations have been elaborated to also apply to the quantum regime by Callen and Welton resulting in the well-known fluctuation dissipation theorem [7].

In the late 1970s one of the first universal relations out of equilibrium was discovered by Bochkov and Kuzovlev. They found a fluctuation relation of work for classical systems which is valid irrespective of how far the system has been driven out of equilibrium [8]. This

and the discovery of further universal fluctuation relations, e.g. the Crooks and Jarzynski relations [9, 10, 11, 12, 13], led to the recognition that fluctuations of the entropy (or heat and work) and micro-reversibility are the key concepts relevant for the dynamics far from equilibrium. These fluctuations become pronounced as the system size decreases. First tests of the fluctuation relations have been carried out in relatively small systems as colloidal particles and biomolecules [14, 15, 16]. Due to the progress in micro-electronics, the fluctuation relations could be demonstrated at the single electron level [17, 18, 19]. However, almost all experimentally obtained results were explained in a classical stochastic picture [13]. Although the fluctuation relations have been generalized to the quantum regime [20, 21, 22], there is still plenty of research activity. For example, experimental [22] and theoretical [23, 24, 25] studies focusing on the Crooks fluctuation relation [10] have been carried out using driven qubits. As the Crooks fluctuation relation is based on the concept of work being performed along each individual trajectory, there may arise a problem to define work in a non-ambiguous way in the quantum regime [26].

In a quantum system however, *energy* is a well defined observable. Hence, measuring the dissipated energy of a system driven out of equilibrium yields an alternative approach to extract information about the system. Such measurements are possible by using a calorimetric approach [27, 28]. The idea behind this approach is to detect single microwave photons emitted by the driven system via a measurement of the temperature change in a resistor coupled to the system [29]. These time-resolved calorimetric measurement techniques have improved within the past few years [30, 31, 32], thereby approaching the single-photon resolution.

A very peculiar fluctuation relation which has not yet been mentioned is the *detailed fluctuation relation* [33] which received its name because of its structure: The detailed fluctuation relation is structurally akin to the detailed balance relation. This relation takes into account an explicit choice of the initial and final states of the system. A very intimately related concept in the context of pre- and post-selection is the *weak measurement* [34, 35] approach to measure a quantum system. The idea of a weak measurement is to perform a slightly invasive measurement on the system. Hence, the system is perturbed very little by the measurement process. On the other hand, very little information is gained because of the weakness of the measurement. Surprisingly, the outcome of a weak measurement of a quantum observable, i.e. a *weak value*, can in principle be way larger than the expectation value of the observable [34]. The concept of the weak measurement has opened up new possibilities in accessing physical quantities experimentally. As an example, in the context of the spin Hall effect, the pre- and post-selection of the weak measurement protocol has been used as an amplification mechanism [36]. In this particular experiment, the achieved enhancement increased the original outcome by four orders of magnitude. In another remarkable experiment the weak measurement technique was used to directly measure the quantum wavefunction of a photon [37], which may be advantageous to the procedure of quantum state tomography [38].

In this context this thesis is devoted to the detailed study of the statistics of energy dissipated by a driven two-level system. The goal of this thesis is to achieve a better understanding of the energy exchange between the system and the heat bath including quantum effects. Motivated by the experimental advances in control and manipulation of two-level systems, e.g. qubits, we analyze the dependence of the statistics of energy dissipation on various external manipulations. We propose to prepare the system in a distinct initial state $|i\rangle$ before the external driving is switched on. After the driving is switched off again, the system undergoes a second strong post-selective measurement to be projected on its final state $|f\rangle$. As we will show and discuss, due to this distinct pre- and post-selection, important quantum corrections induced by the coherences of the density matrix will influence the respective conditional probability distribution.

Furthermore, we extend the analysis by considering a weak measurement approach to the dissipative energy current $\hat{I}_\epsilon$ transferring energy between the system and the bath. We check the self-consistency of the approach by verifying that the integral of the energy current over the measurement time is indeed equivalent to the conditional average of dissipated energy. However, the weak value of the energy current as obtained by that particular approach turns out to be a complex oscillating quantity, which should in principle be detectable.

The content of this thesis is divided into the following chapters:

Chapter 2 (Fundamentals):

In this chapter we review and introduce the principal physical properties of a two-level system. Besides introducing the notation used throughout this thesis, we also discuss how the dynamics of the two-level system is influenced when an external periodic driving is applied. We explain how to treat the generic situation by introducing the Floquet-approach to time-periodic problems [39]. For the situation of relatively simple periodic driving, we explain the widely used transformation into the rotating frame and discuss the consequences arising from it. Furthermore we present the measurement protocol, which we propose to achieve a pre- and post-selection of the two-level system states.

Chapter 3 (Fundamentals):

Here we review the theoretical framework to deal with the dynamics of open quantum systems. In particular, we review the master equation approach. We discuss the necessary conditions for the validity of the equations. Using the example of a two-level system coupled to the bath, we discuss the dissipative effects induced by the bath.

Chapter 4 (Fundamentals):

In this chapter we present a brief review of the concept of full counting statistics. For historical reasons the fundamental idea is explained using the example of the spin-1/2 galvanometer [40]. This is followed by the discussion of the two-point measurement statistics [12], a suitable counting statistics approach in the context of energy exchange.

Chapter 5:

This chapter deals with the energy dissipation of the driven two-level system in the context of the fluctuation relations. We give a brief introduction to the field of research by reviewing the Bochkov-Kuzovlev fluctuation relation [8]. This is followed by a derivation of the characteristic function capable of calculating the energy-exchange-statistics between a periodically driven system and a heat bath. This is achieved by a counting-field-modified master equation approach in the spirit of the two-point measurement statistics [12]. We demonstrate the applicability of the derived equation using the example of a driven two-level system, discussing different limits of coupling between the system and the heat bath, i.e. longitudinal and transversal coupling. We compute the conditional probability distributions with respect to the pre- and post-selection of the states of the system. Within our model we are capable of splitting the characteristic function into a classical part, which is fully determined by the populations of the reduced density operator of the system, and a quantum part, which solely depends on the dynamics of the coherences. Consequently, the conditional probability distributions split into a classical and a quantum part. We find that the quantum part constitutes relatively large contributions to the conditional probability distribution, depending on the choice of pre- and post-selected system states.

Chapter 6:

After discussing the impact of the pre- and post-selection on the conditional probability distributions, we present a detailed analysis on the first two cumulants of the dissipated energy, i.e. the conditional average and the conditional noise of the dissipated energy. The analysis is focused on an interplay between the pre- and post-selection of system states and varying the character of the driving. In particular, we discuss and compare the resonantly driven TLS and the off-resonantly driven TLS. Although quantum features are visible, the most pronounced features can be explained by a classical analysis.

Chapter 7:

In this chapter we provide an alternative approach to the problem by applying a generalized weak measurement scheme [34]. We propose a weak measurement of the energy current $\hat{I}_\epsilon$ including pre- and post-selection of the states of the system. We show that with this approach the conditional average is still accessible, i.e. the integral of the weakly measured energy current is real and equal to the conditional average as obtained by the full counting statistics approach. However, a detailed analysis shows that the weak value of the energy current emerging in this approach turns out to be a complex oscillating quantity.

Chapter 8:

In the last chapter we conclude by reviewing the findings of the thesis and providing an outlook for further studies on the subject.

Throughout the work at hand we will set $\hbar = 1$.

2. Fundamentals: The driven two-level-system

This chapter provides a brief introduction to the physics of two-level-systems (TLSs). Although being part of various standard quantum mechanics textbooks, e.g. [41] or scientific articles [42, 43], the most important fundamental mathematical tools will be briefly reviewed. The mathematical framework of TLSs provides a valuable tool describing various physical systems. The most prominent physical system which serves as a TLS is the well-known spin-1/2 particle. A natural example of a spin-1/2 particle is a silver atom as used in the famous Stern-Gerlach-experiment [44]. In this particular experiment the magnetic moment $\vec{\mu} = \hbar\gamma_M\vec{\sigma}/2$ of a silver atom has been measured. Here, γ_M denotes the gyromagnetic ratio and $\vec{\sigma} = (\sigma_x, \sigma_y, \sigma_z)^T$ denote the Pauli matrices.

However, many other physical systems can be described by the same mathematical tools. For example, superconducting Josephson-circuits in the proper parameter regime serve either as charge, flux or phase-qubits, where their two lowest energy states are well separated from their respective higher-energy states [45, 46]. The same mathematical description, but in a completely different physical context, is attributed to defects in glasses [47, 48], which are usually thought of as TLSs.

This chapter will give a brief review about the mathematical description of a TLS. The most important parts will be reviewed in order for the text to be self-contained and in order to introduce and define the notation which will be used throughout this thesis. For further details we refer to the corresponding special literature.

The notation necessary to describe the driven situation will be introduced using the example of a spin-1/2 in an external magnetic field. In the following, periodic driving due to an external field will be included and the transformation into the rotating frame will be performed and discussed.

2.1. Preliminaries to the TLS

In this section we want to review the basic mathematical and physical framework necessary to describe a quantum TLS. The TLS may be described by Pauli matrices within a two-dimensional Hilbert space

$$\sigma_x = \begin{pmatrix} 0 & 1 \\ 1 & 0 \end{pmatrix}, \quad \sigma_y = \begin{pmatrix} 0 & -i \\ i & 0 \end{pmatrix}, \quad \sigma_z = \begin{pmatrix} 1 & 0 \\ 0 & -1 \end{pmatrix}. \tag{2.1}$$

We chose the representation where the σ_z matrix is diagonal.

In a quite general situation, a spin-1/2 particle may be exposed to an externally applied magnetic field. The most general Hamiltonian has the form

$$\begin{aligned}\hat{H}_{\text{spin}}(t) &= -\vec{\mu}\vec{B}(t) \\ &= -\frac{\gamma_M}{2}\left(\sigma_x B_x(t) + \sigma_y B_y(t) + \sigma_z B_z(t)\right), \end{aligned} \tag{2.2}$$

where $B_i(t)$ denote the possibly time-dependent magnetic field components. Consequently, the orientation of the spin strongly depends on the applied magnetic field.

The dynamics of the TLS is most illustratively described by using the Bloch sphere as depicted in Fig. 2.1. The Hilbert space of the TLS is spanned by the states $|\uparrow\rangle$ and $|\downarrow\rangle$, which are the eigenstates of the σ_z-operator. Within this representation, the state of the TLS is described by

$$|\Psi\rangle = \cos\frac{\theta_L}{2}|\uparrow\rangle + e^{i\phi_L}\sin\frac{\theta_L}{2}|\downarrow\rangle, \tag{2.3}$$

where the angles $\theta_L \in [0, \pi]$ and $\phi_L \in [0, 2\pi]$ denote the rotation around the $\hat{z}$- and $\hat{x}$-axis, respectively. The subscript L is used to indicate that we are referring to the laboratory frame. We note that the dynamics of θ_L and ϕ_L are determined by the the components of the magnetic field $B_i(t)$.

In the context of periodically driven systems, another important reference frame is the *rotating* frame, which will be mainly used throughout this thesis. It will be introduced below.

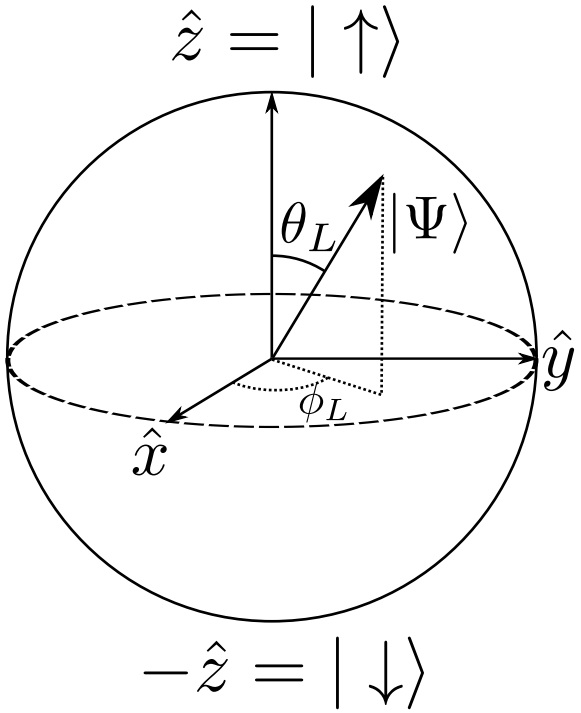

Figure 2.1.: Schematic of the Bloch sphere. The state $|\Psi\rangle$ of the TLS lives on the sphere in an arbitrary superposition of the σ_z basis kets. The angle with respect to the $|\uparrow\rangle$ axis is denoted by θ, whereas the phase ϕ denotes the angle the state is rotated with respect to the $\hat{x}$-axis.

2.2. Periodic driving

The manipulation of TLSs via applying an external driving is a task of practical importance. Thus, it is necessary to understand the behavior of TLSs which are exposed to a time-dependent driving. Prominent examples of practical applications are the nuclear magnetic resonance spectroscopy [49], qubit manipulations [50], driving schemes designed for charge pumping [51, 52] or analyzing defects in amorphous solids [53].

Most of the aforementioned applications use a time-periodic driving scheme. In the following we will present a general theoretical treatment, which is suitable to describe periodically time-dependent problems. It is known as *Floquet theory*. Within this section we will introduce the Floquet formalism. This is followed by an explicit discussion of two very prominent driving schemes, the *linearly polarized* and the *circularly polarized* driving. While the first driving scheme will turn out to be not exactly solvable, the second one belongs to one of the very rare time-dependent problems which are exactly solvable. We will introduce the transformation into the rotating frame and discuss the *rotating wave approximation* (RWA). It turns out that the problem of the linearly polarized driven TLS reduces to the problem of the circularly polarized driven TLS within the limits of the RWA.

2.2.1. Floquet theory

The Floquet approach is applicable to any time periodic problem. Historically, Gaston Floquet studied the properties of periodic differential equations [39]. He was able to show that for any periodic differential equation there are solutions with the same periodicity as the differential equation. The Floquet theory is formally an analog to the Bloch theory but with regard to time periodic problems rather than to space periodic problems. For a detailed presentation of the Floquet theory we refer to [43, 54].

We consider a time-periodic Hamiltonian $\hat{H}(t)$ with $\hat{H}(t) = \hat{H}(t + \tau_p)$, where $\tau_p = 2\pi/\omega$ is the period of the driving. We may write the Schrödinger equation describing the time evolution of the system's state as

$$\underbrace{\left(\hat{H}(t) - i\partial_t\right)}_{\mathcal{H}} |\Psi(t)\rangle = 0, \tag{2.4}$$

where $|\Psi(t)\rangle$ is the state of the system. According to the Floquet-theory, there exists a solution

$$|\Psi(t)\rangle = \sum_\alpha e^{-i\epsilon_\alpha t} |\phi_\alpha(t)\rangle, \tag{2.5}$$

fulfilling

$$\mathcal{H}|\phi_\alpha(t)\rangle = \epsilon_\alpha |\phi_\alpha(t)\rangle, \tag{2.6}$$

where $|\phi_\alpha(t)\rangle$ is the so called time-periodic Floquet-state with $|\phi_\alpha(t)\rangle = |\phi_\alpha(t + \tau_p)\rangle$. The Floquet-energy ϵ_α is real-valued and determined up until to multiples of $\omega = 2\pi/\tau_p$. As both the Hamiltonian and the Floquet states obey the same periodicity, it is useful to perform a Fourier decomposition

$$|\phi_\alpha(t)\rangle = \sum_l e^{-i\omega l t} |\phi_\alpha(l)\rangle, \tag{2.7}$$

$$\hat{H}(t) = \sum_l e^{-i\omega l t} \hat{H}(l), \tag{2.8}$$

of the Floquet modes and the Hamiltonian for further analysis. Inserting both Fourier representations into Eq. (2.6), we obtain

$$\sum_l e^{-i\omega lt}\left(-\omega l - \epsilon_\alpha + \sum_m e^{-im\omega t}\hat{H}(m)\right)|\phi_\alpha(l)\rangle = 0. \tag{2.9}$$

We are now able to project the equation onto a particular Fourier coefficient yielding

$$-l\omega|\phi_\alpha(l)\rangle + \sum_m \hat{H}(l-m)|\phi_\alpha(m)\rangle = \epsilon_\alpha|\phi_\alpha(l)\rangle, \tag{2.10}$$

where we used $1/\tau_p \int_0^{\tau_p} dt e^{i(l-m)\omega t} = \delta_{l,m}$ and $\hat{H}(l-m) = 1/\tau_p \int_0^{\tau_p} dt \hat{H}(t) e^{i(l-m)\omega t}$. We note that each $|\phi_\alpha(n)\rangle$ has the same number of components as the the original Hamiltonian. As an immediate consequence, we can think of Eq. (2.10) as a matrix equation

$$\hat{H}_{m,l}|\phi_\alpha(l)\rangle = \epsilon_\alpha|\phi_\alpha(l)\rangle, \tag{2.11}$$

with coefficients $\hat{H}_{m,l} = -m\omega\delta_{m,l} + \hat{H}(l-m)$. The resulting matrix $\hat{H}$ is infinitely large. The spectrum of $\hat{H}$ is invariant with respect to shifts of values of $n\omega$, where n is an integer, i.e. the eigenvalues ϵ_α do not change under the transformation $\hat{H} \to \hat{H} + n\omega\mathbb{1}$. It turns out to be useful to rewrite the previously introduced index $\alpha = (i, n)$, with $i \in [1, N]$, where N is the dimensionality of the Hamiltonian $\hat{H}(t)$ and $n \in \mathbb{Z}$. The different Floquet energies are connected according to $\epsilon_{i,l+n} = \epsilon_{i,l} + n\omega$. Consequently, an infinite number of copies of the original problem appear, which are connected as

$$|\phi_{i,l+n}(t)\rangle = e^{i\omega nt}|\phi_l(t)\rangle. \tag{2.12}$$

The Fourier components of the Floquet copies are connected in the same way. The connection between different Fourier components of the Floquet copies can analogously be rewritten using a second quantization scheme for the external driving. This seems obvious by the structure of Eq. (2.12). We introduce an additional Fock space and interpret the exponentials as raising and lowering operators, i.e.

$$e^{\pm i\omega t}|n\rangle \to |n \pm 1\rangle, \tag{2.13}$$

where $|n\rangle$ denotes an n photon state in the Fock space. The states are separated by energy quanta of the driving frequency ω. Consequently, the Hilbert space under consideration is extended due to the fact that an infinite set of copies of the original Hamiltonian occurs. We will use this representation to explain the physical processes further below.

An immediate advantage of the Floquet approach is quite obvious. By the structure of Eq. (2.11) one has to deal with an equation similar to the time-independent Schrödinger equation. The price one has to pay is that the number of degrees of freedom of the problem due to the Fourier expansion increase dramatically. However, in the proper parameter regime one is able to approximately truncate the Fourier decomposition of the Hamiltonian so that the analysis only involves a manageable number of Fourier components.

2.2.2. Linearly polarized driving

In a realistic situation one wants to manipulate the system by applying an external field. There are multiple variants to apply an external driving to a TLS depending on its physical nature. Optical TLSs may be controlled by applying an external electric field, whereas spins are exposed to an external magnetic field. A popular driving is the *linearly polarized driving* where the system is exposed to an oscillating classical field. An exemplary Hamiltonian of a TLS exposed to a linearly polarized magnetic field is

$$\hat{H}_{\text{lin}} = -\frac{\omega_0}{2}\sigma_z + \Omega_R \cos\omega t\sigma_x, \tag{2.14}$$

where ω_0 denotes the static magnetic field in $\hat{z}$- direction and ω is the driving frequency. In the case of resonant driving $\omega = \omega_0$, the amplitude of the driving Ω_R is identified with the Rabi-frequency of the system. Interestingly, even such a relatively simple problem turns out to be not exactly solvable.

For illustration we decompose the cosine to exponential functions and rewrite the Hamiltonian as

$$\hat{H}_{\text{lin}} = -\frac{\omega_0}{2}\sigma_z + \frac{\Omega_R}{2}\left(\sigma_+ + \sigma_-\right)\left(e^{i\omega t} + e^{-i\omega t}\right), \tag{2.15}$$

where we introduced $\sigma_\pm = \frac{1}{2}(\sigma_x \pm i\sigma_y)$. Using the above introduced second quantization scheme, we readily see four different processes emerging. Two of them turn out to be energy conserving whereas the other two do not conserve energy. The energy conserving processes involve a spin-flip while emitting or absorbing a photon. For example, we can consider a flip from $|\uparrow\rangle \rightarrow |\downarrow\rangle$ (excitation) while a photon is absorbed by the system, $(\sigma_+ e^{-i\omega t})$ or the vice-versa process where the spin flips from $|\downarrow\rangle \rightarrow |\uparrow\rangle$ (relaxation) while emitting a photon, which corresponds to the process $\sigma_- e^{i\omega t}$.

The energy non-conserving processes involve an excitation while emitting a photon $(\sigma_+ e^{i\omega t})$ or a relaxation of the spin while absorbing a photon $(\sigma_- e^{-i\omega t})$. In the RWA the two non-energy-conserving processes are usually neglected. We will discuss the RWA when introducing the rotating frame in Sec. 2.2.4.

2.2.3. Circularly polarized driving

The circularly polarized driving is one of the few exactly solvable time-dependent problems. In the current thesis we will mostly use this type of driving. However, as we will show further below, in the RWA the circularly polarized driving and linearly polarized driving appear to be equivalent.

The Hamiltonian of a TLS exposed to a circularly polarized magnetic field is given by

$$\hat{H}_{TLS}(t) = -\frac{\omega_0}{2}\sigma_z + \frac{\Omega_R}{2}\left(\cos(\omega t)\sigma_x - \sin(\omega t)\sigma_y\right), \tag{2.16}$$

where the parameters ω_0, ω and Ω_R are analogous to the ones introduced in the previous section. In the same manner we can rewrite the trigonometric functions using exponential functions and find

$$\hat{H}_{TLS}(t) = -\frac{\omega_0}{2}\sigma_z + \frac{\Omega_R}{2}\left(\sigma_+ e^{-i\omega t} + \sigma_- e^{i\omega t}\right). \tag{2.17}$$

We can repeat the above discussion of the second quantization scheme of the driving terms $e^{\pm i\omega t}$. We immediately see that in contrast to the linearly polarized driving only the energy conserving transitions are present. This problem was first studied and solved by Rabi in 1937 [55]. Considering a resonant driving $\omega = \omega_0$ and assuming that the system was initially prepared in the $|\uparrow\rangle$ state, the occupation probabilities are found as

$$\mathcal{P}_t(\uparrow) = \cos^2\frac{\Omega_R t}{2}, \qquad \mathcal{P}_t(\downarrow) = \sin^2\frac{\Omega_R t}{2}, \tag{2.18}$$

which oscillate with the Rabi frequency Ω_R.

2.2.4. Transformation into the rotating frame

The aforementioned situation of the circularly polarized driving is exactly solvable by a transformation into the rotating reference frame. The procedure is equivalent to the Floquet approach. Generally, as soon as the system is driven, the Schrödinger equation

$$i\partial_t|\Psi(t)\rangle = \hat{H}(t)|\Psi(t)\rangle, \tag{2.19}$$

may be quite involving to solve. In the case of the circularly polarized driving we are able to find an exact time-dependent transformation $R_1(t)$ of the system which turns out to make the problem completely time-independent. The same transformation yields an approximate solution to the linearly polarized driving as well, as we will discuss below.

In both cases, the transformation matrix is found to be

$$R_1(t) = \exp\left[-i\frac{\omega t}{2}\sigma_z\right], \tag{2.20}$$

and accordingly the state transforms as

$$|\tilde{\Psi}\rangle = R_1(t)|\Psi\rangle, \tag{2.21}$$

where $|\tilde{\Psi}\rangle$ denotes the state of the system in the rotating frame.

The transformation of the Hamiltonian $\hat{H}_{TLS}(t)$ follows directly from substituting the transformed state into the Schrödinger equation (2.19)

$$\begin{aligned} i\partial_t|\tilde{\Psi}\rangle &= i\dot{R}_1(t)|\Psi\rangle + iR_1(t)\partial_t|\Psi\rangle \\ &= \left(R_1(t)\hat{H}_{TLS}(t)R_1^\dagger(t) + i\dot{R}_1(t)R_1^\dagger(t)\right)|\tilde{\Psi}\rangle, \end{aligned} \tag{2.22}$$

where we identify

$$\begin{aligned} \tilde{H}_{TLS} &= R_1(t)\hat{H}_{TLS}(t)R_1^\dagger(t) + i\dot{R}_1^\dagger(t)R_1^\dagger(t) \\ &= -\frac{\Delta}{2}\sigma_z + \frac{\Omega_R}{2}\sigma_x, \end{aligned} \tag{2.23}$$

the Hamiltonian in the rotating frame, which is totally time-independent. We further introduced the detuning $\Delta = \omega_0 - \omega$. Consequently, in the rotating frame the problem has been reduced to a time-independent problem.

If we perform the exact same transformation onto the Hamiltonian $\hat{H}_{\text{lin}}(t)$, we find

$$\tilde{H}_{\text{lin}} = -\frac{\Delta}{2}\sigma_z + \frac{\Omega_R}{2}\left(\left(1 + e^{-2i\omega t}\right)\sigma_- - \left(1 + e^{2i\omega t}\right)\sigma_+\right). \tag{2.24}$$

We see that the Hamiltonian still is time-dependent as parts of the tunneling matrix elements oscillate with a frequency of 2ω. If the the fast oscillating terms are neglected, we immediately find that $\tilde{H}_{\text{lin}} \approx \tilde{H}_{TLS}$. This procedure is known as rotating wave approximation and may be justified by arguments of energy conservation or simply by the fact that the contributions average out as they oscillate very fast. In a more rigorous perturbation theory analysis, one can show that the leading order contributions of the fast oscillating terms have an amplitude proportional to Ω_R/ω. Thus, the RWA is justified by the perturbation theory for $\omega \gg \Omega_R$.

In the following we use the Floquet picture to describe the transformation into the rotating frame. We demonstrate that the transformation $R_1(t)$ into the rotating frame causes a mixing between two different Floquet copies of the system. By virtue of the transformation $R_1(t)$, it may be unclear to interpret the exponentials as raising and lowering operators of energy quanta of ω since they involve half integer values of the driving frequency. However, the net energy difference between two different states undergoing the transformation $R_1(t)$ is still given by integer values of the driving frequency. To circumvent this problem, we may simply shift the Floquet spectrum by $\omega/2$. Consequently, we write down explicitly the transformation into the rotating frame Eq. (2.21)

$$\begin{aligned} R_1(t)|\Psi\rangle &\equiv e^{-i\frac{\omega t}{2}\sigma_z}\left(a_\uparrow|\uparrow_{n+\frac{1}{2}}\rangle + a_\downarrow|\downarrow_{n+\frac{1}{2}}\rangle\right) \\ &= a_\uparrow|\uparrow_{n+1}\rangle + a_\downarrow|\downarrow_n\rangle, \end{aligned} \tag{2.25}$$

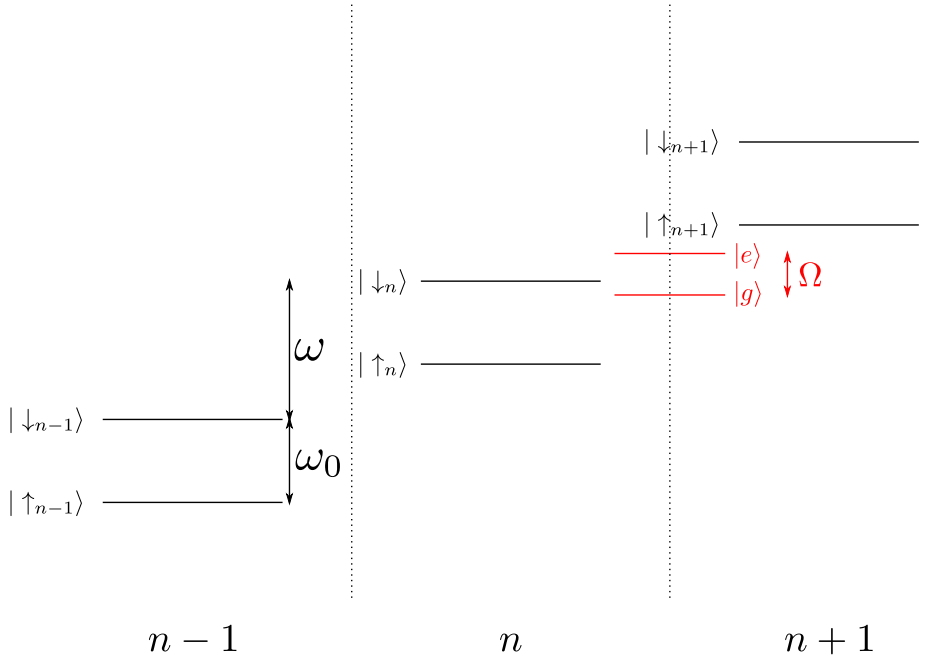

Figure 2.2.: States of the system using the Floquet-picture. The TLS is shifted by integer values of $n\omega$ corresponding to different Floquet modes. The spin statest $|\uparrow_n\rangle$ and $|\downarrow_n\rangle$ are separated by ω_0. The rotation $R_2(\theta)$ yields a diagonalization of the Hamiltonian but invovles a mixing between two different Floquet modes, represented by the states $|g\rangle$ and $|e\rangle$, depicted in red. The two eigenstates are separated by the level splitting Ω.

where the subscript n labels the Floquet copy, i.e. the Floquet mode the state belongs to (see Fig. 2.2), and $a_\uparrow, a_\downarrow$ are the amplitudes of the respective states. The transformed Hamiltonian of the circularly polarized spin using the Floquet picture reads

$$\tilde{H}_{\mathrm{TLS}} = -\frac{\Delta}{2}\left(|\uparrow_{n+1}\rangle\langle\uparrow_{n+1}| - |\downarrow_n\rangle\langle\downarrow_n|\right) + \frac{\Omega_R}{2}\left(|\uparrow_{n+1}\rangle\langle\downarrow_n| + |\downarrow_n\rangle\langle\uparrow_{n+1}|\right). \tag{2.26}$$

The eigenstates of the Hamiltonian are

$$|g\rangle = \cos\frac{\theta}{2}|\uparrow_{n+1}\rangle + \sin\frac{\theta}{2}|\downarrow_n\rangle \tag{2.27}$$

$$|e\rangle = \sin\frac{\theta}{2}|\uparrow_{n+1}\rangle - \cos\frac{\theta}{2}|\downarrow_n\rangle, \tag{2.28}$$

where the angle $\theta = \arctan\Omega_R/\Delta$ denotes the angle between the state of the TLS and the $\hat{z}-$axis in the rotating frame. The energy difference between the two eigenstates is given by

$$\Omega = \sqrt{\Delta^2 + \Omega_R^2} = E_e - E_g. \tag{2.29}$$

For clarification we illustrate both transformations using the Floquet picture depicted in Fig. 2.2. The transformation into the rotating frame causes a mixing between different Floquet modes. The eigenstates obtained by diagonalization are composed of the two compound rotated spin states.

2.3. Measurement protocol

Due to the vast variety of TLSs, many procedures exist to manipulate their states or measure their intrinsic properties. Spin particles may be measured either by using a Stern-Gerlach apparatus or a nuclear magnetic resonance spectrometer. The measurement of

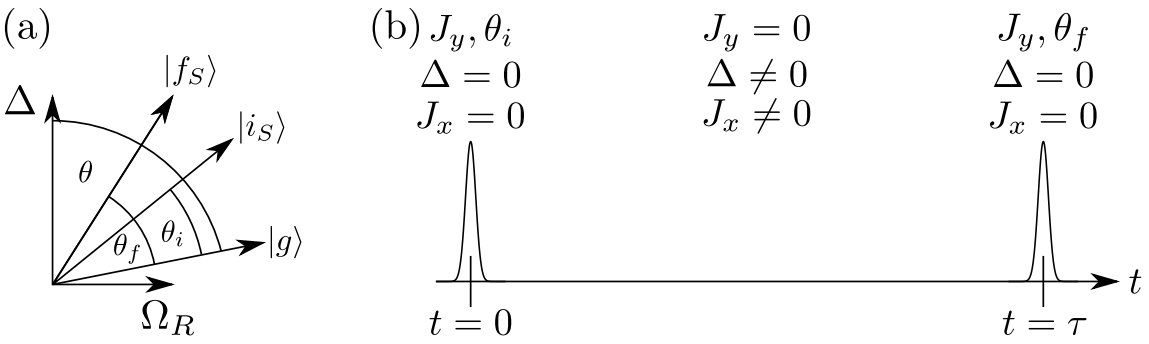

Figure 2.3.: The orientation of the different angles θ, θ_i and θ_f with respect to the $\hat{x}\hat{z}$ plane are depicted in panel (a). In panel (b) the driving protocol is shown schematically. The protocol is discussed in the main text.

the state of a superconducting qubit may be performed capacitively [56, 57] or byf using a resonator in the desired frequency range [58], depending on the design and nature of the qubit. TLSs in glasses are surveyed using measurement devices which could serve qubits themselves [59]. As it becomes obvious by this list of a few examples of TLSs, discussing all different measurement approaches to different types of physical TLSs is far beyond the scope of this thesis.

Throughout this thesis we will consider a pre- and post-selection of the states of the TLS before and after the driving is applied to the TLS. The corresponding measurement protocol has been proposed in [60]. As most of the calculations in this thesis are performed in the energy eigenbasis in the rotating frame, we adjust the measurement protocol accordingly.

The measurement protocol is schematically sketched in Fig. 2.3 (b). At time $t = 0$ before the driving is turned on, the system is prepared in a certain initial state $|i\rangle$, which is characterized by the angle θ_i. The angle denotes a rotation in the $\hat{x}\hat{z}$-plane with respect to the ground state of the system, as depicted in Fig. 2.3 (a). The adjustment of the initial state may be achieved by a strong resonant θ_i pulse around the $\hat{y}$-axis with an amplitude J_y. After the preparation the system is exposed to the possibly off-resonant driving with an amplitude $J_x = \Omega_R$ and $J_y = 0$. Since a change of the driving frequency ω may be cumbersome in a realistic experimental situation, we propose changing the TLS intrinsic quantity ω_0 to obtain off-resonant driving. At $t = \tau$ the driving is turned off and the system state is post-selected onto the desired final state $|f\rangle$ by a second resonant pulse in $\hat{y}$ direction with an amplitude J_y around the angle θ_f.

Transition probability for the circularly polarized driving

Later in this work we will use the measurement scheme introduced above. It will be used in the context of a slightly modified situation where the TLS is coupled to a heat bath. As it will turn out, the coupling to the bath significantly changes the transition probabilities of the TLS as compared to the isolated situation. Thus, it might be insightful to briefly calculate the transition probability for the isolated TLS in order to compare the changes in the transition probability due to the coupling to the bath. The transition probability or more precisely the conditional probability of finding the system in the desired final state $|f\rangle$ at time τ, given it was initially prepared in $|i\rangle$, is obtained as

$$\begin{aligned}\mathcal{P}_{0,\tau}(f|i) &\equiv |\langle f_S|i_S(\tau)\rangle|^2 \\ &= \frac{1}{2}\left(1 + \cos\theta_f \cos\theta_i + \cos\Omega\tau \sin\theta_f \sin\theta_i\right). \end{aligned} \tag{2.30}$$

In the absence of the driving, this formula reduces to $\mathcal{P}_0(f|i) = \cos^2 \frac{\theta_f - \theta_i}{2}$ which gives the expected conditional probability regarding pre- and post-selection of a non-driven spin-system. In the situation of resonant driving $\omega = \omega_0$, for $\theta_i = \pi/2$ and $\theta_f = \pi/2, 3\pi/2$, we obtain the expected Rabi occupation probabilities given by Eq. (2.18).

2.4. Conclusion

In this chapter we presented a review of the mathematical framework which is necessary to describe the physics of TLSs. We introduced an intuitive picture of representing the state of the TLS on the Bloch sphere. Afterwards we provided an introduction to periodically driven systems including a brief survey of the Floquet theory. This was accompanied by discussing two prominent periodic types of driving, namely the linearly polarized driving and the circularly polarized driving. We further examined the transformation into the rotating frame and explained how and in which conditions both types of driving appear to be approximately equivalent. Furthermore, we embedded the circularly polarized driving in the Floquet picture. Finally, we introduced a measurement protocol for probing the TLS, which will be used throughout most of the following parts of this thesis.

3. Fundamentals: Formalisms for open quantum systems

In this chapter we provide an introduction to the standard description to the dynamics of open quantum systems. In this context *open* means that a small subsystem interacts with an environment. The environment usually is assumed to be much larger than the subsystem of interest. As the scope of the work at hand is to analyze the energy dissipation of a driven two-level system to its surroundings, it is instructive to clarify the general treatment of open quantum systems.

There are many different approaches to the problem of open quantum systems which involve an approximate description of the dynamics of the subsystem. Two prominent approaches are, for example, the master equation approach [61] or the Keldysh-technique [62, 63]. We will focus on the master equation approach. The master equation describes the time evolution of the reduced density operator of the system of interest. In this chapter we will provide a derivation of a Markovian master equation. Particular differential equations describing the dynamics of open quantum systems are often called Bloch, Redfield or Bloch-Redfield type master equations. This is attributed to the pioneering work of Bloch and Redfield, who developed those equations in the 1950s [64, 65, 66, 67].

As mentioned above we are interested in the dynamics of a system which is coupled to a bath. The corresponding Hilbert space

$$\mathcal{H} = \mathcal{H}_S \otimes \mathcal{H}_B, \tag{3.1}$$

is spanned by the Hilbert spaces $\mathcal{H}_S$ of the system and $\mathcal{H}_B$ of the bath. Here and in the following, the labeling corresponds to the system (S) and the bath (B) respectively. The generic Hamiltonian describing such a situation consists of three parts,

$$\begin{aligned} \hat{H} &= \hat{H}_S \otimes \mathbb{1}_B + \mathbb{1}_S \otimes \hat{H}_B + \hat{H}_I \\ &= \hat{H}_S \otimes \mathbb{1}_B + \mathbb{1}_S \otimes \hat{H}_B + A_S \otimes B \end{aligned} \tag{3.2}$$

where $\hat{H}_S$ describes the Hamiltonian of the subsystem S, and $\hat{H}_B$ corresponds to the Hamiltonian of the bath. A sketch of the situation is provided in Fig. 3.1. Note that the coupling constant is assumed to be contained in the bath operator B.

The interaction between the system and the bath is given by $\hat{H}_I$. Due to the interaction between the two systems, a non-ambiguous description using the state $|\Psi(t)\rangle$ of the whole

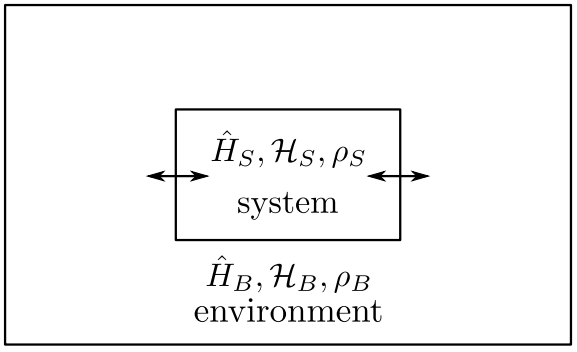

Figure 3.1.: Schematic of the system S surrounded by the environment B. The systems act on their corresponding Hilbert spaces $\mathcal{H}_S$ and $\mathcal{H}_B$ and are described by their density operators ρ_S and ρ_B.

system is not possible anymore. The interaction between the system and the bath leads to a random statistical mixture of states. Consequently, it is more effective to describe the system using the density matrix.

3.1. The density matrix

A quantum mechanical system is usually described by its state $|\Psi(t)\rangle$. The dynamics of the state are governed by the Schrödinger equation

$$i\partial_t|\Psi(t)\rangle = \hat{H}(t)|\Psi(t)\rangle, \tag{3.3}$$

where $\hat{H}(t)$ is the possibly time-dependent Hamiltonian of the system. Situations do exist where the description of a system by its state is impossible. For example, this is the case when one needs to describe a statistical mixture of states. In this situation the use of a density matrix is unavoidable. The density operator has the general form

$$\rho = |\Psi\rangle\langle\Psi|, \tag{3.4}$$

where $|\Psi\rangle$ denotes the state of the system. From Eq. (3.4) it is quite obvious that the density operator has a matrix structure. Hence, it is sometimes also referred to as density matrix. For a detailed study of the density operator we refer to [68].

An important advantage of the density matrix description manifests itself in the context of coupled systems. Interested in the time evolution of a coupled system one may be able to write the initial state of both systems in a product state as $|\Psi_{SB}(0)\rangle = |\phi_S(0)\rangle \otimes |\varphi_B(0)\rangle$, where the states belong to their corresponding Hilbert spaces. However, the time-evolved state $|\Psi_{SB}(t)\rangle$ generally cannot be represented by a product state anymore. As the two states are correlated, an independent analysis of the states of the subsystem S regardless of the subsystem B is no longer possible.

Here is where the advantage of the density matrix description becomes apparent. In accordance to the approach discussed above, we may choose the density matrix ρ_{SB} to be initially represented by a product state, i.e. $\rho_{SB}(0) = \rho_S(0) \otimes \rho_B(0)$. Although the density operator generally cannot be written in a product state at any time $t > 0$ later on, one can trace out the degrees of one system to obtain the reduced density operator of the system of interest,

$$\rho_S(t) = \mathrm{Tr}_B\left[\rho_{SB}(t)\right] = \sum_j \langle\Psi_{B,j}|\rho_{SB}(t)|\Psi_{B,j}\rangle, \tag{3.5}$$

where $|\Psi_{B,j}\rangle$ are the basis states of the subsystem B.

The time evolution of the density operator is called *von Neumann* equation

$$\dot{\rho}(t) = -i\left[\hat{H}(t), \rho(t)\right], \tag{3.6}$$

which directly follows from the Schrödinger equation (3.3). Considering the situation of a system coupled to an infinitely large bath, this equation of motion is impossible to solve exactly. Thus, one needs to derive an approximate equation of motion which governs the time evolution of the density operator.

In the following we will give a brief derivation of a master equation describing the time evolution of the reduced density operator of a system S coupled to a bath B. It turns out that the time evolution of the reduced density matrix of the system is non-unitary as the interaction with the infinitely large bath causes irreversible processes. Since the density operator contains occupation probabilities, the time evolution governed by a master equation needs to fulfill certain conditions. Firstly, the trace of the density operator needs to be preserved. Secondly, the entries corresponding to the occupation probabilities need to remain positive. In other words, the generator given by the master equation must provide a positive and trace-preserving map, i.e. the map $\rho_S \to \mathcal{V}\rho_S$ is called positive if $\mathcal{V}\rho_S$ is positive. Sometimes an even stronger condition onto the mapping is desired, namely complete positivity. This condition is fulfilled if $\mathcal{V} \otimes \mathbb{1}_n$ is positive for all identity operators $\mathbb{1}_n$ with size $n \in \mathbb{Z}$. A map which provides complete positivity for any initial condition of the density operator is ensured by a master equation in Lindblad-Form [69].

3.2. Microscopic derivation of a master equation

A large variety of master equations and their respective derivations can be found in the literature. In the following we will provide a microscopic derivation for a master equation in the weak coupling limit, where we assume the coupling between system and bath to be small. We further discuss the assumptions necessary to derive certain types of master equations. Our presentation is along the lines of [61].

3.2.1. The Bloch-Redfield master equation

As stated above, we are interested in the dynamics of a quantum mechanical system S which is weakly coupled to a bath. The total Hamiltonian is given by

$$\hat{H} = \hat{H}_S + \hat{H}_B + \hat{H}_I, \tag{3.7}$$

where $\hat{H}_S$ denotes the free Hamiltonian of the system. For simplicity we consider the system to be time-independent. The system is coupled to the bath via $\hat{H}_I = \sum_j A_{S,j} \otimes B_j$. The free Hamiltonian of the bath is represented by $\hat{H}_B$. The coupling Hamiltonian consists of system operators $A_{S,j} = A_{S,j}^\dagger$ and bath operators $B_j = B_j^\dagger$, which all are considered to be hermitian. It is useful to perform the derivation of the master equation in the interaction picture. The starting point of the derivation is the von Neumann equation (3.6) which is rewritten in its integral form

$$\rho^I(t) = \rho^I(0) - i\int_0^t ds[\hat{H}_I^I(s), \rho^I(s)], \tag{3.8}$$

where the superscript I denotes the interaction picture. Taking the integral form and putting it back into the von Neumann equation yields

$$\frac{d}{dt}\rho^I(t) = -i[\hat{H}_I(t), \rho^I(0)] - \int_0^t ds[\hat{H}_I^I(t), [\hat{H}_I^I(s), \rho^I(s)]]. \tag{3.9}$$

As we are interested in the time evolution of the reduced density operator $\rho_S(t)$ of the system, the next step is to trace out the bath degrees of freedom. We assume that the density operator can initially be written as a product of the two density operators, i.e. $\rho(0) = \rho_S(0) \otimes \rho_B(0)$. Consequently, we can rewrite Eq. (3.9) for the reduced density operator of the system as

$$\frac{d}{dt}\rho_S^I(t) = -\int_0^t dt' \mathrm{Tr}_B \left[\hat{H}_I^I(t), [\hat{H}_I^I(s), \rho^I(s)]\right], \tag{3.10}$$

where we set

$$\mathrm{Tr}_B \left[\hat{H}_I^I(t), \rho^I(0)\right] = 0. \tag{3.11}$$

Although this may seem to be an additional approximation, Eq. (3.11) is nothing but an energy shift of the system which can be discarded by a proper renormalization. This is achieved as follows. At first one absorbs the term into the free Hamiltonian of the system, i.e. $H_S \to H_S + \sum_j A_{S,j}(t)\langle B_j\rangle$. By a proper renormalization of the bath operators $B_j \to B_j - \langle B_j\rangle$, one readily arrives at Eq. (3.10).

In the weak-coupling limit we are able to perform the Born approximation. This means we restrict the calculations to the lowest order iteration of the above equation of motion. This may easily be understood using a diagrammatic expansion, which we will discuss later in section 3.3.

A second assumption based on the weak-coupling limit is given by

$$\rho^I(t) \approx \rho_S^I(t) \otimes \rho_B, \tag{3.12}$$

i.e. the density operators of the system and the bath factorize. Physically this means that the coupling between the bath and the system is small enough and that the bath itself is large enough for the density operator of the bath to be insignificantly changed by the interaction. We thus obtain a closed differential equation for the reduced systems density operator.

The Markov approximation is more subtle. At first, the density operator depending on the integral time $\rho_S^I(s)$ is replaced by the reduced density operator $\rho_S^I(t)$. This leads to

$$\frac{d}{dt}\rho_S^I(t) = -\int_0^t ds\, \mathrm{Tr}_B \left[\hat{H}_I^I(t), [\hat{H}_I^I(s), \rho_S^I(t) \otimes \rho_B]\right], \tag{3.13}$$

which is local in time as the time evolution of the reduced density operator does not depend on the integral time s anymore. The Markovian approximation has not yet been fully performed. In order to obtain a fully Markovian master equation, one has to substitute $s \to t - s$ and take the upper integral limit to infinity. We finally obtain a master equation

$$\frac{d}{dt}\rho_S^I(t) = -\int_0^\infty ds\, \mathrm{Tr}_B \left[\hat{H}_I^I(t), [\hat{H}_I^I(t-s), \rho_S^I(t) \otimes \rho_B]\right], \tag{3.14}$$

in Born-Markov approximation. This master equation is also known as Bloch-Redfield master equation. The requirement for the Markov equation to be justified is provided by $\tau_B \ll \tau_R$, where τ_B is the decay time of the bath correlation functions and τ_R is the relaxation time of the system. This means that the bath correlation function decays much faster than the system responds to the interaction with the bath. This means that the bath is memoryless with respect to previous physical events. In addition, taking the upper integral limit to infinity requires that the bath correlation function decays sufficiently fast at times $\tau_B \ll s$ so that the integrand in Eq. (3.14) vanishes fast enough.

In principle, this master equation (3.14) allows for a reasonably good description of the weakly coupled open system. However, it does not guaranty complete positivity for the density operator. Furthermore, it may have the disadvantage of only being solvable numerically. Applying a further approximation, one is able to derive the master equation in Lindblad form. This derivation is performed in the subsequent section.

3.2.2. The Lindblad master equation

In this section we provide the derivation of the master equation in Lindblad form. The starting point of the derivation is Eq. (3.14). The necessary approximation to obtain the Lindblad master equation is the *secular* approximation. The secular approximation neglects coupling terms between populations and coherences if they oscillate fast enough. It is a quite similar approximation to the rotating wave approximation which has been discussed in chapter 2.

The secular approximation is most easily explained and performed in the interaction picture using the eigenbasis of the system. We denote the eigenvalues of $\hat{H}_S$ by E_S. The corresponding projector onto the eigenstate of energy E_S is given by $P(E_S)$. We recall the system-bath interaction in the Schrödinger picture $\hat{H}_I = \sum_j A_{S,j} \otimes B_j$. The system part of the interaction is rewritten as a frequency dependent operator, i.e.

$$A_{S_j}(\omega) = \sum_{E'_S - E_S = \omega} P(E_S) A_{S,j} P(E'_S) \tag{3.15}$$

where the sum is taken over all possible energy differences ω regarding the energies E_S and E'_S. We further note that $A^\dagger_{S,j}(\omega) = A_{S,j}(-\omega)$ and $\sum_\omega A_{S,j}(\omega) = \sum_\omega A^\dagger_{S,j}(\omega) = A_{S,j}$ as well as

$$e^{i\hat{H}_S t} A_{S,j}(\omega) e^{-i\hat{H}_S t} = e^{-i\omega t} A_{S,j}(\omega), \tag{3.16}$$

$$e^{i\hat{H}_S t} A^\dagger_{S,j}(\omega) e^{-i\hat{H}_S t} = e^{+i\omega t} A^\dagger_{S,j}(\omega). \tag{3.17}$$

Consequently, we are able to rewrite the system bath interaction in terms of the newly introduced operators

$$\hat{H}_I = \sum_j \sum_\omega A_{S,j}(\omega) \otimes B_j = \sum_j \sum_\omega A^\dagger_{S,j}(\omega) \otimes B^\dagger_j, \tag{3.18}$$

and furthermore

$$\hat{H}^I_I(t) = \sum_j \sum_\omega e^{-i\omega t} A_{S,j}(\omega) \otimes B_j(t) = \sum_j \sum_\omega e^{i\omega t} A^\dagger_{S,j}(\omega) \otimes B^\dagger_j(t), \tag{3.19}$$

where $B_j(t) = e^{iH_B t} B_j e^{-iH_B t}$. Assuming an infinitely large bath in equilibrium, we have $\langle B_j(t) \rangle = \mathrm{Tr}_B \left[B_j(t) \rho_B \right] = 0$.

Next we rewrite the Bloch Redfield equation using the the new representation of the system operators

$$\begin{aligned}
\dot{\rho}^I_S(t) = &\sum_{\omega,\omega'} \sum_{j,k} \int_0^\infty ds e^{i\omega s} \langle B^\dagger_j(s) B_k(0) \rangle e^{i(\omega' - \omega)t} \Big(A_{S,k}(\omega) \rho^I_S(t) A^\dagger_{S,j}(\omega') \\
&\qquad - A^\dagger_{S,j}(\omega') A_{S,k}(\omega) \rho^I_S(t) \Big) \\
&+ \sum_{\omega,\omega'} \sum_{j,k} \int_0^\infty ds e^{-i\omega s} \langle B^\dagger_k(0) B_j(s) \rangle e^{-i(\omega' - \omega)t} \Big(A_{S,j}(\omega') \rho^I_S(t) A^\dagger_{S,k}(\omega) \\
&\qquad - \rho^I_S(t) A^\dagger_{S,k}(\omega) A_{S,j}(\omega') \Big),
\end{aligned} \tag{3.20}$$

where we used that

$$\langle B_j^\dagger(t) B_k(t-s)\rangle = \langle B_j^\dagger(s) B_k(0)\rangle \tag{3.21}$$

is fulfilled. Physically this is achieved if the bath is in a stationary state or in thermal equilibrium. The equation becomes more compact introducing the one-sided Fourier Transforms (Laplace Transforms) of the bath correlation function

$$\Gamma_{jk}(\omega) \equiv \int_0^\infty ds e^{i\omega s}\langle B_j^\dagger(s) B_k(0)\rangle, \tag{3.22}$$

which are-time independent, i.e. do not depend on t anymore. In the Laplace transform $\Gamma_{jk}(\omega)$ the dissipation rates $\gamma_{jk}(\omega)$ as well as the Lamb shift renormalization terms related to the bath are stored. To develop the connection we introduce the Fourier transform of the bath correlation function

$$C_{jk}(\nu) = \int_{-\infty}^\infty dt e^{i\nu s}\langle B_j^\dagger(s) B_k(0)\rangle, \tag{3.23}$$

which is real-valued. We are able to rewrite the Laplace transform (with a convergence generator $\delta > 0$) as

$$\begin{aligned}\Gamma_{jk}(\omega) &= \lim_{\delta\to 0}\int_0^\infty ds e^{i\omega s-\delta s}\langle B_j^\dagger(s) B_k(0)\rangle \\ &= \lim_{\delta\to 0}\int_0^\infty ds e^{i\omega s-\delta s}\int \frac{d\nu}{2\pi} C_{jk}(\nu) e^{-i\nu s} \\ &= \lim_{\delta\to 0} i\int_{-\infty}^\infty \frac{d\nu}{2\pi} C_{jk}(\nu)\frac{1}{\omega-\nu+i\delta},\end{aligned} \tag{3.24}$$

which gives

$$\Re\Gamma_{jk}(\omega) = \frac{1}{2}C_{jk}(\omega) \equiv \frac{1}{2}\gamma_{jk}(\omega), \tag{3.25}$$

$$\Im\Gamma_{jk}(\omega) = P.V.\int_{-\infty}^\infty \frac{d\nu}{2\pi} C_{jk}(\nu)\frac{1}{\omega-\nu}. \tag{3.26}$$

Here, *P.V.* denotes the Cauchy principal value.

As a next step we want to apply the secular approximation, i.e. all terms of Eq. (3.20) oscillating with $e^{i(\omega'-\omega)t}$ for $\omega \neq \omega'$ are discarded. This approximation relies on the separation of time scales of the dynamics of the system and the system bath coupling. It is usually applicable when $|\omega-\omega'| \gg \Gamma_{\text{rel}}, \Gamma_\varphi$ for $\omega \neq \omega'$ where we anticipate the relaxation rate Γ_{rel} and the dephasing rate Γ_φ which we will introduce later on.

Using the secular approximation, we arrive at the master equation in Lindblad form

$$\begin{aligned}\frac{d}{dt}\rho_S^I(t) &= -i[\hat{H}_{LS}, \rho_S^I(t)] \\ &\quad + \sum_\omega\sum_{j,k}\gamma_{jk}(\omega)\left(A_{S,k}(\omega)\rho_S^I(t)A_{S,j}^\dagger(\omega) - \frac{1}{2}\left\{A_{S,j}^\dagger(\omega)A_{S,k}(\omega), \rho_S^I(t)\right\}\right),\end{aligned} \tag{3.27}$$

where we introduced the quasi Lamb shift Hamiltonian

$$\hat{H}_{LS} = \sum_\omega\sum_{jk}\Im\,\Gamma_{jk}(\omega)A_{S,j}^\dagger(\omega)A_{S,k}(\omega). \tag{3.28}$$

The name arises as it evokes a Lamb shift like renormalization of the systems energy levels due to the interaction.

3.2.3. Summary

In the above two subsections we have derived two very prominent master equations from a microscopic approach. We want to briefly compare both equations (3.14) and (3.27), and summarize the approximations which were used in their respective derivations.

Initially a microscopic derivation of the Bloch Redfield equation Eq. (3.14) was provided. The necessary assumptions that have been made to arrive at this equation were the Born and the Markov approximations. Thus, a weak coupling between system and bath as well as an infinitely large bath are necessary to justify the expansion of the exact von Neumann equation to second order. Additionally, the equation relies on a coarse-grained description of time scales and a memoryless bath. This is assured by a sufficient fast decaying bath correlation function, and thus a short bath correlation time $\tau_B \ll \tau_R$ compared to the relaxation time of the system.

The Lindblad equation (3.27) relies on an additional approximation, the secular approximation. It may be applied under the condition of $|\omega - \omega'| \gg \Gamma_{\mathrm{rel}}, \Gamma_\varphi$.

Although the Bloch Redfield equation is more exact than the Lindblad equation, there are a few advantages regarding the latter. For large systems the Bloch Redfield equation may become quite cumbersome to solve and may require a lot of computation power.

The Lindblad equation, although being slightly less exact, may be easier to be solved even analytically. Consequently, it grants an adequate amount of insight to the dynamics of the open system of interest.

3.3. Diagrammatic approach

An alternative approach to the derivation of the master equation is given by a diagrammatic expansion of the time evolution of the density operator. This analysis is based on a perturbative expansion of the time evolution using the Keldysh formalism. In this section we briefly review the framework of the diagrammatic approach which was developed by Schoeller and Schön [63].

Starting point of the diagrammatic expansion is the von Neumann equation (3.6) in the interaction picture

$$\frac{d}{dt}\rho^I(t) = -i[\hat{H}_I^I(t), \rho^I(t)], \tag{3.29}$$

which yields the formal solution

$$\rho^I(t) = \mathcal{T} e^{-i\int_0^t dt' \hat{H}_I^I(t')} \rho^I(0) \bar{\mathcal{T}} e^{i\int_0^t dt' \hat{H}_I^I(t')}, \tag{3.30}$$

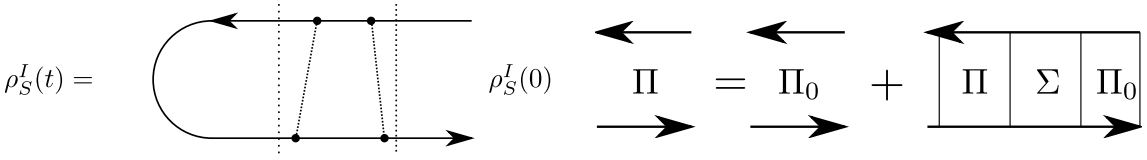

Figure 3.2.: Sketch of the time evolution of the density operator via the propagator Π. The processes inbetween the two dashed lines are exemplary processes.

Figure 3.3.: Diagrammatic representation for the Dyson equation of the propagator Π.

where $\mathcal{T}(\bar{\mathcal{T}})$ denote the chronological (anti-chronological) time ordering operator. If we assume that the initial density operator factorizes, i.e. $\rho^I(0) = \rho_S^I(0) \otimes \rho_B$, we are able to take the trace over the bath and perform an expansion of the exponents in the system bath interaction. Note that this assumption is suitable concerning a Markovian situation, but may disregard non-Markovian effects. We obtain a formal expression for the time evolution of the reduced density operator

$$\rho_S^I(t) = \Pi^I(t,0)\rho_S^I(0), \tag{3.31}$$

where $\Pi(t,t')$ is the propagator of the reduced density operator of the system. The situation is sketched in Fig. 3.2. The propagator fulfills the Dyson equation

$$\Pi = \Pi_0 + \Pi\Sigma\Pi_0, \tag{3.32}$$

where Σ is the self-energy and Π_0 is the free propagator. The corresponding diagrammatic equation is depicted in Fig. 3.3. The self-energy is defined as the contribution of all non-irreducible diagrams to the propagator. Two examples of an irreducible and a reducible diagram are shown in Fig. 3.4. We emphasize that the diagrams used in this work differ from the usual notation as the time direction of time is inverted.

One arrives at the interaction picture differential equation describing the equation of motion of the reduced density operator of the system (often referred as kinetic equation)

$$\frac{d}{dt}\rho_S^I(t) = \int_0^t dt' \Sigma^I(t,t')\rho_S^I(t'), \tag{3.33}$$

where $\Sigma^I(t,t')$ is the interaction picture self energy. If the problem obeys time translational invariance, the self-energy only depends on the time difference, i.e. $\Sigma_I(t,t') = \Sigma_I(t-t')$. The equation of motion (3.33) yields a useful tool to investigate the dynamics of the density operator up to any order of interest by calculating diagrams to the order of interest.

In this thesis we restrict ourselves to the lowest order contribution, which is equivalent to the weak coupling assumption and the Born approximation discussed previously. In the following we briefly want to explain the basic diagrammatic rules which were defined in Ref. [63].

The diagrammatic rules necessary to calculate the diagrams are as follows. The vertices are depicting system-bath interaction contributions at a given time $\hat{H}_I^I(t')$. Propagators inbetween two vertices following the Keldysh contour yield a free time evolution $U_{0,S}(t,t')$ of the system where the time difference is indicated by the arrow of time. Two vertices connected by a dashed line denote a contraction of two bath operators $B(t)$ and $B(t')$ at different times. Note that a vertex can only undergo one contraction. We omitted the indices of different bath operators j,k for the ease of legibility. The time ordering

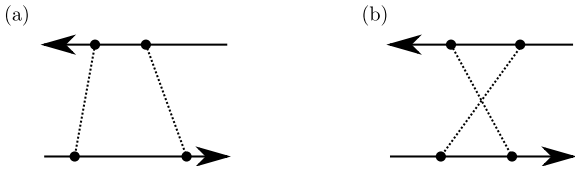

Figure 3.4.: Two exemplary second order contributions to the self-energy Σ. In the situation (a) the diagram is reducible, whereas diagram (b) denotes an irreducible second order process. Diagrams are regarded to be reducible if one can cut vertically without crossing a dashed line.

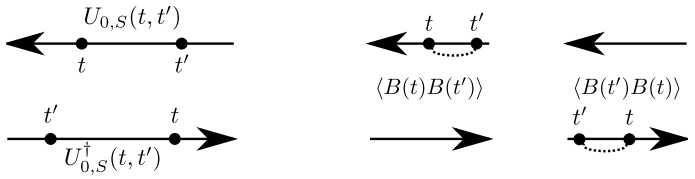

Figure 3.5.: Sketch of diagrammatic rules. The rules are explained in the main text.

depends on the appearance on the Keldysh contour. The rules are depicted in Fig. 3.5. The approximations used within the diagrammatic technique are essentially the same as discussed in the previous section 3.2. Thus, using the Born and the Markov approximations one obtains a Markovian master equation in the Schrödinger picture

$$\frac{d}{dt}\rho_S(t) = \mathcal{L}_S\rho_S(t) + \int_{-\infty}^{\infty} ds\Sigma(s)e^{-\mathcal{L}_S s}\rho_S(t), \tag{3.34}$$

where $\mathcal{L}_S$ with $\mathcal{L}_S\,\rho_S(t) \equiv -i[\hat{H}_S, \rho_S(t)]$ is the free Liouville super operator or *Liouvillian* of the system. If only first order diagrams are considered in the calculation of the self energy Σ, Eq. (3.34) is of Bloch-Redfield form. Thus, it is equivalent to Eq. (3.14).

3.4. Super operator representation

In many situations it is convenient to write the Master equation in super operator form. The advantage of the super operator representation over the regular operator representation is that we directly obtain and see the coupling between different elements of the density operator. Furthermore, in the super operator space (or Liouville space) the master equation obtains a relatively simple matrix differential equation, which is quite handy to analyze.

The master equation for the reduced system density operator is given by

$$\frac{d}{dt}\vec{\rho}_S(t) = \mathcal{L}\vec{\rho}_S(t), \tag{3.35}$$

where $\mathcal{L}$ is a $N^2 \times N^2$ dimensional super operator with N being the dimensionality of the Hilbert space of the system. The N-dimensional density operator $\rho_S(t)$ has been rewritten as a vector of with N^2 rows. The ordering of the resulting vector can be chosen quite arbitrarily. A super operator, consisting of two operators A and B acting from two sides onto third operator C in Hilbert space, is constructed as (see for example Ref. [70])

$$\overrightarrow{ACB} = \left(A \otimes B^T\right)\vec{C}, \tag{3.36}$$

where $\otimes$ denotes the tensor product which is in this situation equivalent to the the Kronecker product. In the same spirit the super operator $\mathcal{M}$ is determined from Eq. (3.14) or Eq. (3.33). We note that this transformation refers to a specific arrangement of the resulting vector

$$C = \begin{pmatrix} c_{11} & c_{12} & \dots & c_{1n} \\ c_{21} & c_{22} & \dots & c_{2n} \\ \dots & \dots & \dots & \dots \\ \dots & \dots & \dots & \dots \\ \dots & \dots & \dots & \dots \\ c_{n1} & c_{n2} & \dots & c_{nn} \end{pmatrix} \rightarrow \vec{C} = \begin{pmatrix} c_{11} \\ c_{12} \\ \dots \\ c_{21} \\ \dots \\ c_{nn} \end{pmatrix}, \tag{3.37}$$

such that the rows are counted first. The advantage of this particular representation becomes obvious regarding the master equation in Bloch Redfield form. One obtains a set of N^2 coupled linear differential equations where the solution is accessible via the matrix diagonalization of the super operator $\mathcal{L}$, which is in the literature often referred as the *Redfield tensor*.

3.5. The bath correlation functions

The properties of the bath are usually characterized by the bath correlation functions. Depending on the physical properties of the bath, it may influence the system in various ways. In this thesis we will treat the bath as an infinite set of harmonic oscillators which can be represented by bosonic operators. The discussion in this section is restricted to autocorrelation functions only.

Within the master equation approach discussed above, the bath correlation function appears usually in the time domain

$$C_{BB}(t) \equiv \langle B^\dagger(t)B(0)\rangle = \mathrm{Tr}_B\left[B^\dagger(t)B(0)\rho_B\right], \tag{3.38}$$

where ρ_B is the density operator of the bath. Assuming that the system couples to the coordinate of the oscillator, we are able to rewrite the coordinate using the bosonic creation and annihilation operators $b^\dagger$ and b yielding

$$B = \sum_j \lambda_j \left(b_j^\dagger + b_j\right), \tag{3.39}$$

where $\lambda_j = g_j\sqrt{1/(2m_j\omega_j)}$ and g_j is the coupling constant. Consequently, the correlation function is

$$\begin{aligned}\langle B^\dagger(t)B(0)\rangle &= \sum_j \lambda_j^2 \left(\langle b_j^\dagger(t)b_j\rangle + \langle b_j(t)b_j^\dagger\rangle\right)\\ &= \sum_j \lambda_j^2 \left(e^{i\omega_j t}n_B(\omega_j) + e^{-i\omega_j t}(n_B(\omega_j)+1)\right),\end{aligned} \tag{3.40}$$

where $n_B(\omega_j)$ is the Bose function. In the literature one often finds

$$\langle B^\dagger(t)B(0)\rangle = \frac{2}{\pi}\int_0^\infty d\omega J(\omega)\left(e^{i\omega t}n_B(\omega) + e^{-i\omega t}\left(n_B(\omega)+1\right)\right), \tag{3.41}$$

where $J(\omega)$ is the spectral density is given by

$$J(\omega) \equiv \frac{\pi}{2}\sum_j \lambda_j^2\delta(\omega-\omega_j). \tag{3.42}$$

The spectral density can be understood as a density of states of the bath. The structure of $J(\omega)$ contains the complete information about the properties of the bath. In this thesis we restrict the bath to be *ohmic* which is represented by a linear spectral density $J(\omega) = g\omega\pi/2$, where g is the dimensionless coupling constant.

Concerning the transition rates used within the master equations discussed in the previous sections, we introduced the Fourier transform of the bath correlation functions

$$C_{BB}(\omega) = \int dt e^{i\omega t}\langle B^\dagger(t)B(0)\rangle, \tag{3.43}$$

which is real-valued as $C_{BB}(t) = C^*_{BB}(-t)$. Furthermore, the correlation function obeys the property

$$\frac{C_{BB}(-\omega)}{C_{BB}(\omega)} = e^{-\beta\omega}, \tag{3.44}$$

where $\beta = 1/T$ is the inverse temperature. Inserting this property to the transition rates Γ_{ij} in Eqs. (3.54) and (3.55), we obtain the detailed balance relation

$$\frac{\Gamma_{eg}}{\Gamma_{ge}} = e^{-\beta E}, \tag{3.45}$$

where Γ_{eg} is the excitation rate and Γ_{ge} is the relaxation rate. Physically this means that the transition of the system to a state of lower energy is more probable as the inverse transition is suppressed by a Boltzmann factor characterized by energy difference of the two states. Introducing the symmetrized and anti symmetrized correlation functions

$$S_{BB}(\omega) = \frac{1}{2}\left(C_{BB}(\omega) + C_{BB}(-\omega)\right), \tag{3.46}$$

$$A_{BB}(\omega) = \frac{1}{2}\left(C_{BB}(\omega) - C_{BB}(-\omega)\right), \tag{3.47}$$

we immediately find

$$S_{BB}(\omega) = \coth\frac{\beta\omega}{2} A_{BB}(\omega), \tag{3.48}$$

which is the fluctuation dissipation theorem (FDT) derived by Callen and Welton [7]. We may emphasize that Eq. (3.48) is not affected by the choice of the bath's spectral density $J(\omega)$.

3.6. Example: a two-level system coupled to a heat bath

In this section we want to give an example of the application of the master equation approach by discussing the dissipative treatment of a two-level system. For a comprehensive and extensive analysis of the dissipative two-level system we refer to a review by Leggett *et al.* [42]; for a detailed discussion in the context of Josephson qubits wrefer to [71].

Quite generally the Hamiltonian of a non-driven TLS (see Chapter 2) coupled to a heat bath may be written as

$$\begin{aligned}\hat{H} &= \hat{H}_{\mathrm{TLS}} + \hat{H}_I + \hat{H}_B \\ &= \underbrace{-\frac{E}{2}\sigma_z}_{=\hat{H}_{\mathrm{TLS}}} + \underbrace{\frac{1}{2}\left(\cos\vartheta\sigma_x + \sin\vartheta\sigma_z\right)\otimes B}_{\hat{H}_I} + \hat{H}_B,\end{aligned} \tag{3.49}$$

where E denotes the level splitting of the TLS and B is a bath operator. The angle ϑ determines the nature of the system bath coupling enjoined by the physical properties of the TLS. The bath does not yet need to be specified except for the property of being infinitely large. The master equation in Lindblad is obtained as (in Liouville space)

$$\frac{d}{dt}\vec{\rho}_S(t) = \begin{pmatrix} -\Gamma_{eg} & \Gamma_{ge} & 0 & 0 \\ \Gamma_{eg} & -\Gamma_{ge} & 0 & 0 \\ 0 & 0 & -\Gamma_\varphi - i(E+E_{LS}) & 0 \\ 0 & 0 & 0 & -\Gamma_\varphi + i(E+E_{LS}) \end{pmatrix} \begin{pmatrix} \rho_{gg} \\ \rho_{ee} \\ \rho_{eg} \\ \rho_{ge} \end{pmatrix}, \tag{3.50}$$

where Γ_{ij} denote the transition rates between different populations of the density operator induced by the bath. We also introduced the dephasing rate Γ_φ which characterizes the decay of the coherences. The energy shift (Lamb shift) induced by the bath is indicated by E_{LS}. The secular approximation results in the absence of the matrix elements coupling the coherences and the populations. Thus, the dynamics of the coherences and the populations totally decouple and can be solved separately.

The solution of the master equation (3.50) is

$$\rho_z(t) = \rho_{\text{th}} + (\rho_z(0) - \rho_{\text{th}})\, e^{-t\Gamma_{\text{rel}}}, \tag{3.51}$$

$$\rho_{eg}(t) = \rho_{eg}(0) e^{-i(E+E_{LS})t} e^{-t\Gamma_\varphi} = \rho_{ge}(t)^*, \tag{3.52}$$

where $\rho_{\text{th}} = (\Gamma_{ge} - \Gamma_{eg})/(\Gamma_{eg} + \Gamma_{ge})$ is the thermal steady state of the TLS. Thus, the system reaches the state of thermal equilibrium as $\rho_z(t \to \infty) \equiv \rho_{\text{th}}$. The relaxation rate is given by $\Gamma_{\text{rel}} = \Gamma_{ge} + \Gamma_{eg}$, characterizing the decay to thermal equilibrium. In the literature the relaxation rate and the dephasing rate are often referred by their inverse, the relaxation time $T_1 = \Gamma_{\text{rel}}^{-1}$ and the dephasing time $T_2 = \Gamma_\varphi^{-1}$. They also are connected via

$$\frac{1}{T_2} = \frac{1}{2T_1} + \frac{1}{T_2^*}, \tag{3.53}$$

where $(T_2^*)^{-1}$ is called the *pure* dephasing rate. The rates within this particular model are given by

$$\Gamma_{ge} = \frac{\cos^2\vartheta}{4} C_{BB}(\omega = E) \tag{3.54}$$

$$\Gamma_{eg} = \frac{\cos^2\vartheta}{4} C_{BB}(\omega = -E) \tag{3.55}$$

$$\Gamma_\varphi = \frac{\Gamma_{ge} + \Gamma_{eg}}{2} + \frac{\sin^2\vartheta}{4} C_{BB}(\omega = 0), \tag{3.56}$$

where $C_{BB}(\omega) \equiv \int dt e^{i\omega t} \langle B(t)B(0)\rangle$ is the Fourier transform of the bath correlation function. The pure dephasing rate in this particular scenario is obtained from Eq. (3.53) as $(T_2^*)^{-1} = \sin^2\vartheta/4 C_{BB}(\omega = 0)$ which depends only on the zero frequency correlation function. Physically this effect is due to the longitudinal coupling of the TLS to the bath which is not capable of flipping the state of the system. Thus, the transitions in the bath induced by this coupling do not carry any energy. We can identify two physical processes contributing to the dephasing: First, the zero energy phase loss by the pure dephasing and, second, the relaxation of the coherence which is also known as *decoherence*.

In general, the pure dephasing or loss of phase coherence does not have to be an exponential decay, i.e. the decay of the coherences may be written as $\rho_{eg} \sim e^{-t/(2T_1)} f(t)$. Here, $f(t)$ determines the loss of phase coherence due to the low frequency noise spectrum of the bath. A very prominent example is the phenomenon of $1/f$ noise, where the low frequency bath correlation function $C_{BB}(\omega \approx 0) \propto A/\omega$ tends to diverge [72]. Regarding a free induction decay (Ramsay decay), the decay function turns out to be cutoff dependent and one finds [71, 73] $f(t) \approx \exp[-t^2 A \ln 1/(\omega_{\text{ir}} t)]$ where ω_{ir} is a low-frequency cutoff. However, these effects are beyond the scope of the work at hand.

The coupling parameter ϑ allows for distinguishing between two different physical coupling limits between the system and the bath. In the situation of $\vartheta = 0$ we obtain a pure transversal coupling to the bath, i.e $\hat{H}_I \sim \sigma_x B$. In this situation the pure dephasing rate becomes immaterial regarding the decay of the coherences. Although the pure dephasing is absent, the dephasing rate Γ_φ is still finite due to the decoherence.

Another interesting situation occurs for $\vartheta = \pi/2$, where the system is purely longitudinally coupled to the bath. In this situation the populations of the system do not change as the relaxation rate $\Gamma_{\text{rel}} = 0$ vanishes. The dephasing rate is determined solely by the pure dephasing, i.e. $\Gamma_\varphi = (T_2^*)^{-1}$.

In the previous section 3.2.2 we saw that the level splitting of the system is renormalized by the interaction with the bath. The renormalization only emerges from the transverse coupling to the system. It is evaluated as

$$\begin{aligned} E_{LS} &= \frac{\sin^2\vartheta}{2} P.V. \int_{-\infty}^{\infty} \frac{d\nu}{2\pi} \frac{C_{BB}(\nu) + C_{BB}(-\nu)}{\nu - E}, \\ &= -\frac{\sin^2\vartheta}{2} P.V. \int_{-\infty}^{\infty} \frac{d\nu}{2\pi} E \frac{C_{BB}(\nu) + C_{BB}(-\nu)}{\nu^2 - E^2}. \end{aligned} \tag{3.57}$$

As we have discussed in the previous section, the bath is characterized by the spectral density $J(\omega)$. In most situations one can model the bath consisting of an infinite set of harmonic oscillators. Although the bath is supposed to be of infinite size, an infinite frequency range of the oscillators in the bath would be clearly unphysical. Thus, one may incorporate a high frequency cut-off ω_c to the bath. In the situation of ohmic dissipation, one finds that $E_{LS} \sim E \ln(\omega_c/E)$.

3.7. Conclusion

This chapter provided a compact review of the theoretical treatment of open quantum systems. A detailed derivation of a quantum master equation was given and the underlying assumptions have been discussed. The differences between two different types of master equations, i.e. the Bloch-Redfield and the Lindblad master equations have been pointed out and we have annotated their respective advantages. Additionally, we provided a brief survey of the real-time Keldysh diagrammatic approach, which turns out to lead to the same results with respect to the applied approximations.

The derivation of the master equation was followed by a more thorough and explicit treatment of the autocorrelation functions of the bath. This was carried out to be self-contained concerning the bath correlation functions used throughout the thesis.

We concluded the chapter by providing an intuitive example on the basis of a non-driven TLS weakly coupled to the bath. In the example we discussed the physical processes induced by the system-bath interaction, such as the relaxation and the dephasing as well as the Lamb shift like energy shift.

4. Fundamentals: Full counting statistics

One of the main mathematical tools used in this thesis is that of *full counting statistics* (FCS). It is a very powerful tool to calculate transport statistics properties. The FCS was first used in charge transport calculations by Levitov and Lesovik [40] and has been generalized for a variety of transport problems. The idea is to calculate the transport statistics of a system using the characteristic function (CF) of a probability distribution rather than the probability distribution itself.

In this section we will briefly review the general idea of the FCS technique in the context of its first application to the problem of electron counting statistics. This is followed by a discussion of two quite similar approaches of FCS, which will be used to determine the energy exchange statistics between two systems.

4.1. An intuitive example: The spin-1/2 galvanometer

To give a brief idea of the power of the FCS, we want to quickly review the basic idea on the basis of the original work by Levitov and Lesovik [40]. In their work they developed a theoretical framework to calculate the statistics of the current in a conductor by 'counting' the number of electrons running past a measurement device. We will review their approach to the problem of electron transport in the following.

Concerning the statistics of electrical charge flowing through a constriction during a certain measurement time τ one could ask the following question: What is the probability $\mathcal{P}_{N,\tau}$ of N electrons passing the constriction during the measurement time τ? Even more precisely rephrased, the question is: What is the probability distribution for N electrons passing the constriction during a measurement of time τ? For clarification we included a schematic of that approach in Fig. 4.1.

The CF $\chi_\tau(\lambda)$ is calculated rather than the distribution function itself. They are connected via Fourier transform, i.e.

$$\chi_\tau(\lambda) = \sum_N e^{iN\lambda}\mathcal{P}_{N,\tau}, \tag{4.1}$$

where λ is the counting field. Note that the CF itself still depends on the measurement time τ.

In a realistic experimental situation, one is not capable of directly measuring the traversed charge but the current flowing through the constriction is observed instead. The classical

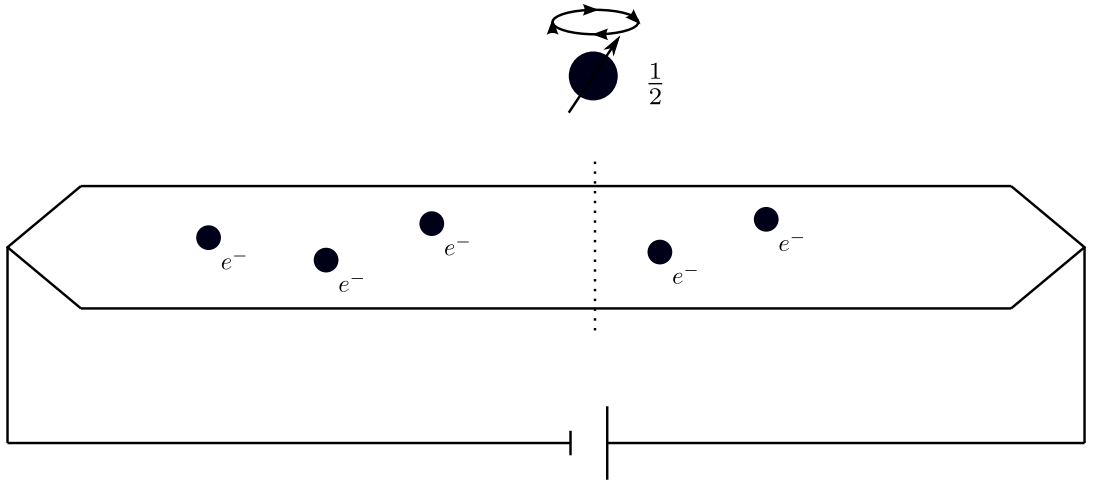

Figure 4.1.: Schematic of the spin-1/2 galvanometer: The spin precesses as an electron e^- traverses the constriction, which is indicated by the dashed line.

connection between charge and current is easily obtained by taking the integral over the current

$$Q(\tau) = \int_0^\tau dt' I(t'). \tag{4.2}$$

However, the reliability of this connection in the quantum regime is rather questionable, as the current is a quantum mechanical operator which does not necessarily need to commute with itself at different times.

The theoretical strategy is to incorporate a measurement device that is capable of measuring the charge directly instead of the current. Here, this is performed by coupling a spin-1/2 galvanometer to the constriction. The coupling between the current and the spin is given by

$$\hat{H}_{\text{coup}} = -\int \frac{1}{c}\vec{j}\vec{A}, \tag{4.3}$$

where $\vec{j}$ is the current density and $\vec{A}$ is the vector potential. By hand, the vector potential $\vec{A}$ is modified in such a way, that the spin only couples to the current whenever a charge passes the constriction, i.e. $A_j = \frac{\lambda\phi_0}{4\pi}\sigma_z\nabla_j\Theta(f(r) - f_0)$. Here $\phi_0 = 2\pi c/e$, $f(r) = f_0$ defines the surface of the constriction, Θ denotes the Heaviside step function and λ has been introduced as coupling constant. The latter will turn out to be the counting field in the following. The effective coupling Hamiltonian is obtained by integrating the current density over the surface of the constriction resulting in

$$\hat{H}_{\text{coup}} = -\frac{\lambda}{2e}\sigma_z I \tag{4.4}$$

where $I = \int_S \vec{j}d\vec{s}$ is the total current through the constriction. The modification of the spin-current interaction makes it possible to actually count the number of electrons traversing the intersection to which the spin is coupled.

This is easily verified by having a look at the density operator of the spin

$$\rho_{\text{spin}}(\tau) = \text{Tr}_e\left[e^{-i\hat{H}_\sigma\tau}\rho_{\text{spin}}(0)\otimes\rho_e(0)e^{i\hat{H}_\sigma\tau}\right], \tag{4.5}$$

where $\hat{H}_\sigma$ is the total Hamiltonian depending on the modified vector potential. As the choice of basis for the spin system is arbitrary, one can choose the eigenstates of σ_z and obtain

$$\rho_{\text{spin}}(\tau) = \begin{pmatrix} \rho_{\uparrow\uparrow}(0) & \chi_\tau(\lambda)\rho_{\uparrow\downarrow}(0) \\ \chi_\tau(-\lambda)\rho_{\downarrow\uparrow}(0) & \rho_{\downarrow\downarrow}(0) \end{pmatrix}, \tag{4.6}$$

where

$$\chi_\tau(\lambda) = \text{Tr}_e \left[e^{i\hat{H}_{-\lambda}\tau} \rho_e(0) e^{-i\hat{H}_\lambda \tau} \right] \tag{4.7}$$

turns out to be the desired CF [40]. The Hamiltonian $\hat{H}_\lambda$ is obtained by disregarding the σ_z dependence in the coupling Hamiltonian $\hat{H}_{\text{coup}} \to \hat{H}_\lambda = -\frac{\lambda}{2e} I$. Note that in Eq. (4.6) the spin degree of freedom is taken care of explicitly.

The main advantage of the FCS approach is rather obvious. Since one is capable of deriving the CF of the desired probability distribution, one can determine the statistical properties of the probability distribution quite comfortably. These properties, i.e. the cumulants, are connected to the CF by taking the derivative of the logarithm

$$\langle\langle \mathcal{C}^n \rangle\rangle \equiv (\partial_{i\lambda})^n \ln \chi_\tau(\lambda)|_{\lambda=0}\,, \tag{4.8}$$

at $\lambda = 0$, where we abbreviated $\partial_{i\lambda} \equiv \frac{1}{i}\frac{\partial}{\partial\lambda}$. This is readily seen by applying the derivative to the representation of the CF, Eq. (4.1),

$$\begin{aligned} \partial_{i\lambda} \ln \chi_\tau(\lambda)|_{\lambda=0} &= \sum_N N P_{N,\tau} \\ &= \langle N \rangle, \end{aligned} \tag{4.9}$$

which in this situation gives the average number N of electrons passing the constriction.

4.2. The two-point measurement statistics

The two-point measurement statistics is a very similar yet quite different technique to the above discussed FCS approach. It has been developed by Esposito, Harbola and Mukamel [12] and is used in the context of the fluctuation relations. The purpose of the two-point measurement statistics is to calculate the energy and the matter transfer statistics between coupled open systems. In this section we will review the necessary parts of this particular technique used in this thesis.

Instead of the charge, the quantity of interest is the energy exchanged between two systems. To be more precise we restrict ourselves to the energy ϵ emitted to the bath by a subsystem S. We aim to calculate the CF of the probability distribution of dissipated energy ϵ to the bath. As the energy in this case does not need to be quantized like in the previously discussed scenario, the connection is given by the continuous Fourier-transform

$$\chi_\tau(\lambda) = \int_{-\infty}^{\infty} d\epsilon\, e^{i\lambda\epsilon} \mathcal{P}_\tau(\epsilon), \tag{4.10}$$

where $\mathcal{P}_\tau(\epsilon)$ is the probability of dissipating the amount of ϵ energy to the bath. One can think of the dissipated energy ϵ as a difference of two measurement outcomes of energy: First, the energy of the bath is determined by a measurement resulting in ϵ_0. At a later time $t = \tau$ the energy again is measured resulting in ϵ_τ, yielding $\epsilon = \epsilon_\tau - \epsilon_0$. Thus, the probability distribution of the dissipated energy is rewritten as

$$\mathcal{P}_\tau(\epsilon) = \sum_{\epsilon_\tau, \epsilon_0} \delta(\epsilon - (\epsilon_\tau - \epsilon_0)) \mathcal{P}[\epsilon_\tau, \epsilon_0], \tag{4.11}$$

where

$$\mathcal{P}[\epsilon_\tau, \epsilon_0] \equiv \mathrm{Tr}\left[P_{\epsilon_\tau} U(\tau,0) P_{\epsilon_0} \rho(0) P_{\epsilon_0} U^\dagger(\tau,0) P_{\epsilon_\tau}\right] \tag{4.12}$$

is the joint probability of measuring ϵ_τ at time $t = \tau$ and ϵ_0 at time $t = 0$. Here, the projection operators $P_{0/\tau}$ onto the eigenstates of the corresponding energy $\epsilon_{0/\tau}$ have been introduced and

$$U(\tau,0) = \mathcal{T} \exp\left[-i \int_0^\tau dt \hat{H}(t)\right] \tag{4.13}$$

is the full time evolution operator. Here, $\mathcal{T}$ is the time-ordering operator and $\hat{H}(t)$ is the full Hamiltonian of the problem of interest.

Using this approach it turns out [12] that the CF Eq. (4.10) can be calculated via

$$\chi_\tau(\lambda) = \mathrm{Tr}\left[\rho(\lambda,\tau)\right], \tag{4.14}$$

where

$$\rho(\lambda,\tau) \equiv U_{\lambda/2}(\tau,0)\rho(0)U^\dagger_{-\lambda/2}(\tau,0), \tag{4.15}$$

is the counting field dependent density operator. Furthermore a modified time-evolution operator

$$\begin{aligned} U_\lambda(\tau,0) &\equiv e^{i\lambda\hat{H}_B(\tau)} U(\tau,0) e^{-i\lambda\hat{H}_B(0)} \\ &= e^{i\lambda\hat{H}_B} U(\tau,0) e^{-i\lambda\hat{H}_B}, \end{aligned} \tag{4.16}$$

has been introduced. This particular modification may be achieved by a transformation of the Hamiltonian according to

$$\hat{H}(t) \to \hat{H}_\lambda(t) = e^{i\lambda\hat{H}_B} \hat{H}(t) e^{-i\lambda\hat{H}_B} \tag{4.17}$$

providing the exact same result with the explicit form of the modified time evolution operator given by

$$U_\lambda(\tau,0) = \mathcal{T} \exp\left[-i \int_0^\tau dt \hat{H}_\lambda(t)\right]. \tag{4.18}$$

In the limit of zero counting field, i.e. $\lambda \to 0$, the operator $\rho(0,\tau)$ reduces to the density operator of the full system as the complete modification becomes obsolete.

For later purposes it is useful to define the corresponding energy current to the dissipated energy

$$\hat{I}_\epsilon \equiv i\left[\hat{H}(t), \hat{H}_B\right], \tag{4.19}$$

which is nothing but the total derivative of the dissipated energy. This is obvious by changing to the Heisenberg picture, where we find

$$\hat{I}^H_\epsilon(t) = \frac{d}{dt}\hat{H}^H_B(t). \tag{4.20}$$

Note that we introduced the superscript H to indicate the Heisenberg picture where $\hat{I}^H_\epsilon(t) = U^\dagger(t,0)\hat{I}_\epsilon U(t,0)$. With the definition of the energy current Eq. (4.19) we can rewrite Eq. (4.17)

$$\begin{aligned} \hat{H}_\lambda(t) &= e^{i\lambda\hat{H}_B}\hat{H}(t)e^{-i\lambda\hat{H}_B} \\ &= \sum_{m=0}^{\infty} \frac{1}{m!}\left[i\lambda\hat{H}_B, \hat{H}(t)\right]_m \\ &= \hat{H}(t) - \lambda\hat{I}_\epsilon + \mathcal{O}(\lambda^2), \end{aligned} \tag{4.21}$$

where $[A,B]_m = [A,[A,B]_{m-1}]$ with $[A,B]_0 = B$ is the nested commutator. If we go to the interaction picture with respect to the energy current $\hat{I}_\epsilon$, we immediately find

$$\chi_\tau(\lambda) = \mathrm{Tr}\left[\mathcal{T}\exp\left[-i\frac{\lambda}{2}\int_0^\tau dt\hat{I}_\epsilon^H(t)\right]\rho(0)\mathcal{T}\exp\left[-i\frac{\lambda}{2}\int_0^\tau dt\hat{I}_\epsilon^H(t)\right]\right]. \tag{4.22}$$

The structure of Eq. (4.22) is equivalent to the generating function derived by Nazarov and Kindermann [74]. We will discuss and comment on that in the next section, where we will review the Nazarov-Kindermann approach for FCS.

4.3. The Nazarov-Kindermann-approach to energy counting statistics

In this section we review an alternative approach to FCS as suggested by Nazarov and Kindermann [74]. In contrast to their original work, which provided the full analysis of the FCS of a general quantum mechanical variable, we will restrict ourselves to the FCS of the dissipated energy. As anticipated in the previous section, the outcome of the FCS will be equivalent to the two point measurement statistics, however, it involves a slightly different approach.

In contrast to the two-point measurement approach, where the counting field becomes incorporated more or less 'by hand', this proposal introduces and includes an actual detector (we will sometimes refer to it as meter or measurement device) to the discussion. The detector is based on the pioneering measurement proposal by von Neumann [75] and is supposed to be a quantum system with coordinate $\hat{X}_M$ and momentum $\hat{P}_M$, satisfying $[\hat{X}_M,\hat{P}_M] = i$.

The detector is coupled to a current-like quantity similar to the original proposal by Levitov and Lesovik [40]. Considering the situation of system coupled to a heat bath represented by the Hamiltonian $\hat{H}_{SB}$, the current is identified with the energy current $\hat{I}_\epsilon = -i[\hat{H}_B,\hat{H}_I]$ in our problem where $\hat{H}_I$ is the system-bath interaction Hamiltonian. The full Hamiltonian including the meter reads

$$\hat{H} = \hat{H}_{SB} - \hat{I}_\epsilon\hat{P}_M + \hat{H}_M, \tag{4.23}$$

with $\hat{H}_M$ being the free Hamiltonian of the meter. In the following we completely discard the internal dynamics of the detector and set $\hat{H}_M = 0$. Being interested in the outcome of the meter, we have to study the reduced density operator of the meter ρ_M. By tracing out the system and bath degrees of freedom, we obtain

$$\rho_M(\tau) = \mathrm{Tr}_{SB}\left[U_{SBM}(\tau,0)\rho_S(0)\otimes\rho_B\otimes\rho_M U_{SBM}^\dagger(\tau,0)\right], \tag{4.24}$$

where $U_{SBM}(\tau,0)$ is the full time evolution operator for system bath and measurement device. We further assumed that the initial density operator can be written as a product $\rho_{SBM}(0) = \rho_S(0)\otimes\rho_B\otimes\rho_M$. Introducing the eigenstates of the momentum operator as

$$\hat{P}_M|\lambda\rangle = \lambda|\lambda\rangle, \tag{4.25}$$

we are able to evaluate a certain matrix element of the density operator of the detector. We find

$$\langle\lambda/2|\rho_M(\tau)|-\lambda/2\rangle = \chi_\tau(\lambda)\langle\lambda/2|\rho_M(0)|-\lambda/2\rangle, \tag{4.26}$$

where $\chi_\tau(\lambda)$ is the desired CF and $\langle\lambda/2|\rho_M(0)|\lambda/2\rangle$ yields the initial deflection of the meter. It is quite simple to verify that the CF as obtained by Eq. (4.26) is equivalent to Eq. (4.22).

The calculation of the average dissipated energy is straightforward. As discussed above in Eq. (4.8), we find

$$\begin{aligned}\langle \epsilon_\tau \rangle &= \partial_{i\lambda} \ln \chi_\tau(\lambda)|_{\lambda=0} \\ &= \int_0^\tau dt\, \langle \hat{I}_\epsilon^H(t) \rangle,\end{aligned} \tag{4.27}$$

where $\hat{I}_\epsilon^H(t) = U_{SB}(t,0)\hat{I}_\epsilon U_{SB}^\dagger(t,0)$ is the energy current in the Heisenberg picture.

Until now, we had anticipated the CF to be the Fourier-transform of the probability distribution. Strictly speaking, as we are dealing with a quantum mechanical density operator, a more careful analysis may be necessary. Hence, in a rigorous treatment, the CF should be identified with a Wigner distribution [76] function

$$\mathcal{W}(x,p) = \int_{-\infty}^{\infty} d\lambda\, \langle p + \lambda/2|\rho_M(\tau)|p - \lambda/2\rangle e^{-ix\lambda}, \tag{4.28}$$

which may involve problems in actually interpreting the result as a probability distribution function. This is due to the fact that the Wigner transform is not completely positive and, thus, may contain negative values. A discussion about this peculiarity in the context of superconductors can be found in [77]. Consequently, we need to check if the generating function obtained by

$$\langle p + \frac{\lambda}{2}|\rho_M(\tau)|p - \frac{\lambda}{2}\rangle = \chi_\tau(p,\lambda)\langle p + \frac{\lambda}{2}|\rho_M(0)|p - \frac{\lambda}{2}\rangle, \tag{4.29}$$

is independent of p. We obtain

$$\begin{aligned}\chi_\tau(p,\lambda) &= \mathrm{Tr}_{SB}\left[e^{i\hat{H}_B(p+\frac{\lambda}{2})}U_{SB}(\tau,0)\rho_S(0)e^{-i\hat{H}_B(p+\frac{\lambda}{2})}\rho_B(0)e^{i\hat{H}_B(p-\frac{\lambda}{2})}U_{SB}^\dagger(\tau,0)e^{-i\hat{H}_B(p-\frac{\lambda}{2})}\right] \\ &= \chi_\tau(\lambda),\end{aligned} \tag{4.30}$$

where we used that $[\hat{H}_B, \rho_B] = 0$ and the invariance of the trace regarding cyclic permutation. Therefore, the interpretation of the FCS approach to the statistics of dissipated energy in terms of a probability distribution is in fact possible.

4.4. Conclusion

In this chapter an introduction to the FCS was presented. To present the general idea behind the FCS we reviewed the original proposal by Levitov and Lesovik [40] via the example of the spin 1/2-galvanometer. We highlighted the benefit of the FCS, which allows access to the CF of the problem and, consequently, to the complete transport statistics.

This was followed by the introduction of the two-point measurement statistics [12] of energy which will be used for most of the calculations within this thesis. We discussed the consistency of the two-point measurement statistics by reviewing the energy counting statistics in the full-fledged Nazarov-Kindermann approach [74]. Within this discussion we convinced ourselves that the CF derived within this approach is indeed connected to a classical probability distribution function via Fourier transform.

5. The driven two-level system in the context of fluctuation relations

This chapter deals with the topic of fluctuation relations (FRs). The FRs are exact relations for the probability distributions of thermodynamic quantities such as heat or entropy production. Interestingly, the relations are exact even if the system under consideration is far from equilibrium. Although they were discovered more than 30 years ago, they have recently attracted great attention. This is due to several reasons. Firstly, the impact of fluctuations becomes pronounced as the system size decreases. Thus, from an experimental point of view it is very difficult to test the FRs. Consequently, experiments needed to be improved to detect the small fluctuations of the thermodynamic quantities. Secondly, besides the first FR derived by Bochkov and Kuzovlev [8] in the late 1970s, which considered fluctuations of work, there have been found FRs of entropy production [10] and heat. Hence, a study of several thermodynamic quantities and their fluctuations in mesoscopic systems is possible, opening an avenue towards thermodynamics in the quantum regime [78].

The thermodynamics of macroscopic systems is well-understood in the picture of statistical mechanics. However, the description is restricted to equilibrium or near to equilibrium situations only. The FRs enable the study of the dynamics of the system even far from equilibrium. The mathematical form of the FRs quite generally has a structure of [11]

$$\mathcal{P}(x) = \mathcal{P}_B(x) e^{a(x-b)} \tag{5.1}$$

which relates the probability density $\mathcal{P}(x)$ of a thermodynamic quantity x undergoing a certain possibly non-equilibrium process to the corresponding reversed (backward) probability density $\mathcal{P}_B(x)$. Despite the fact that the equality holds for quite arbitrary non-equilibrium processes, one still needs to know the initial equilibrium properties of the system. Here, this information is stored in the quantities a and b. Two main elements are obligatory for the FRs: Firstly, as already mentioned, one needs to know about the equilibrium initial conditions of the system of interest. Secondly, the FRs rely on the principle of microreversibility. These two building blocks of the FRs will be discussed further below.

In this chapter we will present our results in the context of the FRs. Before we do so we will introduce the concept of the FRs on the basis of the very first appearance in the literature derived by Bochkov and Kuzovlev in the late 1970s [8]. We then comment on the current experimental situation and briefly discuss a related state-of-the-art experiment [19]. For a detailed review on the general topic we refer to Campisi *et al.* [11]; a more technical guidance is found in Esposito *et al.* [12].

5.1. Introduction of the fluctuation relations

As an introduction to the FRs we will review and discuss the work FR derived by Bochkov and Kuzovlev. Later on we will comment on the subtlety of defining work and give a short comparison between the Bochkov-Kuzovlev and the Jarzynski fluctuation relations. As it will become apparent, they both not only rely on two different protocols but also use two different definitions of work. Finally, we will introduce the detailed fluctuation relation which will be involved in our analysis.

5.1.1. The Bochkov-Kuzovlev fluctuation relation

In 1977 Bochkov and Kuzovlev discovered a first exact fluctuation relation covering fluctuations of all orders [8]. In order to introduce the concept of the FRs, we will provide a derivation of the FR. We note that the FR is only valid for classical systems; thus, the discussion and calculation in this section is restricted to classical systems only.

Here, a classical system with the Hamiltonian $H_0 = H_0(q, p)$, depending on its coordinates q and the conjugated momenta p, is considered. The system is supposed to be in an equilibrium state at time $t < 0$, characterized by a Gibbs distribution

$$\rho_G(q, p) = \frac{1}{Z} e^{-\beta H_0(q,p)}, \tag{5.2}$$

where Z is the partition function. Note that this condition is one of the two crucial basic elements necessary for the FR.

At time $t = 0$ an external force $F_Q(t)$ is applied onto the system, such that the new Hamiltonian becomes

$$H(t) = H_0(q, p) - F_Q(t)Q(q(t), p(t)), \tag{5.3}$$

where $Q(q(t), p(t))$ is the generalized conjugate coordinate to $F_Q(t)$. The generalized conjugate coordinate is expressed in terms of

$$Q(t) \equiv Q(q(t), p(t)) = Q_t[q_0, p_0; F_Q(t')], \tag{5.4}$$

where $Q_t[q_0, p_0; F_Q(t')]$ is a functional depending on the initial values q_0, p_0 and a distinct realization of the external force $F_Q(t')$ for $0 \leq t' \leq t$.

As a next step one makes use of the principle of time reversal symmetry. This means that time-odd parameters, such as momenta, change sign when the direction of time is inverted. In the time symmetric case we have $H_0(q, -p) = H_0(q, p)$, which can be achieved in the presence of other odd parameters by changing their direction accordingly. The generalized coordinate $Q(t)$ is assumed to have a non-ambiguous parity $\varepsilon = \pm 1$ under the time reversal operation $Q(q, -p) = \varepsilon Q(q, p)$. This leads to the microreversibility condition for the generalized coordinate at time τ inbetween $[0, t]$

$$Q(\tau) = Q_\tau[q_0, p_0; F_Q(t')] = \epsilon Q_{t-\tau}[q_t, -p_t; \varepsilon F_Q(t - t')], \tag{5.5}$$

where q_t, p_t are the initial values for the time reversed protocol starting at time t. This microreversibilty condition is the second crucial building block of the FR.

The situation is depicted in Fig. 5.1 as a sketch of the phase space. Starting at an inital point (q_0, p_0) in phase space, the systems evolves according to the functional $Q_\tau[q_0, p_0; F_Q(t')]$ following a distinct realization of $F_Q(t')$ to the point (q_τ, p_τ). The time reversed process starts at $(q_t, -p_t)$ and traverses through the phase space according to the time reversed functional with respect to the exact same but time reversed realization $F_Q(t - t')$ of the external force.

Being interested in the statistics of the coordinate $Q(\tau)$, one can calculate the characteristic function for a given realization of $F_Q(t)$, given by

$$\left\langle \exp\left(\int_0^t d\tau u(\tau)Q(\tau)d\tau\right)\right\rangle\Big|_{F_Q(\tau)} = \int dq_0 dp_0 \exp\left(\int_0^t d\tau u(\tau) Q_\tau[q_0, p_0; F_Q(t')]\right)\rho_G(q_0, p_0), \tag{5.6}$$

where $u(\tau)$ is an arbitrary test function and the integration is taken over the distribution of the initial state. The characteristic function for the reversed process undergoing the same but time reversed force protocol is obtained as

$$\begin{aligned}&\left\langle \exp\left(\int_0^t d\tau u(t-\tau)Q(t-\tau)\right)\right\rangle\Big|_{F_Q(t-\tau)} \\ &= \int dq_t dp_t \exp\left(\int_0^t d\tau u(t-\tau) Q_{t-\tau}[q_t, -p_t; \varepsilon F_Q(t-t')]\right)\frac{e^{-\beta H_0(q_t,p_t)}}{Z},\end{aligned} \tag{5.7}$$

which is averaged over the distribution of the final coordinates q_t and momenta p_t. In the following we want to derive the relation between the two characteristic functions. To do so one defines work as

$$W = \int_0^t d\tau F_Q(\tau)\frac{dQ(\tau)}{d\tau} = \int_0^\tau F_Q(\tau) dQ(\tau), \tag{5.8}$$

the integral of a given realization of the externally applied force $F_Q(t)$ over the traversed trajectory of $Q(t)$ during that process. By virtue of Eq. (5.8), the work is defined as the change of the internal energy of the system as a response to the applied external realization

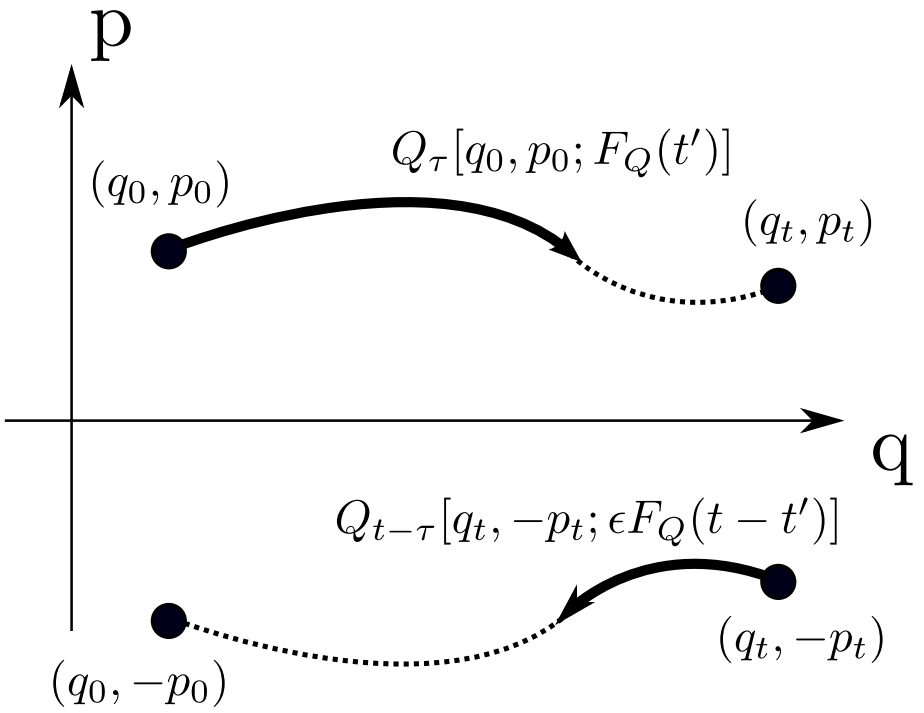

Figure 5.1.: A sketch of the traversed path in phase space is shown. The forward protocol starts at (q_0, p_0) traversing according to $Q_\tau[q_0, p_0; F_Q(t')]$ until it finally reaches the point (q_t, p_t) in phase space . The corresponding time-reversed process following the protocol $Q_{t-\tau}[q_t, -p_t; \varepsilon F_Q(t-t')]$ is depicted as well.

of the force. This is obtained by the Hamiltonian equations of motion, where

$$\begin{aligned}\frac{d}{dt}H &= \frac{\partial H}{\partial q}\frac{dq}{dt} + \frac{\partial H}{\partial p}\frac{dp}{dt} + \frac{\partial H}{\partial F_Q}\frac{dF_Q}{dt} \\ &= -Q(t)\dot{F_Q}(t),\end{aligned} \tag{5.9}$$

yielding

$$\frac{dH_0}{dt} = \frac{d}{dt}\left(H + F_Q(t)Q(t)\right) \tag{5.10}$$

$$= F_Q(t)\dot{Q}(t). \tag{5.11}$$

Hence, the work is given by

$$W(q_0, p_0) = H_0(q_t(q_0), p_t(q_0)) - H_0(q_0, p_0), \tag{5.12}$$

which can be written as a function of the initial internal coordinates q_0 and momenta p_0. The connection between the characteristic function of the forward protocol and the characteristic function of the backward protocol is established by

$$\begin{aligned}&\left\langle \exp\left(\int_0^t u(\tau)Q(\tau)d\tau\right)\right\rangle\Bigg|_{F_Q(\tau)} \\ &= \int dq_0 dp_0 \exp\left(\int_0^t u(\tau)Q_\tau[q_0, p_0; F_Q(t')]d\tau\right)\frac{1}{Z}e^{-\beta H_0(q_0,p_0)} \\ &= \int dq_0 dp_0 \exp\left(\int_0^t u(\tau)\epsilon Q_{t-\tau}[q_t, -p_t; \epsilon F_Q(t-t')]d\tau\right)\frac{1}{Z}e^{-\beta H_0(q_0,p_0)} \\ &= \int dq_t dp_t \exp\left(\int_0^t u(\tau)\epsilon Q_{t-\tau}[q_t, -p_t; \epsilon F_Q(t-t')]d\tau\right)\frac{1}{Z}e^{-\beta H_0(q_0(q_t),q_0(q_t))} \\ &= \int dq_t dp_t \exp\left(\int_0^t u(\tau)\epsilon Q_{t-\tau}[q_t, -p_t; \epsilon F_Q(t-t')]d\tau\right)\frac{1}{Z}e^{-\beta(H_0(q_t,p_t)+W(q_t,p_t))}.\end{aligned} \tag{5.13}$$

Here, it was utilized that the distribution function is symmetric under time reversal, i.e. $\rho_G(q,p) = \rho_G(q,-p)$. In addition the quantity

$$W(q_t, p_t) = -W(q_0, p_0) = H(q_0, p_0) - H(q_t, p_t) \tag{5.14}$$

has been introduced. It is identified as the work performed onto the system during the backward process. The starting and end position of the drive can be chosen arbitrarily yielding

$$\left\langle \exp\left(\int_{-\infty}^{\infty} u(\tau)Q(\tau)d\tau\right)\right\rangle\Bigg|_{F_Q(t')} = \left\langle \exp\left(\int_{-\infty}^{\infty} u(-\tau)\epsilon Q(\tau)d\tau\right)e^{\beta W(q_0,p_0)}\right\rangle\Bigg|_{\epsilon F_Q(-t')}, \tag{5.15}$$

which is the famous result derived by Bochkov and Kuzovlev. To demonstrate the physical implications one may consider the statistics of $Q(\tau)$ following a given realization of the force protocol $F_Q(t)$. We introduce the probability density $\mathcal{P}(Q; F_Q)$ in the space of trajectories $Q(\tau)$. The analog of the fluctuation relation Eq. (5.15) written in terms of the probability density reads

$$\mathcal{P}_F(Q(\tau); F_Q)e^{-\beta W} = \mathcal{P}_B(\varepsilon Q(-\tau); \epsilon F_Q(-\tau)), \tag{5.16}$$

where the subscripts F,(B) label the forward (backward, time reversed) protocol. The integration on both sides yields

$$\langle e^{-\beta W}\rangle = 1, \tag{5.17}$$

	Bochkov Kuzovlev	**Jarzynski**
Fluctuation relation	$\langle e^{-\beta W}\rangle = 1$	$\langle e^{-\beta W_{\mathrm{tot}}}\rangle = e^{-\beta \Delta F}$
Work	$W = H_0(q_t, p_t) - H_0(q_0, p_0)$ $= \int_0^t dt' F_Q(t') \frac{dQ(t')}{dt'}$	$W_{\mathrm{tot}} = H(q_t, p_t) - H(q_0, p_0)$ $= \int_0^t dt' \frac{dF_Q(t')}{dt'} Q(t')$

Table 5.1.: Two different fluctuation relations of work.

which is probably the most widely used form of the Bochkov-Kuzovlev formula. A physical intuitive result immediately follows by using Jensens inequality $\langle e^{-\beta W}\rangle \geq e^{-\beta\langle W\rangle}$, which gives

$$\langle W\rangle \geq 0. \tag{5.18}$$

Here, the equality sign applies to idealized reversible processes of closed systems, whereas in a more general situation a system perturbed by an external force always absorbs energy. Thus, Eq. (5.18) is often denoted as the FR equivalent of the second law of thermodynamics for work performed onto a system.

5.1.2. The subtlety of defining work

Yet, classical FRs have been derived for various different thermodynamic quantities such as entropy production ΔS. The FR derived by Crooks [10] is given by

$$\frac{\mathcal{P}(\Delta S)}{\mathcal{P}_B(-\Delta S)} = e^{\Delta S}, \tag{5.19}$$

where ΔS denotes the entropy production of a driven system and $\mathcal{P}_{(B)}(\Delta S)$ is the corresponding probability distribution following a certain forward (backward) protocol. From the Crooks relation (5.19) the second law of thermodynamics is directly obtained by applying the Jensens inequality, providing $\langle \Delta S\rangle \geq 0$.

Another relation widely discussed in the literature is the Jarzynski equality [9]

$$\langle e^{-\beta W_{\mathrm{tot}}}\rangle = e^{-\beta \Delta F}\ , \tag{5.20}$$

which incorporates the equilibrium free energy difference ΔF of the initial and final states in the parameter space of the system subjected to external driving. The relation derived by Jarzynski relies on a different protocol as the Bochkov-Kuzovlev FR. This leads to a different definition of work W_{tot} as compared to the Bochkov-Kuzovlev approach. In comparison, both relations and the corresponding definition of work are shown in table 5.1. Indeed, the definition of work following the Jarzynski protocol is obtained as $W_{\mathrm{tot}} = H(\tau) - H(0)$, being the total work performed onto the system.

For a meaningful comparison of the two relations it is convenient to introduce the difference

$$W_{\mathrm{tot}} - W = F_Q(0)Q(0) - F_Q(t)Q(t). \tag{5.21}$$

Setting $F_Q(0) = 0$ and inserting the difference into Eq. (5.17) yields

$$\langle e^{-\beta\left(W_{\mathrm{tot}}+F_Q(t)Q(t)\right)}\rangle = 1. \tag{5.22}$$

Comparing this relation with Eq. (5.20) shows that both equations refer to two different random quantities W_{tot} and $W_{\mathrm{tot}}+F_Q(t)Q(t)$. A very enlightening and detailed discussion about the relation between those two equations has been given in [79].

5.1.3. A detailed fluctuation relation

In this thesis we study the energy dissipation of a driven TLS. Hence, an analysis in the context of FRs is reasonable. Since the previous discussions in this section dealt with fluctuation relations of work, one could naturally ask for a quantum definition of work. Such definitions exist in the literature [26], however, there is an ongoing discussion about the controversial definition. To circumvent this problem we will stick to the energy dissipated by the driven system.

As discussed in Chapter 2.3 we use a certain measurement protocol. We include two additional strong measurements, which select the initial and the final state of the system. Hence, we expect the quantum version of the detailed fluctuation relation [33]

$$\frac{\mathcal{P}_\tau(\epsilon, f|i)}{\mathcal{P}_{\tau,B}(-\epsilon, i|f)} = e^{-\beta\epsilon} \tag{5.23}$$

to be satisfied. The detailed FR explicitly considers the initial and the final state of the system. In Eq. (5.23) we introduced the conditional probability distribution $\mathcal{P}_\tau(\epsilon, f|i)$ of the dissipated energy ϵ given that the system was initially prepared in a distinct initial state $|i_S\rangle$ and post selected onto a chosen final state $|f_S\rangle$. The subscript τ denotes the driving time. To fulfill the detailed FR the corresponding CF needs to possess a certain symmetry [80]

$$\chi_\tau(\lambda, f|i) = \chi_{\tau,B}(-\lambda + i\beta, i|f), \tag{5.24}$$

where λ is the counting field of the dissipated energy. A demonstration of Eq. (5.24) is provided in the appendix A.

5.1.4. Experimental situation

Since the rediscovery of the FRs by Jarzynski and Crooks, many experiments have been performed to test and verify the FRs. Experimental tests are a subtle task since very small system sizes as well as very precise measurement techniques are required. Thanks to the progress in recent years, the test of the FRs has become a feasible task. One of the first experimental verifications of the FRs has been demonstrated by Wang *et al.* [14], monitoring a colloidal particle in an optical trap. More recent experiments have been carried out on mesoscopic electronic circuits [17, 19, 81].

Referring to [19] in particular, the authors Kooski *et al.* were able to obtain the thermodynamic entropy production $\Delta s^{\mathrm{th}}_{\mathrm{tot}}$ by directly measuring the number of electrons tunneling inbetween a normal conducting single electron box and a superconducting Cooper pair box. The superconductor insulator normal conductor (SIN) junction, which was used in this experiment, is depicted and sketched in Fig 5.2. The tunneling of the electrons was controlled via the manipulation of the gate voltage V_g.

The distribution of the entropy production $\Delta s^{\mathrm{th}}_{\mathrm{tot}}$ obtained in the experiment is depicted in Fig. 5.3 for different temperatures. Furthermore, they were able to test the detailed FR of the entropy production

$$\frac{P_{\rightleftarrows}(\Delta s^{\mathrm{th}}_{\mathrm{tot}})}{P_{\rightleftarrows}(-\Delta s^{\mathrm{th}}_{\mathrm{tot}})} = e^{\Delta s^{\mathrm{th}}_{\mathrm{tot}}}, \tag{5.25}$$

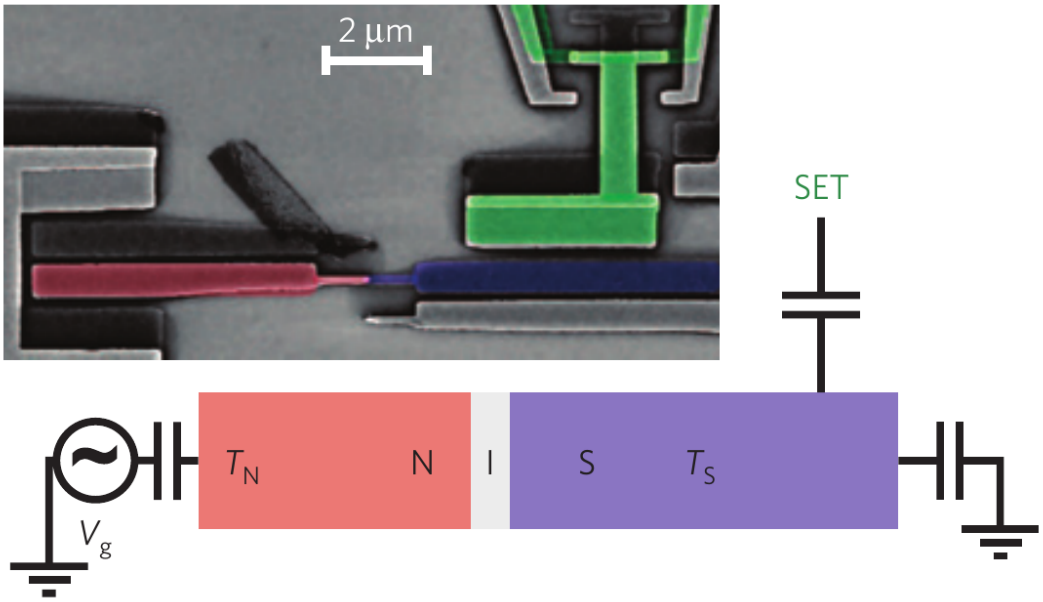

Figure 5.2.: Electron scanning micrograph and sketch of the device used in the experiment by the Kooski *et al.* [19], taken from [19] (Reprinted by permission from Macmillan Publishers Ltd: Nat. Phys. [19], copyright 2013). The content is explained in the main text.

with their results. However, even though the experiment was carried out at the single electron level at temperatures well below 1 K, the results were understood and well described on a classical level. For further details on the experiments we refer to [19].

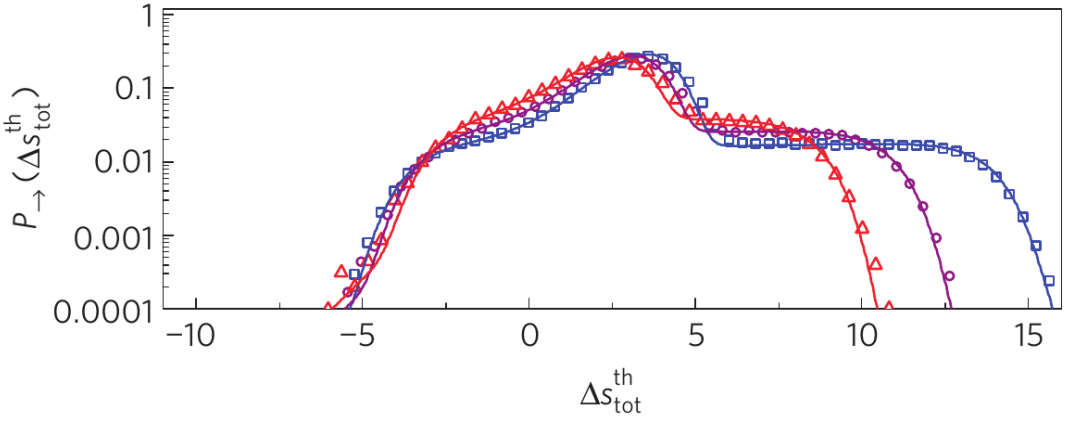

Figure 5.3.: Experimental result for the measurement of the distribution of the thermodynamic entropy production $P_{\rightarrow}(\Delta s_{\mathrm{tot}}^{\mathrm{th}})$, taken from [19] (Reprinted by permission from Macmillan Publishers Ltd: Nat. Phys. [19], copyright 2013). The different symbols indicate different temperatures of the sample while the measurement has been carried out.

5.2. Probability distribution of energy dissipated by the driven two-level system

After providing an introduction to the FRs in the previous Sec. 5.1, we focus on one particular physical situation in the following. We study the energy dissipation at the example of the well-known spin-boson model, considering a periodically driven TLS which is coupled to a bosonic heat bath.

The probability distribution function is calculated via the method of FCS which has been introduced in Ch. 4. In order to calculate the corresponding CF we will use the master equation approach for the reduced density operator of the system. The derived master equation is used to calculate the CF of the energy dissipated by the driven TLS. Furthermore, the TLS will be manipulated according to the measurement protocol which was presented in Ch. 2.3. Hence, the system will be pre- and post-selected in two distinct states $|i\rangle$ and $|f\rangle$. Consequently, the conditional probability distribution function (PDF) is determined as

$$\mathcal{P}_\tau(\epsilon, f|i) = \sum_n \sum_k \sum_{\sigma=-1,0,1} p_\tau^{k,n,\sigma}(f|i)\delta(\epsilon - n\omega - \sigma\Omega_k), \tag{5.26}$$

where ϵ is the dissipated energy.The time-dependent weights $p_\tau^{k,n,\sigma}(f|i)$ indicate the height of the peaks of the distribution function. The peak positions are quantized to multiples of the driving frequency ω plus the level splitting Ω_k in the rotating frame. The results presented in this section have been published in [82].

5.2.1. Counting field dependent master equation for the driven system

We derive a master equation in order to obtain the CF of the conditional PDF. The Floquet theory introduced in Ch. 2.2 will become helpful within this approach. The resulting master equation will be of Lindblad-form, i.e. we perform a full secular approximation.

The Hamiltonian of the complete system is given by

$$\hat{H}(t) = \hat{H}_S(t) + \hat{H}_B + \hat{H}_I, \tag{5.27}$$

where $\hat{H}_S(t) = \hat{H}_S(t+\tau_p)$ is the periodically driven Hamiltonian of the system with period $\tau_p = 2\pi/\omega$. The bath is described by an infinite set of harmonic oscillators. Accordingly, the Hamiltonian of the bath is given by $\hat{H}_B = \sum_\alpha \omega_\alpha b_\alpha^\dagger b_\alpha$, where $b_\alpha^\dagger$ and b_α are the bosonic creation and annihilation operators. The frequencies of the bath are given by ω_α. The system is coupled to the bath via $\hat{H}_I = \sum_\alpha A_\alpha B_\alpha$, where A_α, B_α are system and bath operators, respectively.

In the following we will focus on the situation, where the time-dependency of the free Hamiltonian of the system is removed by a transformation into the rotating frame. A generalization suitable to more complicated time periodic problems using the full-fledged Floquet approach is straightforward and can be found, for example, in [83].

Even though the free Hamiltonian of the system has become time-independent, in the general situation the system bath coupling may become time-dependent. Consequently, the Hamiltonian we have to consider reads

$$\tilde{H} = \tilde{H}_S + \tilde{H}_I(t) + \hat{H}_B, \tag{5.28}$$

where

$$\tilde{H}_S = R(t)\hat{H}_S(t)R^\dagger(t) + i\dot{R}(t)R^\dagger(t), \tag{5.29}$$

and

$$\tilde{H}_I(t) = \sum_\alpha R(t) A_\alpha R^\dagger(t) \otimes B_\alpha, \tag{5.30}$$

where $R(t)$ denotes the transformation into the rotating frame. Note that the Hamiltonian of the bath $\hat{H}_B$ remains invariant under the transformation $R(t)$. Furthermore, as we employ a FCS calculation, we have to incorporate the counting field into the problem. This is achieved by the two-point measurement approach introduced in Ch. 4.2.

In the following we present the derivation of the master equation with counting field dependency in full secular approximation. All the approximations which are used in this derivation have been described in detail in Ch. 3.2. The starting point of the derivation is a master equation structurally equivalent to Eq. (3.14) with an additional counting field dependency,

$$\begin{aligned}\frac{d}{dt}\rho(t) = \int_0^\infty ds \tilde{H}_I(\lambda,t)\rho(t)\tilde{H}_I(-\lambda,t-s) + \tilde{H}_I(\lambda,t-s)\rho(t)\tilde{H}_I(-\lambda,t) \\ - \tilde{H}_I(\lambda,t)\tilde{H}_I(\lambda,t-s)\rho(t) - \rho(t)\tilde{H}_I(-\lambda,t-s)\tilde{H}_I(-\lambda,t),\end{aligned} \tag{5.31}$$

where $\rho(t)$ is the full density matrix of the system and the bath and

$$\tilde{H}_I(\lambda,t) = \sum_\alpha \tilde{A}_\alpha(t) \otimes e^{i\hat{H}_B\lambda/2} B_\alpha e^{-i\hat{H}_B\lambda/2}, \tag{5.32}$$

is the time-dependent and counting-field-dependent system-bath interaction. We emphasize that the only term of the Hamiltonian, which is affected by the counting field, is the system-bath interaction $\tilde{H}_I(\lambda,t)$. Employing the Born and the Markov approximation $\rho(t) \approx \rho_S(t) \otimes \rho_B$ and assuming that the bath is in thermal equilibrium, we are able to trace out the bath degrees of freedom. As the counting field appears in terms of bath operators, we note that the arising bath correlation functions may contain a counting field dependence. We find two different types of correlation functions

$$\begin{aligned}\mathrm{Tr}_B\left[B_\beta(\lambda,t-s)\rho_B B_\alpha^\dagger(-\lambda,t)\right] &= \mathrm{Tr}_B\left[B_\beta\rho_B e^{iH_B(s-\lambda)}B_\alpha^\dagger e^{-iH_B(s-\lambda)}\right] \\ &= \langle B_\alpha^\dagger(s-\lambda)B_\beta(0)\rangle\ , \end{aligned} \tag{5.33}$$

$$\begin{aligned}\mathrm{Tr}_B\left[B_\beta(\lambda,t)\rho_B B_\alpha^\dagger(-\lambda,t-s)\right] &= \mathrm{Tr}_B\left[e^{iH_B(s+\lambda)}B_\beta e^{-iH_B(s+\lambda)}\rho_B B_\alpha^\dagger\right] \\ &= \langle B_\alpha^\dagger(0)B_\beta(s+\lambda)\rangle\ , \end{aligned} \tag{5.34}$$

containing information about the counting field. The counting field appears as a quasi time shift with respect to λ. We are able rewrite Eq. (5.31) as a master equation for the reduced density operator of the system $\rho_S(t)$

$$\begin{aligned}\frac{d}{dt}\rho_S(t) = \sum_{\alpha,\beta}\int_0^\infty ds\Big[&\langle B_\beta^\dagger(0)B_\alpha(s+\lambda)\rangle\ \tilde{A}_\alpha(t)\rho_S(t)\tilde{A}_\beta^\dagger(t-s) \\ &+ \langle B_\alpha^\dagger(s-\lambda)B_\beta(0)\rangle\ \tilde{A}_\beta(t-s)\rho_S(t)\tilde{A}_\alpha^\dagger(t) \\ &- \langle B_\alpha^\dagger(s)B_\beta(0)\rangle\ \tilde{A}_\alpha^\dagger(t)\tilde{A}_\beta(t-s)\rho_S(t) \\ &- \langle B_\beta^\dagger(0)B_\alpha(s)\rangle\ \rho_S(t)\tilde{A}_\beta^\dagger(t-s)A_\alpha(t)\Big].\end{aligned} \tag{5.35}$$

We note that by construction the counting field in the latter two bath correlation functions drops out.

Since the free Hamiltonian of the system in the rotating frame is time-independent, we are able to perform a spectral decomposition of the operators $\tilde{A}(t)$ with respect to $\tilde{H}_S$. Thus, we write

$$\tilde{A}(t) = \sum_{n,n'} |n\rangle\langle n|A(t)|n'\rangle\langle n'| = \sum_{n,n'} |n\rangle\langle n'|A^{nn'}(t), \tag{5.36}$$

$$\tilde{A}^\dagger(t) = \sum_{n,n'} \left(|n\rangle\langle n|A(t)|n'\rangle\langle n'|\right)^\dagger = \sum_{n,n'} |n'\rangle\langle n|A^{nn'}(t), \tag{5.37}$$

where $|n\rangle$ denote the systems eigenstates. Inserting the spectral decomposition into the master equation (5.35), we obtain

$$\begin{aligned}
\frac{d}{dt}\rho_S(t) =& \int_0^\infty ds \langle B_\alpha^\dagger(s-\lambda)B_\beta(0)\rangle e^{-i\omega_{nn'}(t-s)}|n\rangle\langle n'|A_\alpha^{nn'}(t-s)\rho_S(t)|m'\rangle\langle m|A_\beta{}^{m'm}(t)e^{i\omega_{mm'}t} \\
&+ \int_0^\infty ds \langle B_\alpha^\dagger(0)B_\beta(s+\lambda)\rangle e^{-i\omega_{mm'}t}|m\rangle\langle m'|A_\beta^{mm'}(t)\rho_S(t)|n'\rangle\langle n|A_\alpha{}^{n'n}(t-s)e^{i\omega_{nn'}(t-s)} \\
&- \int_0^\infty ds \langle B_\alpha^\dagger(s)B_\beta(0)\rangle e^{i\omega_{mm'}t}|m'\rangle\langle m|A_\alpha{}^{m'm}(t)|n\rangle\langle n'|\rho_S(t)A_\beta^{nn'}(t-s)e^{-i\omega_{nn'}(t-s)} \\
&- \int_0^\infty ds \langle B_\alpha^\dagger(0)B_\beta(s)\rangle \rho_S(t)e^{i\omega_{nn'}(t-s)}|n'\rangle\langle n|A_\alpha{}^{n'n}(t-s)A_\beta^{mm'}|m\rangle\langle m'|e^{-i\omega_{mm'}t} \ .
\end{aligned} \tag{5.38}$$

Here we introduced the energy differences $\omega_{nn'} = E_n - E_{n'}$ of the Hamiltonian of the system in the rotating frame. We further simplify the equation by applying the secular approximations, i.e., we neglect fast oscillating parts of the master equation oscillating with frequencies $\omega_{nn'} \neq \omega_{mm'}$. It is useful to perform a Fourier decomposition of the periodic matrix elements,

$$A_\alpha^{nn'}(t) = \sum_k e^{i\omega kt} A_\alpha^{nn'}(k), \tag{5.39}$$

$$A_\alpha^{nn'}(k) = \frac{1}{\tau_p}\int_0^{\tau_p} dt e^{-i\omega kt} A_\alpha^{nn'}(t), \tag{5.40}$$

where $A_\alpha^{nn'}(k)$ denote the Fourier coefficients. Using the Fourier representation, the full secular approximation is achieved by neglecting fast oscillating terms which oscillate with the driving frequency ω. This approximation is in agreement with the usual secular approximation in the regime $\omega > \omega_{nn'}$. We finally obtain

$$\begin{aligned}
\frac{d}{dt}\rho_S(t) =& -i[H_{LS}, \rho_S(t)] \\
&+ \sum_{\alpha,\beta}\sum_{n,n'}\sum_k \gamma_{\alpha\beta}(\omega_{nn'} - k\omega)\Big[e^{i\lambda(\omega_{nn'}-k\omega)}A_\beta^{nn'}(k)A_\alpha^{nn'*}(k)|n\rangle\langle n|\rho_S^{n'n'}(t) \\
&- \frac{1}{2}\left\{A_\alpha^{nn'*}(k)A_\beta^{nn'}(k)|n'\rangle\langle n'|, \rho_S(t)\right\}\Big],
\end{aligned} \tag{5.41}$$

where

$$\gamma_{\alpha\beta}(\omega_{nn'} - k\omega) = \int_{-\infty}^\infty ds e^{i(\omega_{nn'}-k\omega)s}\langle B_\alpha^\dagger(s)B_\beta(0)\rangle \tag{5.42}$$

are the transition rates and

$$H_{LS} = \sum_{\alpha,\beta}\sum_{nn'}\sum_k \Im\Gamma(\omega_{nn'} - k\omega)A_\alpha^{nn'*}(k)A_\beta^{nn'}(k)|n'\rangle\langle n'|, \tag{5.43}$$

denotes the Lamb shift like part of the Hamiltonian, which is independent of the counting field. In the limit of $\lambda \to 0$ the above master equation (5.41) reduces to a master equation in Lindblad form. Consequently, the master equation is applicable to systems where the previously discussed transformation into the rotating is possible.

5.2.2. Structure of the generating function

In the following we determine and evaluate the conditional CF of the conditional PDF. Before we do so we will discuss several properties of the conditional CF. The general structure is given by

$$\chi_\tau(\lambda, f|i) = \mathrm{Tr}\left[P_f e^{\mathcal{L}(\lambda)\tau}\rho_i(\lambda, 0)\right], \tag{5.44}$$

where $P_f = |f\rangle\langle f|$ is the projector onto the desired final state of the system responsible for the post-selection. The initial density operator is represented by $\rho_i(\lambda, 0)$. At first, a simple check in accordance with Eq. (4.30) yields

$$\chi_\tau(p, \lambda, f|i) = \chi_\tau(\lambda, f|i). \tag{5.45}$$

Thus, the characteristic function is connected to the conditional PDF via Fourier-transform, i.e.

$$\chi_\tau(\lambda, f|i) = \int d\epsilon e^{i\epsilon\lambda}\mathcal{P}_\tau(\lambda, f|i). \tag{5.46}$$

Another interesting property of the CF is generated by the secular approximation. Due to the secular approximation, the dynamics of the populations and the coherences of the system decouple. Consequently, the CF for the conditional PDF splits into a classical part $\chi_\tau^{cl}(\lambda, f|i)$ which solely depends on the dynamics of the populations and a quantum part $\delta\chi_\tau(\lambda, f|i)$ which is characterized by the dynamics of the coherences. This effect migrates to the conditional PDF. Hence, the PDF separates into a classical and a quantum part,

$$\begin{aligned}\mathcal{P}_\tau(\epsilon, f|i) &= \mathcal{P}_\tau^{cl}(\epsilon, f|i) + \delta\mathcal{P}_\tau(\epsilon, f|i) \\ &= \frac{1}{2\pi}\int d\lambda e^{-i\lambda\epsilon}\left(\chi_\tau^{cl}(\lambda, f|i) + \delta\chi_\tau(\lambda, f|i)\right).\end{aligned} \tag{5.47}$$

Although the secular approximation allows for a separate analysis of the classical and the quantum component of the conditional probabilities, we wish to emphasize that the quantum corrections only appear when the system was initially prepared in a superposition state. In other words, if no initial coherences are present, the quantum corrections to the CF $\delta\chi_\tau(\lambda, f|i)$ and to the PDF vanish.

5.2.3. Results for the driven two-level system

Having established the mathematical framework to derive the CF we will now apply the technique to the driven spin-boson model by using the example of the circularly polarized driving. We recall the full Hamiltonian

$$\hat{H}(t) = \hat{H}_{TLS}(t) + \hat{H}_I(\vartheta) + \hat{H}_B, \tag{5.48}$$

$$\hat{H}_{\mathrm{TLS}}(t) = -\frac{\omega_0}{2}\sigma_z + \frac{\Omega_R}{2}\left(\cos(\omega t)\sigma_x - \sin(\omega t)\sigma_y\right), \tag{5.49}$$

$$\hat{H}_I(\vartheta) = (\cos\vartheta\sigma_x + \sin\vartheta\sigma_z) \otimes B, \tag{5.50}$$

$$\hat{H}_B = \sum_\alpha \omega_\alpha b_\alpha^\dagger b_\alpha. \tag{5.51}$$

By transforming the system into the rotating frame (cf. Ch. 2.2.4), the free Hamiltonian of the system becomes time-independent. However, the system bath interaction will be affected by the rotation.

For convenience we present the master equation in Liouville space

$$\frac{d}{dt}\vec{\rho}(t) = \tilde{\mathcal{L}}(\lambda)\vec{\rho}(t)\ , \tag{5.52}$$

where the reduced density operator of the system is represented by a four component vector with

$$\vec{\rho}_S(t) = \begin{pmatrix} \rho_{gg}(t) \\ \rho_{ee}(t) \\ \rho_{eg}(t) \\ \rho_{ge}(t) \end{pmatrix}. \tag{5.53}$$

The super operator generating the dynamics of the reduced density operator is given by

$$\tilde{\mathcal{L}}(\lambda) = \begin{pmatrix} -\Gamma_{gg}(\lambda) & \Gamma_{ge}(\lambda) & 0 & 0 \\ \Gamma_{eg}(\lambda) & -\Gamma_{ee}(\lambda) & 0 & 0 \\ 0 & 0 & +i\Omega - \Gamma_{\varphi}(\lambda) & 0 \\ 0 & 0 & 0 & -i\Omega - \Gamma_{\varphi}(\lambda) \end{pmatrix}, \tag{5.54}$$

where $\Gamma_{ij}(\lambda)$ are the counting field dependent transition rates and $\Gamma_{\varphi}(\lambda)$ is the dephasing rate. Consequently, the CF is obtained as

$$\chi_\tau(\lambda, f|i) = \vec{f} e^{\tilde{\mathcal{L}}(\lambda)\tau} \vec{\rho}_S^{\,i}, \tag{5.55}$$

where $\vec{f}$ is the projector onto the final state, represented by a four component vector.

To perform the desired initial and final state selection, we use the measurement protocol introduced in Ch. 2.3. According to the protocol, the initial density operator as well as the final state projector are parametrized as

$$\vec{\rho}_S^{\,i} = \begin{pmatrix} \cos^2\frac{\theta_i}{2} \\ \sin^2\frac{\theta_i}{2} \\ \frac{\sin\theta_i}{2} \\ \frac{\sin\theta_i}{2} \end{pmatrix}, \qquad \vec{f} = \begin{pmatrix} \cos^2\frac{\theta_f}{2} \\ \sin^2\frac{\theta_f}{2} \\ \frac{\sin\theta_f}{2} \\ \frac{\sin\theta_f}{2} \end{pmatrix}, \tag{5.56}$$

such that the pre-selected initial state as well as the post-selected final state is the ground state of the system for $\theta_i = \theta_f = 0$.

In the following we investigate two different limits. At first we study the situation where the system in the laboratory frame is purely longitudinally coupled to the bath, referring to $\vartheta = \pi/2$. The second limit of study considers a purely transversal system-bath coupling with $\vartheta = 0$.

Longitudinal system bath coupling:

In the situation of $\vartheta = \pi/2$ the system-bath coupling acquires the form $\hat{H}_I(\pi/2) = \sigma_z \otimes B$. We find that the transformation into the rotating frame itself does not affect the system bath interaction, i.e. $\tilde{H}_I(\pi/2) = R_1(t)\hat{H}_I(\pi/2)R_1^\dagger(t) = \hat{H}_I(\pi/2)$. For clarification we use the Floquet picture introduced in Ch. 2 to clarify what the possible energy transfer between system and bath can be. We thus consider the driving exponents $e^{\pm i\omega t}$ as raising or lowering operators of energy quanta of ω absorbed or emitted by the bath. With $\hat{H}_I(\pi/2)$ being invariant with respect to the rotation $R_1(t)$, we immediately note that the energy exchange between system and bath of energy quanta of ω are not possible. Consequently, the only energy transfer between the system and the bath allowed by this coupling is restricted to energy dissipation of the level splitting Ω in the rotating frame.

This becomes apparent by the structure of the CF

$$\chi_\tau^z(\lambda, f|i) = \vec{f} e^{\tilde{\mathcal{L}}_z(\lambda)\tau} \vec{\rho}_S^{\,i}, \tag{5.57}$$

where

$$\tilde{\mathcal{L}}_z(\lambda) = \begin{pmatrix} -\sin^2\theta\gamma(-\Omega) & \sin^2\theta e^{i\Omega\lambda}\gamma(\Omega) & 0 & 0 \\ e^{-i\Omega\lambda}\sin^2\theta\gamma(-\Omega) & -\sin^2\theta\gamma(\Omega) & 0 & 0 \\ 0 & 0 & -i\Omega - 2\cos^2\theta\gamma(0) & 0 \\ 0 & 0 & 0 & i\Omega - 2\cos^2\theta\gamma(0) \end{pmatrix} \tag{5.58}$$

is the super operator yielding the dynamics of the TLS governed by a fully longitudinal coupling. Here $\gamma(\omega) = \int dt e^{i\omega t}\langle B^\dagger(t)B(0)\rangle$ are the Fourier transforms of the autocorrelation functions of th bath. The only counting field dependency is apparent within the rates that are responsible for changes of the respective system state.

The conditional PDF is calculated via Fourier transform yielding

$$\begin{aligned}\mathcal{P}_\tau^z(\epsilon, f|i) &= \int \frac{d\lambda}{2\pi} e^{-i\lambda\epsilon}\chi_\tau^z(\lambda, f|i) \\ &= \mathcal{P}_\tau^{z,c}(\epsilon, f|i) + \delta\mathcal{P}_\tau^z(\epsilon, f|i),\end{aligned} \tag{5.59}$$

where the classical part is given by

$$\mathcal{P}_\tau^{z,c}(\epsilon, f|i) = \delta(\epsilon)p_\tau^{z,0}(f|i) + \delta(\epsilon+\Omega)p_\tau^{z,-1}(f|i) + p_\tau^{z,1}(f|i)\delta(\epsilon-\Omega). \tag{5.60}$$

The corresponding weights are given by

$$\begin{aligned}p_\tau^{z,0}(f|i) = \frac{\sin^2\theta}{\Gamma_{\text{rel}}^z}\Bigg(&\gamma(\Omega)\left(\cos^2\frac{\theta_i}{2}\cos^2\frac{\theta_f}{2} + e^{-\Gamma_{\text{rel}}^z\tau}\sin^2\frac{\theta_i}{2}\sin^2\frac{\theta_f}{2}\right) \\ &+ \gamma(-\Omega)\left(e^{-\Gamma_{\text{rel}}^z\tau}\cos^2\frac{\theta_i}{2}\cos^2\frac{\theta_f}{2} + \sin^2\frac{\theta_i}{2}\sin^2\frac{\theta_f}{2}\right)\Bigg),\end{aligned} \tag{5.61}$$

$$p_\tau^{z,-1}(f|i) = \frac{\sin^2\theta\gamma(\Omega)}{\Gamma_{\text{rel}}^z}\cos^2\frac{\theta_f}{2}\sin^2\frac{\theta_i}{2}\left(1 - e^{-\Gamma_{\text{rel}}^z\tau}\right), \tag{5.62}$$

$$p_\tau^{z,1}(f|i) = \frac{\sin^2\theta\gamma(-\Omega)}{\Gamma_{\text{rel}}^z}\cos^2\frac{\theta_i}{2}\sin^2\frac{\theta_f}{2}\left(1 - e^{-\Gamma_{\text{rel}}^z\tau}\right), \tag{5.63}$$

$$\tag{5.64}$$

where $\Gamma_{\text{rel}}^z = \sin^2\theta(\gamma(\omega) + \gamma(-\omega))$. The quantum part yields a shift to the weight of the zero energy peak, i.e.

$$\delta\mathcal{P}_\tau^z(\epsilon, f|i) = \frac{1}{2}\sin\theta_i\sin\theta_f\cos\Omega\tau e^{-2\cos^2\theta\gamma(0)\tau}\delta(\epsilon), \tag{5.65}$$

which decays according to the dephasing rate $\Gamma_\varphi^z = 2\cos^2\theta\gamma(0)$.

The resulting conditional PDFs $\mathcal{P}_\tau^z(\epsilon, f|i)$ of energy emitted to the bath are shown in Fig. 5.4. Four different PDfs regarding different pre- and post-selected states are presented. A pre- or post-selection of the $|\downarrow\rangle$ state of the system corresponds to $\theta_i = \theta_f = 5\pi/4$, whereas the selection for the system being in the state $|\uparrow\rangle$ is achieved by $\theta_i = \theta_f = \pi/4$. As expected, there are three peaks visible in the picture. A central peak at $\epsilon = 0$ and two side peaks at $\epsilon = \pm\Omega$.

Transversal system bath coupling:

The situation of transversal system-bath coupling with $\vartheta = 0$ is more interesting. Since the transformation into the rotating frame does not commute with $\hat{H}_I$, we obtain a time dependency of the system bath interaction in the rotating frame yielding

$$\tilde{H}_I(t) = \left(e^{i\omega t}\sigma_+ + e^{-i\omega t}\sigma_-\right)\otimes B. \tag{5.66}$$

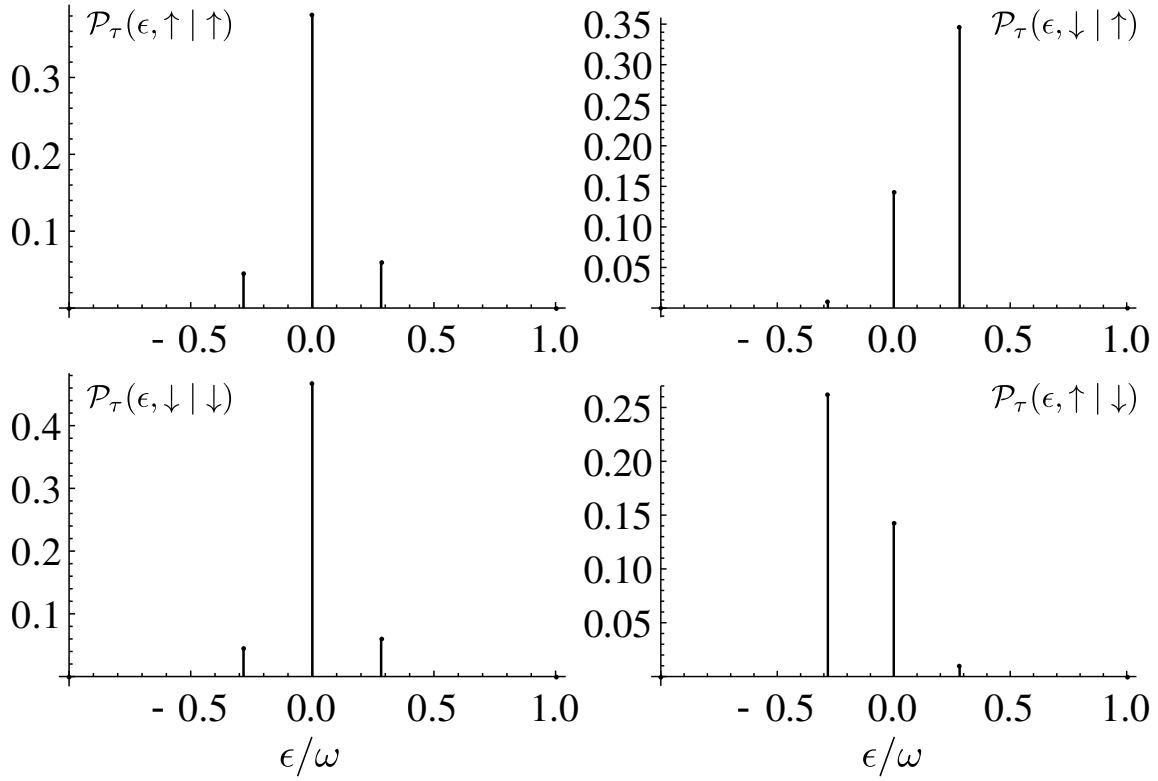

Figure 5.4.: Conditional probability densities $\mathcal{P}_\tau^z(\epsilon, f|i)$ of energy emitted to the bath. Here, $f(i)$ indicates the final (initial) state selection in the rotating frame. The energy ϵ is normalized to the driving frequency ω. The probability densities are plotted for coupling $\gamma_0 = 0.01$, temperature $\beta = 1/\omega$, detuning $\Delta = 0.2\omega$, Rabi-frequency $\Omega_R = 0.2\omega$ and a driving time $\omega\tau = 200$.

We immediately see that with the transversal system-bath couplingm the energy exchange of quanta of the driving frequency ω is possible between the system and the bath. To illustrate the possible transitions of the system with respect to energy transfer to the bath we use the Floquet picture as illustrated in Fig. 5.5. The available transitions depend on the current state of the system. For example, the system could be in the ground state $|g\rangle$ of the rotating frame. Consequently, the system can either make transitions with frequency $\pm\omega$ to neighboring Floquet mode ground states $|g\rangle$ or to neighboring Floquet mode excited states $|e\rangle$, corresponding to transition frequencies $\pm\omega - \Omega$. Transitions with frequencies $\pm\omega + \Omega$ are blocked as there are no final states available. In the opposite scenario, where the system is in the excited state $|e\rangle$ of a particular Floquet mode, it can either change to an excited state of a neighboring Floquet mode by exchanging $\pm\omega$ quanta of energy to the bath or it ends up in a neighboring ground state corresponding to an energy exchange of $\pm\omega + \Omega$ with the bath. Due to the lack of an available final state, the transitions with frequencies $\pm\omega - \Omega$ are blocked. Thus, the conditional PDF depends on the initial state of the system.

In the same manner as for the longitudinal coupling, we obtain the PDF via Fourier transform of the characteristic function $\chi_\tau^x(\lambda, f|i)$ given by Eq. (5.55). With the separation into the classical part, depending only on the dynamics of the populations of the reduced density operator, and the respective quantum part, only depending on the dynamics of

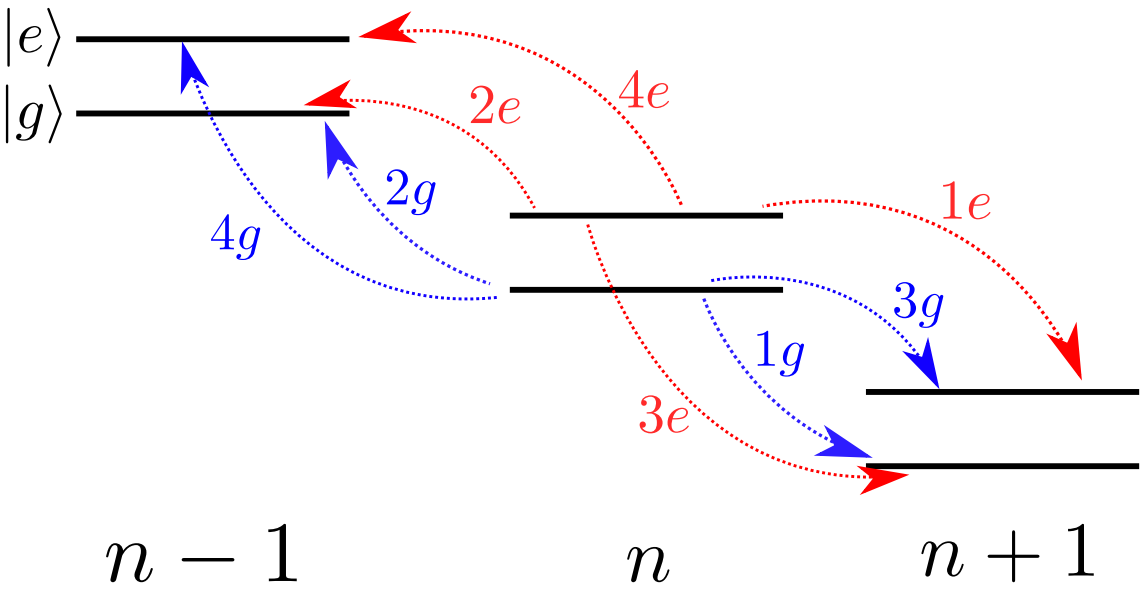

Figure 5.5.: Floquet-picture of the two level system in the energy-eigenbasis in the case of transversal coupling. The index n depicts the n-th Floquet-mode of the system, which is energetically shifted to the system by the Frequency $n\,\omega$. There are 8 possible transitions. If the system was in the ground state $|g\rangle$ of the rotated frame, then only (blue) transitions with energy exchange of $\pm\omega$ $(1g, 2g)$ or $\pm\omega - \Omega$ $(3g, 4g)$ are possible. If the system has been in it's excited state $|e\rangle$, only the (red) transitions $(1e - 4e)$ are possible.

the coherences, we find

$$\chi_\tau^{x,cl}(\lambda, f|i) = \frac{e^{-\frac{\tau}{2}(\Gamma_{gg}(\lambda)+\Gamma_{ee}(\lambda)-2\Lambda(\lambda))}}{2\Lambda(\lambda)} \times \\ \times \left(\frac{A(\lambda,\theta_f,\theta_i) + B(\lambda,\theta_f,\theta_i)}{4} - \frac{A(\lambda,\theta_f,\theta_i) - B(\lambda,\theta_f,\theta_i)}{4} e^{-2\Lambda(\lambda)\tau} \right), \quad (5.67)$$

$$\delta\chi_\tau^{x}(\lambda, f|i) = \frac{1}{2}\cos(\Omega\tau)\,\sin\theta_i \sin\theta_f e^{-\Gamma_\varphi(\lambda)\tau}, \quad (5.68)$$

where

$$A(\lambda,\theta_f,\theta_i) = (\cos\theta_i + \cos\theta_f)\,(\Gamma_{ge}(0) - \Gamma_{eg}(0)) \\ - (\cos\theta_f - 1)(\cos\theta_i + 1)\Gamma_{eg}(\lambda) - (\cos\theta_f + 1)(\cos\theta_i - 1)\Gamma_{ge}(\lambda) \quad (5.69)$$

$$B(\lambda,\theta_f,\theta_i) = 2\Lambda(\lambda)(1 + \cos\theta_f\cos\theta_i) \quad (5.70)$$

$$\Lambda(\lambda) = \frac{1}{2}\sqrt{4\Gamma_{eg}(\lambda)\Gamma_{ge}(\lambda) + (\Gamma_{ee}(\lambda) - \Gamma_{gg}(\lambda))^2} \quad (5.71)$$

The matrix elements for the time evolution of the reduced density operator of the system are computed as

$$\Gamma_{gg}(\lambda) = \Gamma_{eg}(\lambda = 0) - \gamma^-(\omega, \lambda)\ , \quad (5.72)$$

$$\Gamma_{ge}(\lambda) = \cos^4\frac{\theta}{2}\gamma(\Omega + \omega)e^{i\lambda(\Omega+\omega)} + \sin^4\frac{\theta}{2}\gamma(\Omega - \omega)e^{i\lambda(\Omega-\omega)}\ , \quad (5.73)$$

$$\Gamma_{eg}(\lambda) = \cos^4\frac{\theta}{2}\gamma(-\Omega - \omega)e^{i\lambda(-\Omega-\omega)} + \sin^4\frac{\theta}{2}\gamma(-\Omega + \omega)e^{i\lambda(-\Omega+\omega)}\ , \quad (5.74)$$

$$\Gamma_{ee}(\lambda) = \Gamma_{ge}(\lambda = 0) - \gamma^-(\omega, \lambda)\ , \quad (5.75)$$

which reflect the energetically possible transitions based on their counting field dependency. The dephasing rate is obtained as

$$\Gamma_\varphi(\lambda) = \gamma^+(\omega,\lambda) + \frac{1}{2}\left(\Gamma_{eg}(0) + \Gamma_{ge}(0)\right). \tag{5.76}$$

In all the rates ((5.72) - (5.76)) we have obtained contributions

$$\gamma^\pm(\omega,\lambda) = \frac{\sin^2\theta}{4}\left(\gamma(\omega)\left(e^{i\lambda\omega}\pm 1\right) + \gamma(-\omega)\left(e^{-i\lambda\omega}\pm 1\right)\right), \tag{5.77}$$

which originate from processes where only the Floquet index is changed and the state of the system remains unchanged. Consequently, those contributions provide an energy exchange of quanta $\pm\omega$ with the bath and are belonging to the transitions $1g, 2g, 1e$ and $4e$ in Fig. 5.5.

The conditional PDFs $\mathcal{P}_\tau^x(\epsilon, f|i)$ are depicted in Fig. 5.6 for four different choices of pre- and post-selected system states. We chose two different pre- and post-selected states of the system, i.e. the $|\uparrow\rangle$ state corresponding to a choice of $\theta_i = \theta_f = \pi/4$ the $|\downarrow\rangle$ state, which is achieved by choosing $\theta_i = \theta_f = 5\pi/4$. The conditional PDFs have been obtained by numerical Fourier transform of Eq. (5.55). We find that the PDF consists of peaks positioned at $n\omega + \sigma\Omega$ with $\sigma = 0, +, -$ and n being integer. As discussed above, the conditional PDFs contain considerable quantum contributions (see Fig. 5.6), most pronounced in Fig. 5.6 (d), which we calculate analytically. Interestingly, these corrections appear only for $\epsilon = n\omega$ and thus only for the central peaks. Via Fourier transform of Eq. (5.68) we obtain

$$\delta\mathcal{P}_\tau^x(\epsilon, f|i) = \frac{1}{2}\sin\theta_i \sin\theta_f \cos(\Omega\tau)\, e^{-\tau\Gamma_\varphi^0} \times \sum_n \delta(\epsilon - n\omega)\left(\frac{i\gamma(\omega)^{1/2}}{\gamma(-\omega)^{1/2}}\right)^n J_n\left[i\eta\tau\right], \tag{5.78}$$

where $J_n[i\eta\tau]$ is the Bessel function of the first kind. The factor in the argument has been abbreviated for legibility reading $\eta = \sin^2\theta(\gamma(\omega)\gamma(-\omega)^{1/2})/2$. A detailed calculation of the dephasing rate is found in the Appendix B. The dephasing rate is given by

$$\Gamma_\varphi^0 \equiv (\Gamma_{eg}(0) + \Gamma_{ge}(0))/2 + \gamma^+(\omega, 0)/2, \tag{5.79}$$

which characterizes the decay of the quantum contribution to the conditional PDF. Consequently, the quantum contribution decays over time, oscillating with the frequency of the level splitting. We observe that the quantum corrections to the PDF are maximized for a selection of $\theta_i = \theta_f = \pi/2, 3\pi/2$, corresponding to a state selection of maximal coherence of the eigenstates of the rotating frame Hamiltonian of the system. As expected, in the situation of the system being prepared or post-selected in an eigenstate of the Hamiltonian of the system in the rotating frame, the quantum correction vanishes. The quantum corrections to several probability weights are depicted in Fig. 5.7 as a function of the driving time. For convenience they are calculated for $\theta_i = \theta_f = \pi/4$. The dotted vertical line is used to indicate the time $\omega\tau = 200$ at which the PDFs in Fig. 5.6 where calculated.

On a technical level we are able to explain why only the central peaks corresponding to integer values of ϵ/ω are affected by the quantum corrections. The quantum corrections arise from the coherences and hence are assigned to the dephasing rate Eq. (5.76). The two parts are given by Eq. (5.77) and $\frac{1}{2}(\Gamma_{eg}(0) + \Gamma_{ge}(0))$. The first part yields only transitions between different Floquet modes without changing the state of the system with an associated energy transfer of $\pm\omega$. The second part consists of the two diagonal components of the matrix of rates which are, by construction, independent of the counting field λ. Consequently, they do not contribute to the distribution function of dissipated energy.

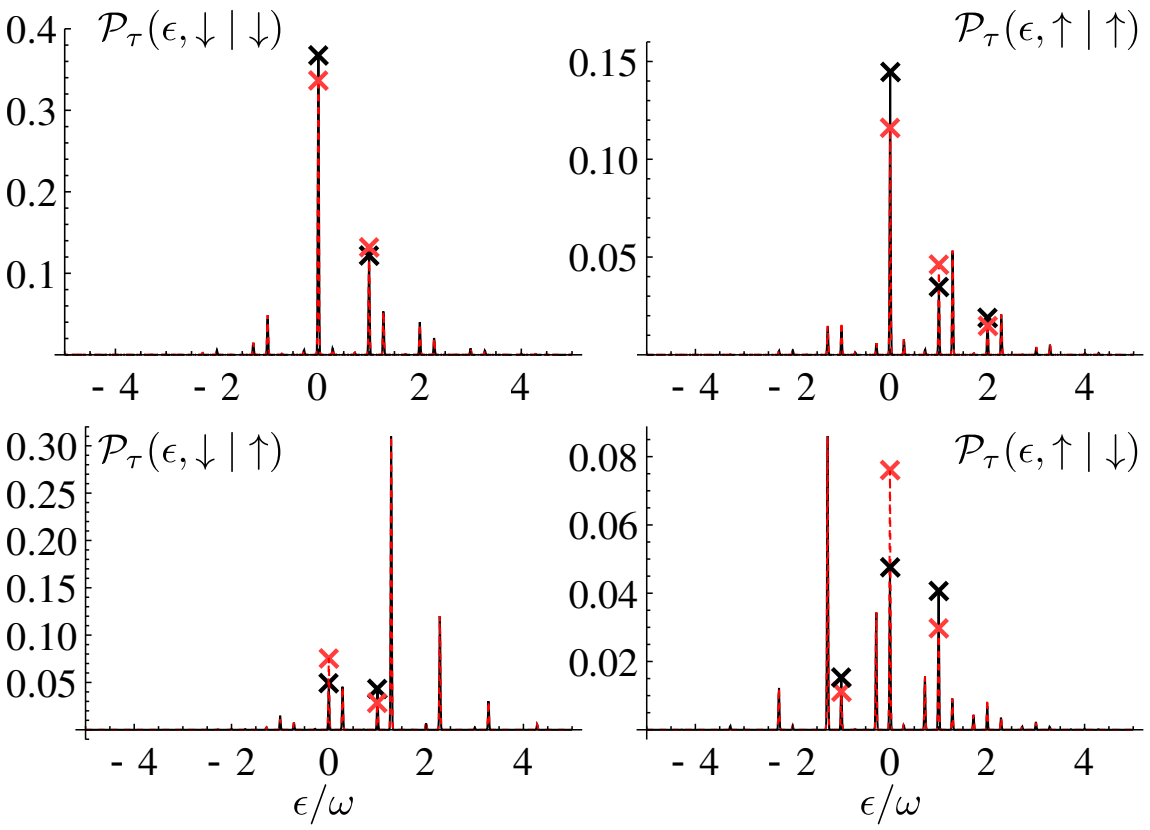

Figure 5.6.: Conditional probability densities $\mathcal{P}_\tau(\epsilon, f|i)$ as a function of normalized energy ϵ/ω. The distances between the peaks are given by the driving frequency ω or the level splitting Ω. The parameters are the same as in Fig. 5.4. The distinct choice of initial and final state drastically changes the structure of the probability densities. The markers denote the difference between the PDF with (black solid) and without (red dashed) quantum corrections $\delta\mathcal{P}_\tau(\epsilon, f|i)$ at peak positions with integer values of ϵ/ω.

In the context of the aforementioned FRs, we can successfully check that our generating function obeys

$$\chi_\tau(\lambda, f|i) = \chi_\tau(-\lambda + i\beta, i|f), \tag{5.80}$$

which is in agreement with Eq. (5.24). Hence, the detailed FR

$$\frac{\mathcal{P}_\tau(\epsilon, f|i)}{\mathcal{P}_\tau(-\epsilon, i|f)} = e^{\epsilon\beta} \tag{5.81}$$

is satisfied. Note that in a general situation, the PDF $\mathcal{P}_\tau$ should be related to the time-reversed PDF $\mathcal{P}_{\tau,B}$, where not only the state but, in addition, the driving protocol is time-reversed. In our case the driving protocol only contributes a phase shift, which is immaterial within the RWA.

5.3. Conclusion

After providing an introduction to the general topic of the FRs and discussing the current experimental situation, we presented our results on the energy dissipation of the driven TLS.

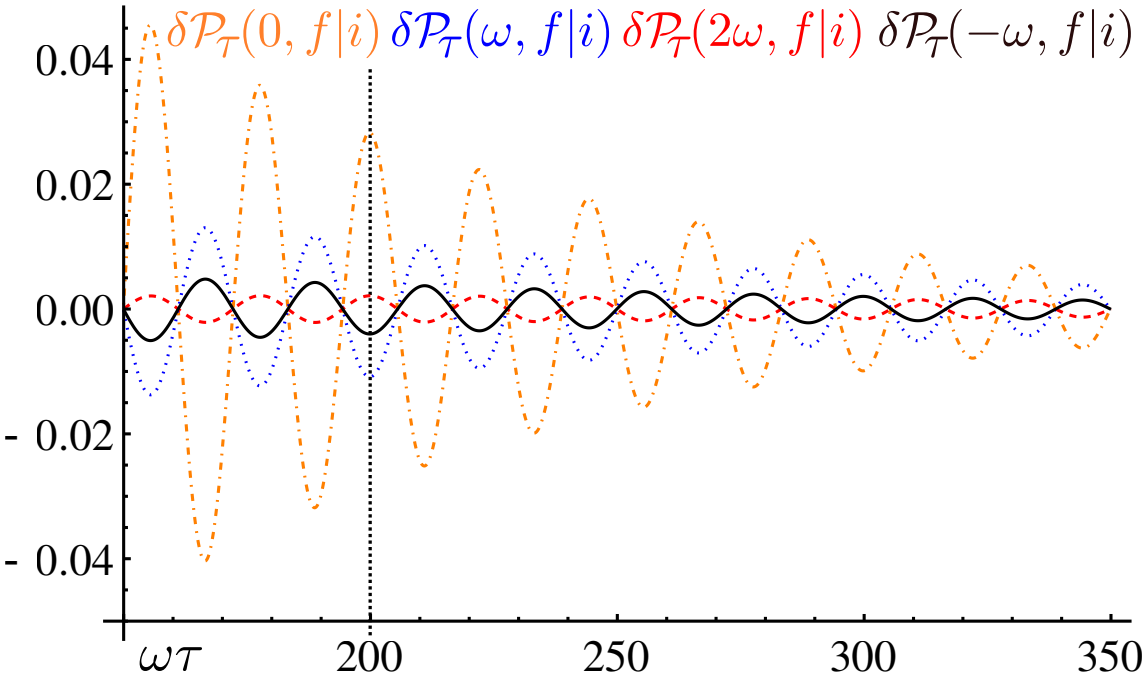

Figure 5.7.: Quantum correction $\delta\mathcal{P}_\tau(\epsilon, f|i)$ for $\theta_f = \theta_i = \pi/4$ as a function of time for different values of $\epsilon = 0$ (orange, dashed dotted), $\epsilon = \omega$ (blue, dotted), $\epsilon = 2\omega$ (red, dashed) and $\epsilon = -\omega$ (black). The intersection at $\tau = 200/\omega$ denotes the time, where the conditional probabilities of Fig. 5.6 have been calculated.

We calculated the conditional PDFs of the dissipated energy for certain pre- and post-selected system states. The obtained conditional PDFs fulfilled the quantum version of the detailed fluctuation relation.

We discussed two different system-bath couping scenarios. In the situation of pure longitudinal coupling it turned out that the energy pumped into the system by the external driving cannot be dissipated to the surrounding heat bath. Instead, only relaxation processes with energy dissipation of quanta of the energy splitting of the TLS $\pm\Omega$ were visible in the conditional PDF.

In the situation of transversal system-bath coupling, the situation became more interesting. The coupling allowed for energy exchange of quanta of the driving frequency ω between the system and the bath. The energy exchanged between the system and the bath turned out to be quantized to multiples of the driving frequency ω shifted by $\pm\Omega$, the level splitting of the TLS in the rotating frame. Consequently, the structure of the PDF resulted in peaks positioned at integer values of ω with side peaks appearing at $\pm\Omega$ next to them.

The main result were relatively large quantum corrections to the conditional probabilities due to the coherences of the density operator of the system. The quantum corrections turned out to solely influence the weights to the central peaks, i.e. the peaks of $n\omega$ with integer n. Furthermore, the quantum corrections were found to decay with respect to the dephasing rate Γ_φ^0. An observation of the quantum corrections would constitute a first test of the FRs in the quantum regime, explicitly taking into account quantum effects.

6. The conditional cumulants of dissipated energy

The previous chapter was devoted to the analysis of the conditional probability distributions of the dissipated energy. In this chapter we present a detailed analysis of the first two conditional cumulants, i.e. the conditional average and the conditional noise. The cumulants are computed using the FCS technique. Our analysis focuses on how the external manipulation of the TLS influences the energy dissipation as well as the noise of dissipated energy. Consequently, the analysis contains the effect of pre- and post-selection of the states of the TLS. Additionally, we consider and analyze two different situations, where the TLS is either driven in resonance or off resonance. We focus on the situation of transversal system bath coupling $\hat{H}_I(\vartheta = 0) = \sigma_x B$. Although quantum features are visible in our results, the most pronounced features are explained by a classical analysis. The results presented in this chapter have partially been published by the author in [60].

6.1. Numerical analysis of the cumulants

To obtain an overall picture, as to how the energy dissipation is influenced either by the choice of pre- and post-selection of system states or the type of the drive, we first perform a numerical analysis. Hence, we first investigate the qualitative picture of the conditional average and the conditional noise.

6.1.1. Analysis of the conditional average

We start our investigations with the analysis of the conditional average of dissipated energy

$$\begin{aligned} \langle \epsilon_\tau \rangle_{i\to f} &\equiv \int d\epsilon\, \epsilon \tilde{\mathcal{P}}_\tau(\epsilon, f|i) \\ &= \partial_{i\lambda} \ln \chi_\tau(\lambda, f|i)|_{\lambda=0}\,, \end{aligned} \tag{6.1}$$

where

$$\tilde{\mathcal{P}}_\tau(\epsilon, f|i) = \frac{\mathcal{P}_\tau(\epsilon, f|i)}{\int d\epsilon\, \mathcal{P}_\tau(\epsilon, f|i)}\,, \tag{6.2}$$

$$= \frac{\mathcal{P}_\tau(\epsilon, f|i)}{\mathcal{P}_\tau(f|i)}. \tag{6.3}$$

In the second line of Eq. (6.1) we used the fact that the conditional average is connected to the CF by the derivative with respect to the counting field λ. As discussed in the previous Ch. 5, the FR demands a lower bound on the conditional average. Indeed, utilizing Jensen's inequality on the conditional probabilty densities yields

$$\int d\epsilon\, \tilde{\mathcal{P}}_\tau(\epsilon, f|i) e^{-\beta\epsilon} \geq \exp\left[-\beta \int d\epsilon\, \epsilon \tilde{\mathcal{P}}_\tau(\epsilon, f|i)\right]. \tag{6.4}$$

Using Eqs. (6.1) and (6.4) one obtains

$$\begin{aligned}\langle\epsilon\rangle_{i\to f} = -\beta \frac{\int d\epsilon\, \epsilon\, \mathcal{P}_\tau(\epsilon, f|i)}{\mathcal{P}_\tau(f|i)} &\leq \ln\left(\frac{\int d\epsilon\, \mathcal{P}_\tau(\epsilon, f|i) e^{-\beta\epsilon}}{\int d\epsilon\, \mathcal{P}_\tau(\epsilon, f|i)}\right) \\ &= \ln\left(\frac{\int d\epsilon\, \mathcal{P}_{\tau,B}(-\epsilon, i|f)}{\int d\epsilon\, \mathcal{P}_\tau(\epsilon, f|i)}\right),\end{aligned} \tag{6.5}$$

which results in

$$\langle\epsilon\rangle_{i\to f} \geq \frac{1}{\beta} \ln\left(\frac{\mathcal{P}_\tau(f|i)}{\mathcal{P}_{\tau_B}(i|f)}\right). \tag{6.6}$$

Eq. (6.6) can be undestood as the second law of thermodynamics for the pre- and post-selected ensemble. Interestingly, the lower bound for the conditional average of dissipated energy can in general be negative, depending on the selection of initial and final states of the system.

In Fig. 6.1 the conditional average $\langle\epsilon\rangle_{i\to f}$ is depicted as a function of the two pre- and post-selective measurement angles θ_i and θ_f for a finite driving time $\omega\tau = 30 \times 2\pi$ and finite temperature $T = \omega$. The driving time is chosen to be of the order of the characteristic relaxation times $\Gamma_{\text{rel}}^{-1}, \Gamma_\varphi^{-1}$ of the spin. At such time scales the effect of the pre- and post-selection is prevailing. The longer the driving lasts, the more the statistics of the conditional average will be characterized by the properties of the stationary state, irrespective of the systems initial state preparation.

Furthermore, in Fig. 6.1 a comparison of two different driving scenarios is shown: Panel (a) shows the situation of finite detuning $\Delta = 0.2\omega$, whereas panel (b) depicts the resonantly driven scenario ($\Delta = 0$). We immediately notice that the detuning has a pronounced impact on the amount of energy being dissipated. Furthermore, the conditional average of the energy dissipated by the detuned driven TLS exhibits regions where it is negative. The corresponding selection angles are in the in the vicinity of $\theta_i = 0, \theta_f = \pi$, which correspond to a pre-selection of the system in its ground state $|g\rangle$ and a post-selection in the systems excited state $|e\rangle$.

In both driving schemes we note that the largest value of dissipated energy lies at $\theta_i = \pi$ and $\theta_f = 0$, which corresponds to a preparation in the excited state and a final state selection in the ground state of the rotating frame. Interestingly, for this choice of driving time and temperature, the absolute value of $\langle\epsilon\rangle_{e\to g}$ turns out to be larger at finite detuning as compared to the case of resonant driving.

A deeper understanding of the results depicted in Fig. 6.1 may be achieved by considering special pairs of pre- and post-selected system states which we will study in the following. We start our analysis by a choice of θ_i and θ_f, either being 0 or π, which corresponds to a pre- and post-selection of the systems eigenstates in the rotating frame. As discussed in the previous Ch. 5.2.2, with this choice of states coherences are neither initially present, nor are they ever generated. By that means we do not expect any coherent oscillations to appear and the result is completely determined by the classical part of the CF.

We start with the conditional average $\langle \epsilon_\tau \rangle_{g\to e}$ (corresponding $\theta_i = 0$ and $\theta_f = \pi$) and its respective lower bound, cf. Eq. (6.6) depicted in Fig. 6.2 (a) as a function of the normalized temperature T/ω for a fixed driving time $\omega\tau = 30 \times 2\pi$. We observe a sign change of the dissipated energy at a transition temperature which we denote by T_0. Above the transition temperature the bath is more likely to provide the energy required for the transition to the energetically unfavorable state. Below T_0 the bath is not capable of exciting the system. Consequently, the system solely receives its energy from the driving source which is partly dissipated to the bath, yielding a positive value for the dissipated energy. The aforementioned transition temperature T_0 referring to this particular pre- and post-selection scenario is depicted in Fig. 6.2 as a function of the driving time. The transition temperature tends to diverge the longer the drive lasts. Indeed, the longer the drive lasts, the more energy has been pumped into the system by the driving source. Consequently, after enough energy has been pumped into the system the average dissipated energy will become positive irrespective of the magnitude of the temperature of the bath.

We further show the conditional average and the corresponding lower bounds in Fig. 6.2 (c) for two different pairs of pre- and post-selected system states. Referring to the energetically unfavorable process $|g\rangle \to |e\rangle$, the average dissipated energy is negative and increasing with the driving time. Finally we depict the conditional average for the $|e\rangle \to |e\rangle$ process in Fig. 6.2 (d) for different temperatures. With increasing temperature the the amount of dissipated energy decreases. Indeed, the bath is more likely to transfer energy to the system than to receive energy from the system as temperature increases.

In a next step we analyze pairs of pre- and post-selected system states corresponding to the spin states in the rotating frame, i.e. the state $|\uparrow\rangle$ and $|\downarrow\rangle$ (along the $\hat{z}$-axis in the rotating frame). For finite detuning $\Delta = \Omega_R = 0.2\omega$ the angle between the ground state and the $\hat{z}$-axis is given by $\theta = \pi/4$. Consequently a pre selected state $|\uparrow\rangle$ corresponds to $\theta_i = \pi/4$, whereas a pre-selection of the $|\downarrow\rangle$ state is achieved by a rotation angle $\theta_i = 5\pi/4$. The same holds true for the selection angle θ_f regarding the post-selected systems state. In

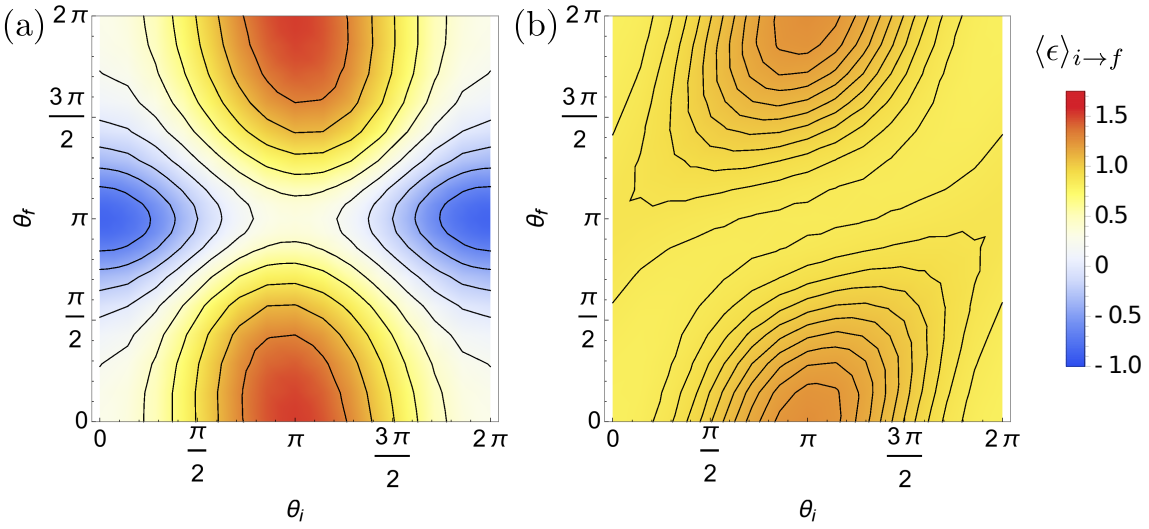

Figure 6.1.: The conditional average $\langle \epsilon \rangle_{i\to f}$ depicted at finite temperature $T = \omega$ and finite driving time $\omega\tau = 30 \times 2\pi$. In panel (a) we have a finite detuning $\Delta = 0.2\omega$. Panel (b) corresponds to the case of resonant driving with $\Delta = 0$. The dimensionless coupling strength between system and bath is set to $\gamma_0 = 0.01$. The Rabi-frequency is set to $\Omega_R = 0.2\omega$. Lines of equal energy have been included for clarity.

Fig. 6.3 we show results similar to those of Fig. 6.2, however with respect to the selection to the spin states. Since the pre- and post-selected states are no longer eigenstates of the Hamiltonian in the rotating frame, in addition to the above discussed features the results undergo coherent oscillations which decay with respect to the relaxation and dephasing processes. However, the qualitative characteristics of the results remain unchanged despite the coherent oscillations.

Regarding to Fig 6.3 (d) in particular, we observe that the amplitude of the oscillations decreases with increasing temperatures. In conclusion, most of the observed features seem to be explainable by the classical part of the CF. We will provide an analysis of the corresponding contribution $\chi_\tau^{cl}(\lambda, f|i)$ in the subsequent Sec. 6.2.

6.1.2. Analysis of the conditional noise

After having provided a qualitative analysis of the conditional average in the previous section we will now turn our attention to the second cumulant, the conditional noise, with

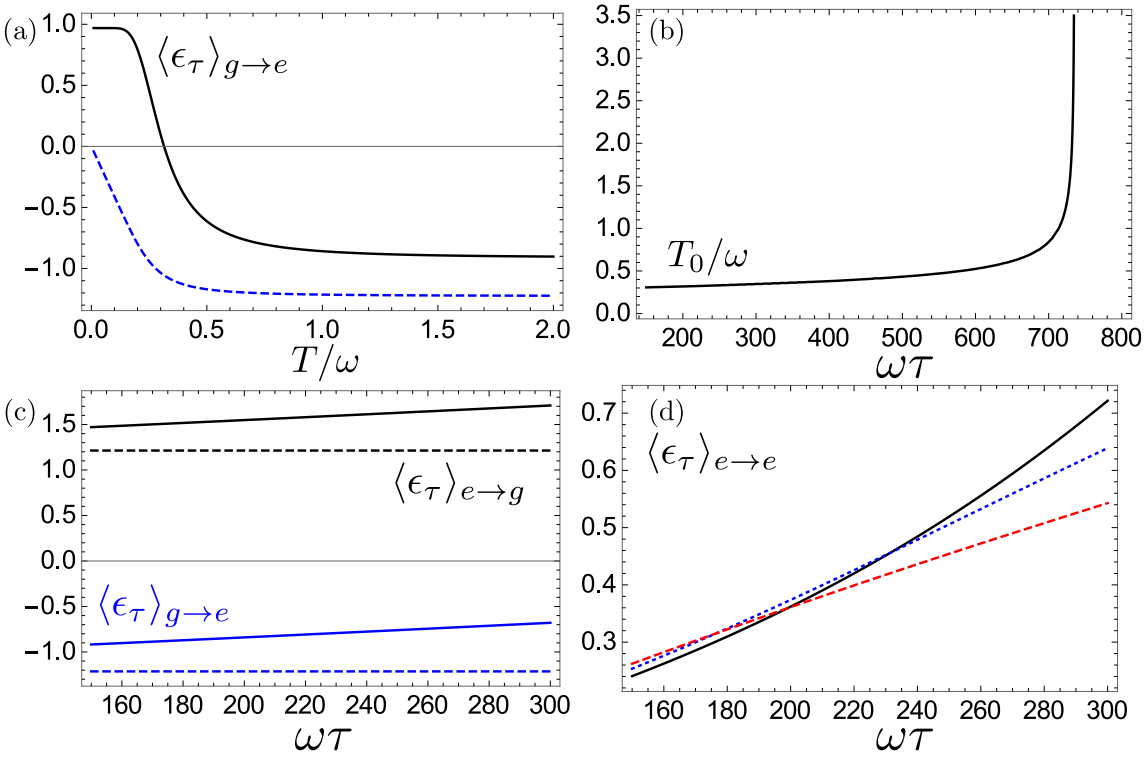

Figure 6.2.: Conditional average of the energy dissipated to the bath for various choices of the pre- and post-selected states. In all panels $\Delta = \Omega_R = 0.2\omega$. In panel (a) the conditional average $\langle\epsilon_\tau\rangle_{g\to e}$ (black) and its lower bound (blue, dashed) is shown as a function of the temperature T (driving time $\omega\tau = 30 \times 2\pi$). Panel (b) shows the transition temperature T_0/ω for the same pre and post selection as a function of the driving time $\omega\tau$. In panel (c) and (d) we show the behavior of the conditional average as a function of the driving time. Panel (c) shows the conditional average $\langle\epsilon_\tau\rangle_{e\to g}$ (black) and the corresponding lower bound (black, dashed) as well as the the conditional average $\langle\epsilon_\tau\rangle_{g\to e}$ (blue) and the lower bound (blue, dashed), respectively. In panel (d) we show the dependence of the conditional average $\langle\epsilon_\tau\rangle_{e\to e}$ on the driving time for three different temperatures: $T = 0.01\omega$ (black), $T = 0.5\omega$ (blue,dotted) and $T = \omega$ (red, dashed).

respect to the impact of the pre- and post selection

$$\begin{aligned}\langle \Delta\epsilon_\tau^2\rangle_{i\to f} &\equiv \langle \epsilon_\tau^2\rangle_{i\to f} - \langle \epsilon_\tau\rangle_{i\to f}^2 \\ &= -\partial_\lambda^2 \ln(\chi_\tau(\lambda, f|i))|_{\lambda=0}\,. \end{aligned} \tag{6.7}$$

In a similar manner as in the previous section, we show the results for the conditional noise after a driving time of $\omega\tau = 30\times 2\pi$ in Fig. 6.4. We show the situation for finite detuning $\Delta = 0.2\omega$ in Fig. 6.4 (a), whereas in Fig. 6.4 (b) we show the resonant case, $\Delta = 0$. As one would expect, the magnitude of the noise is generally enhanced for a resonant drive. Furthermore, the variance reaches a maximum in the situation of the $|e\rangle \to |g\rangle$ pre- and post-selection scenario. In the situation of finite detuning $\Delta = 0.2\omega$, the exact same choice of pre- and post-selected system states yields a suppressed noise. We will discuss this in more detail in the subsequent section.

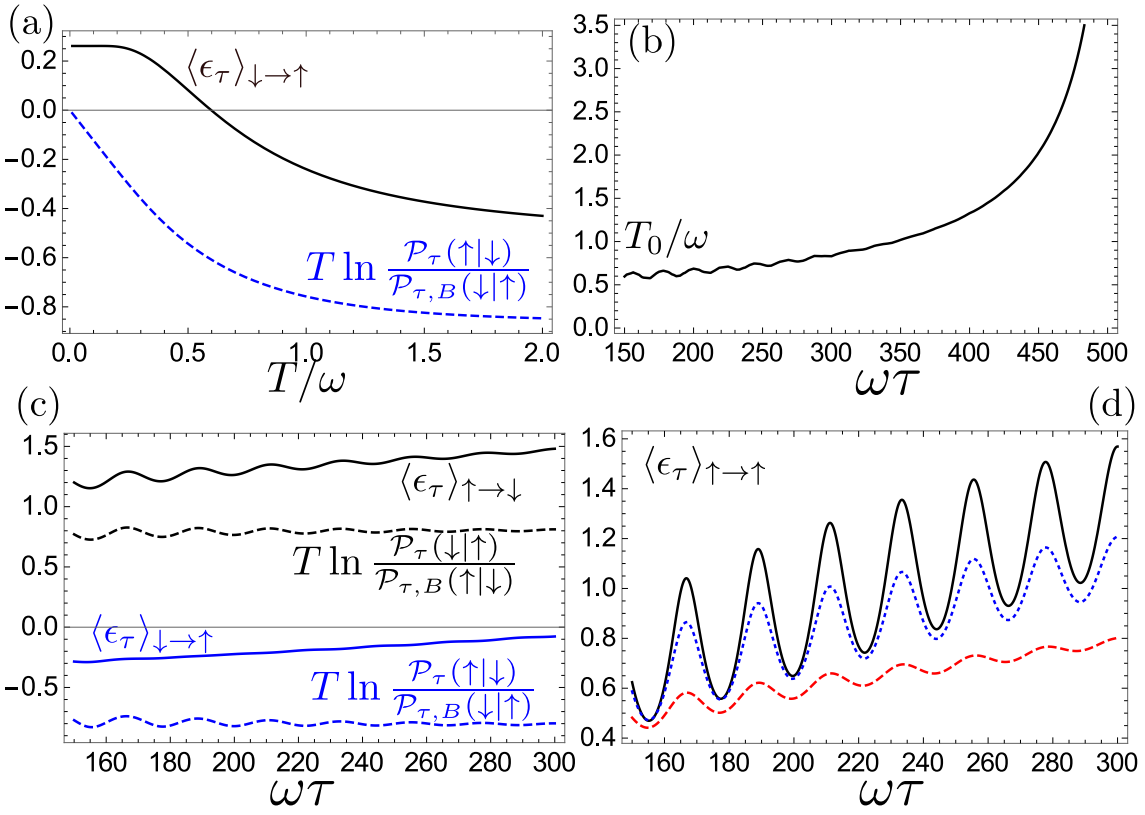

Figure 6.3.: Conditional average of the energy dissipated to the bath for various choices of the pre- and post-selected states. In all panels $\Delta = \Omega_R = 0.2\omega$. In panel (a) the conditional average $\langle\epsilon_\tau\rangle_{\downarrow\to\uparrow}$ (black) and its lower bound (blue, dashed) (both measured in units of the driving frequency ω) is shown as a function of temperature T (driving time $\omega\tau = 30\times 2\pi$). Panel (b) shows the transition temperature normalized to the driving frequency T_0/ω as a function of the driving time $\omega\tau$. The transition temperature is plotted for the conditional average $\langle\epsilon_\tau\rangle_{\downarrow\to\uparrow}$. Panels (c) and (d) depict the time dependence of the conditional average. In panel (c) we show the conditional averages and the corresponding lower bounds for different pre- and post-selected states, i.e. $\langle\epsilon_\tau\rangle_{\downarrow\to\uparrow}$ (blue, bottom) and its lower bound (blue, dashed, bottom) as well as $\langle\epsilon_\tau\rangle_{\uparrow\to\downarrow}$ (black, top) and its lower bound (black, dashed, top). Finally panel (d) depicts $\langle\epsilon_\tau\rangle_{\uparrow\to\uparrow}$ as a function of $\omega\tau$ for different temperatures $T = 0.01\omega$ (black), $T = 0.5\omega$ (blue, dotted) and $T = \omega$ (red, dashed).

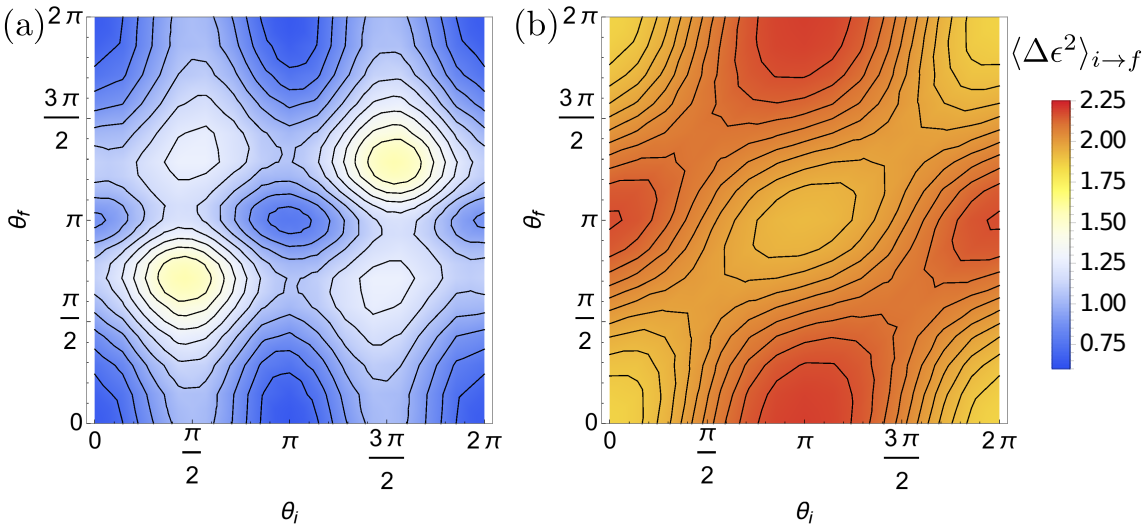

Figure 6.4.: Conditional variance as a function of the initial and final states characterized by the angles θ_i and θ_f. The conditional variances are plotted at the time $\omega\tau = 30 \times 2\pi$ and temperature $T = \omega$. In Panel (a) we consider a finite detuning $\Delta = 0.2\omega$. Panel (b) shows the case of resonant driving. Lines indicating equal noise amplitude have been included for clarity.

6.2. Discussion and analytics to the conditional cumulants

Within this section we provide an analytic analysis of the conditional cumulants. This is carried out to recover the main features as depicted in Figures 6.1 and 6.4 from the classical part of the CF.

As discussed in the previous Ch. 5.2.2, the CF derived with the help of a master equation in full secular approximation, splits into a classical part, fully determined by the dynamics of the populations and a quantum part, solely depending on the dynamics of the coherences. In the following we will focus on an analysis of the classical part of the CF. We will discuss and argue that it is responsible for most of the pronounced features appearing in Figs. 6.1 and 6.4. This is also attributed to the fact that at the timescale of the order of the relaxation time of the system, the conditional average of dissipated energy is strongly affected by the expectation values of energy differences with respect to the pre- and post-selected states. This effect should be clearly visible at very long driving times $\tau \to \infty$ but obviously will be overpowered by the contribution of the energy current growing linear in time. Hence the information about the state selection should be found as a time-independent part of the classical part of the CF. In the following we will analyze the classical part of the CF

$$\begin{aligned}\ln \chi^p_\tau(\lambda, f|i) = \frac{\tau}{2}(-\Gamma_{gg}(\lambda) - \Gamma_{ee}(\lambda) + 2\Lambda(\lambda)) \\ - \ln 2\Lambda(\lambda) + \ln \frac{A(\lambda,\theta_f,\theta_i) + B(\lambda,\theta_f,\theta_i)}{4} \\ + \ln\left(1 - \frac{A(\lambda,\theta_f,\theta_i) - B(\lambda,\theta_f,\theta_i)}{A(\lambda,\theta_f,\theta_i) + B(\lambda,\theta_f,\theta_i)} e^{-2\Lambda(\lambda)\tau}\right).\end{aligned} \tag{6.8}$$

The quantities used within Eq. (6.8) are given by

$$\begin{aligned}A(\lambda,\theta_f,\theta_i) = (\cos\theta_i + \cos\theta_f)\left(\Gamma_{ge}(0) - \Gamma_{eg}(0)\right) - (\cos\theta_f - 1)(\cos\theta_i + 1)\Gamma_{eg}(\lambda) \\ - (\cos\theta_f + 1)(\cos\theta_i - 1)\Gamma_{ge}(\lambda)\ ,\end{aligned} \tag{6.9}$$

$$B(\lambda,\theta_f,\theta_i) = 2\Lambda(\lambda)(1 + \cos\theta_f \cos\theta_i)\ . \tag{6.10}$$

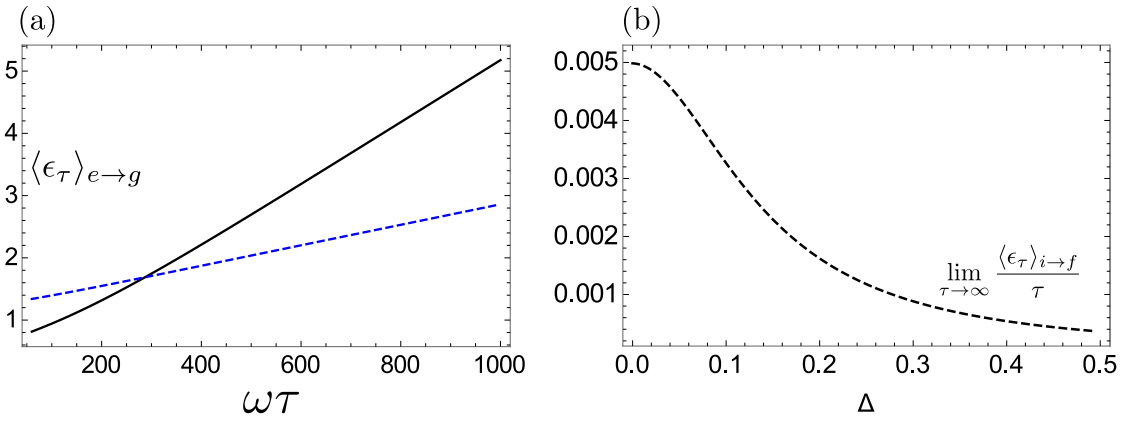

Figure 6.5.: Conditional average of energy for $|e\rangle \to |g\rangle$ pre- and post-selection shown in panel (a) for resonant driving $\Delta = 0$ (black, solid) and with finite detuning $\Delta = 0.2\omega$ (blue, dashed). Panel (b) depicts the average heat current $\lim_{\tau\to\infty}\langle\epsilon_\tau\rangle_{i\to f}/\tau$ as a function of the detuning Δ.

The first line of the above Eq. (6.8) is related to the vanishing eigenvalue of the superoperator Eq. (5.54) for $\lambda = 0$. This eigenvalue in particular determines the long time behavoir of the CF. The second line of Eq. (6.8) denotes a time-independent offset carrying information about the pre- and post-selected states of the system. The last contribution to the CF are transient contributions. They decay on timescales of order of the relaxation time Γ_{rel}^{-1}. For zero driving time $\tau = 0$ we can check that $\chi_0(\lambda, f|i)$ becomes independent of λ and consequently all cumulants vanish.

For convenience we present in Fig. 6.5 the results for the conditional average as obtained from Eq. (6.8). In Fig. 6.5 panel (a) the conditional average $\langle\epsilon_\tau\rangle_{e\to g}$ is depicted for both the resonant driving $\Delta = 0$ as well as the detuned driving scheme $\Delta = 0.2\omega$. We observe that for a shorter driving time more energy is emitted in the detuned case rather than in the resonantly driven situation. On the other hand, the longer the driving lasts, the more energy tends to be dissipated during the resonant drive.

For long driving times $\tau \to \infty$ the energy dissipation should be dominated by the stationary state heat current, being independent of the state selection. Indeed, we obtain the heat current of dissipated energy as

$$\begin{aligned}\lim_{\tau\to\infty}\frac{\langle\epsilon_\tau\rangle_{i\to f}}{\tau} &= \lim_{\tau\to\infty}\frac{\partial_{i\lambda}\,\ln\chi_\tau(\lambda, f|i)|_{\lambda=0}}{\tau}\\ &= \frac{\sin^2\theta\,\omega}{4\Gamma_{\text{rel}}}\left(\Gamma_{\text{rel}}\gamma(\omega)\left(1-e^{-\beta\omega}\right) + \frac{\sin^2\theta}{2}\gamma(\omega+\Omega)\gamma(\omega-\Omega)\left(1-e^{-2\beta\omega}\right)\right).\end{aligned} \tag{6.11}$$

It is clearly independent of the choice of pre- and post-selected states of the system. Furthermore, as expected, the heat current is sensitive to the detuning, maximal for the resonant drive $\Delta = 0$ and decreasing as the detuning increases. For convenience we plot the heat current in Fig. 6.5 (b) as a function of the detuning.

Next, we analyze the time-independent part of the CF, given by line 2 of Eq. (6.8), or to be more precise, its contributions to the conditional cumulants. This contribution dominates the selection sensitivity of the cumulants at long driving times $\tau \to \infty$ since all other selection sensitive contributions will have vanished by then. Hence they determine the landscape of $\lim_{\tau\to\infty}\langle\epsilon_\tau\rangle_{i\to f}$ as a function of the selection angles θ_i and θ_f. Dropping out

the selection insensitive contribution of Eq. (6.8) we readily define

$$c_n(\theta_i,\theta_f) \equiv \partial_{i\lambda}^n \ln \frac{A(\lambda,\theta_i,\theta_f)+B(\lambda,\theta_i,\theta_f)}{4}\bigg|_{\lambda=0}. \tag{6.12}$$

Consequently, the contribution to the first cumulant, the conditional average of dissipated energy, is given by

$$\begin{aligned} c_1(\theta_i,\theta_f) = \frac{1}{2(\Gamma_{\rm rel}+\cos\theta_f(\Gamma_{ge}-\Gamma_{eg}))}\Big((1-\cos\theta_f)(\cos\theta_i+1)\Gamma'_{eg}+(\cos\theta_f+1)(1-\cos\theta_i)\Gamma'_{ge} \\ +\frac{2}{\Gamma_{\rm rel}}(1+\cos\theta_f\cos\theta_i)(\Gamma_{ge}\Gamma'_{eg}+\Gamma'_{ge}\Gamma_{eg})\Big)\ , \end{aligned} \tag{6.13}$$

where $\Gamma'_{ij} \equiv \partial_{i\lambda}\Gamma_{ij}|_{\lambda=0}$. We show $c_1(\theta_i,\theta_f)$ as a function of the selection angles for the detuned drive $\Delta = 0.2\omega$ in Fig. 6.6 (a) and for the resonant drive in Fig. 6.6 (b). A comparison to the numerically obtained results in Fig. 6.1 yields a high degree of similarities in both pictures. Considering the detuned driving scenario, cf. Figs 6.1 (a) and 6.6 (a), we observe that the effects of pre- and post-selection are much more pronounced in comparison to the resonantly driven situation, depicted in Figs 6.1 (b) and 6.6 (b). In order to explain this effect of higher sensitivity to the pre- and post-selection of states to the detuned regime, we analyze the $|e\rangle \to |g\rangle$ state selection. The corresponding angles are $\theta_i = \pi$ and $\theta_f = 0$. The constant contribution is determined to be

$$\begin{aligned} c_1(\pi,0) &= \frac{\Gamma'_{ge}}{\Gamma_{ge}} \\ &= \omega+\Omega-\frac{2\omega\gamma(\omega-\Omega)}{\gamma(\omega-\Omega)+e^{\beta(\omega-\Omega)}\cot^4\frac{\theta}{2}\gamma(\omega+\Omega)}. \end{aligned} \tag{6.14}$$

This particular state selection identifies the relevant contributions to the $|e\rangle \to |g\rangle$ transition, which is solely determined by the corresponding matrix element $\Gamma_{ge}(\lambda)$. The matrix element is given by (cf. Eq. (5.74))

$$\Gamma_{ge}(\lambda) = \cos^4\frac{\theta}{2}\gamma(\Omega+\omega)e^{i\lambda(\Omega+\omega)} + \sin^4\frac{\theta}{2}\gamma(\Omega-\omega)e^{i\lambda(\Omega-\omega)}\ . \tag{6.15}$$

Both processes contained in this matrix element involve a transition process of energy exchance of quanta $\Omega \pm \omega$. At elevated temperatures $T \sim \omega$ and in the resonant regime $\Delta = 0, \theta = \pi/2$, both processes have comparable rates. This results in an average energy dissipation of quanta of Ω. Hence, $c_1(\pi,0) \approx \Omega$ with respect to the resonant regime. However, by increasing the detuning, the first rate within this process is favored. Consequently, an additional process emitting energy of the amount of $\omega+\Omega$ has to occur. This is reflected by $c_1(\pi,0) \approx \omega+\Omega$ for the detuned driving scheme, which results in a much higher amount of energy dissipated as compared to the resonantly driven situation. Furthermore, this result explains the enhancement of energy dissipation for short driving times regarding the detuned drive as compared to the resonant situation shown in Fig. 6.5 (a). In this regime the enhancement is dramatically larger than the natural increase of energy difference $\Omega = \sqrt{\Delta^2+\Omega_R^2}$ due to the detuning. What we observe is related to the effect of detuning on the Mollow-Triplet [84, 85, 86].

Finally, we want to discuss the state selection sensitive contribution $c_2(\theta_i,\theta_f)$ to the conditional variance. The time-independent contribution to the noise $c_2(\theta_i,\theta_f)$ is depicted in Fig. 6.6 (a) for finite detuning and for the resonant situation in Fig. 6.6 (b). A comparison shows a qualitative similarity to the numerically obtained results in Fig. 6.4. Regarding the resonant regime, the noise is generally enhanced and relatively insensitive to the pre-

and post-selection of system states. Again, the situation with finite detuning yields a more versatile dependency on the pre- and post-selection. Interestingly, the noise appears to be minimal in the vicinity of the $|e\rangle \to |g\rangle$ transition, which yielded a maximal energy dissipation. We find

$$\begin{aligned} c_2(\pi,0) &= \frac{\Gamma''_{ge}}{\Gamma_{ge}} - \left(\frac{\Gamma'_{ge}}{\Gamma_{ge}}\right)^2 \\ &= \frac{\sin^4\theta e^{\beta(\omega-\Omega)}\omega^2\gamma(\omega-\Omega)\gamma(\omega+\Omega)}{4\left(\sin^4\frac{\theta}{2}\gamma(\omega-\Omega)+e^{\beta(\omega-\Omega)}\cos^4\frac{\theta}{2}\gamma(\omega+\Omega)\right)^2}\,, \end{aligned} \tag{6.16}$$

which leads to a suppression of the conditional variance as the detuning increases due to the $\sin^4\theta$ dependency in the numerator. The physical explanation of the noise suppression is completely analogous to that of the time-independent contribution to the conditional average. The state selection identifies the matrix element of the master equation responsible for the $|e\rangle \to |g\rangle$ transition, $\Gamma_{ge}(\lambda)$. In the resonant regime, both transitions with energy exchange of quanta $\Omega+\omega$ and $\Omega-\omega$ are equally probable, resulting in an enhanced

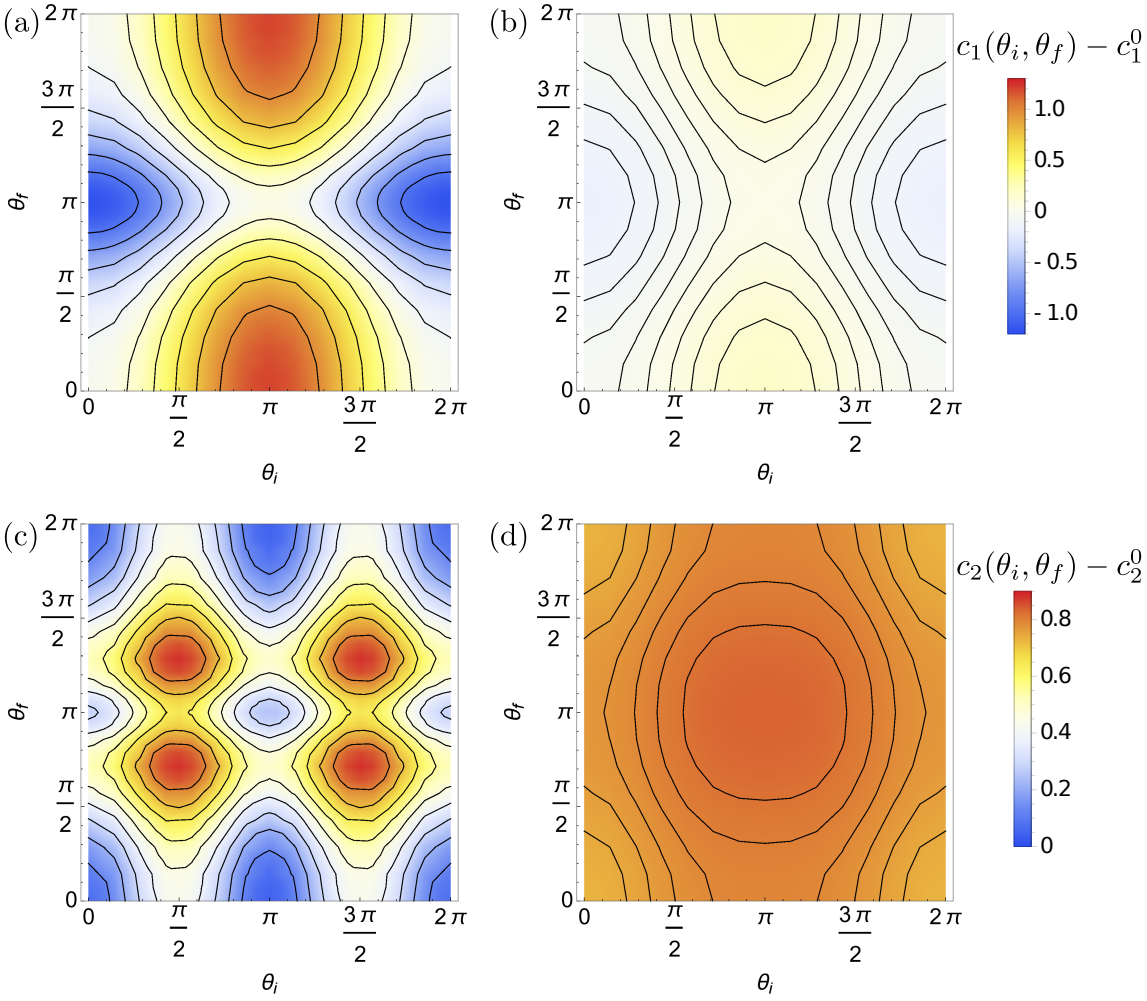

Figure 6.6.: Top panels: Selection sensitive contribution $c_1(\theta_i,\theta_f)$ to the conditional average. Panel (a) depicts the situation with $\Delta = 0.2\omega$. In Panel (b) the situation for resonant driving $\Delta = 0$ is shown. Bottom panels: Selection sensitive contribution $c_2(\theta_i,\theta_f)$ to the conditional noise. The panels compare the situation (c) with finite detuning $\Delta = 0.2\omega$ and (d) resonant driving.

noise. As the detuning tends to favor the energy exchange of $\Omega + \omega$, i.e. this transition is favored; the noise is suppressed.

6.3. Quantum part of the dissipated energy

So far we have provided a detailed analysis of the effect of pre- and post-selection of states of the TLS on the conditional average. We showed that the most pronounced features are due to the classical contributions of the CF. In Sec. 6.1 we observed that quantum features, i.e. coherent oscillations are observable but relatively small. Referring to our analysis in the previous Ch. 5, the CF, as obtained by a master equation in Lindblad form, splits into a classical and a quantum part. Hence, we can extract the quantum part from Eq. (5.47)

$$\delta\chi_\tau^x(\lambda, f|i) = \frac{1}{2}\cos(\Omega\tau)\,\sin\theta_i \sin\theta_f e^{-\Gamma_\varphi(\lambda)\tau}. \tag{6.17}$$

Consequently, the quantum part of the conditional average is obtained as

$$\begin{aligned}\langle\delta\epsilon_\tau\rangle_{i\to f} &= \frac{\partial_{i\lambda}\,\delta\chi_\tau^x(\lambda, f|i)|_{\lambda=0}}{\mathcal{P}_\tau(f|i)} \\ &= \frac{-\tau\cos\Omega\tau e^{-\Gamma_\varphi(0)\tau}}{8\mathcal{P}_\tau(f|i)}\sin^2\theta\sin\theta_i\sin\theta_f\omega\left(\gamma(\omega)-\gamma(-\omega)\right).\end{aligned} \tag{6.18}$$

where

$$\mathcal{P}_\tau(f|i) = \mathcal{P}_\tau^{x,cl}(f|i) + \delta\mathcal{P}_\tau^x(f|i) \tag{6.19}$$

denotes the conditional transition probabilty of the system to end up in the post-selected state $|f\rangle$, given it was prepared in the state $|i\rangle$. As expected, the quantum effect on the dissipated energy is largest if the driving time is chosen in the vicinity of the dephasing time $\Gamma_\varphi(0)$. Furthermore, it is largest for a set of pre- and post-selected states of maximal coherence, i.e. $\theta_i = \theta_f = \pi/2$, with respect to the eigenstates of the TLS in the rotating frame.

In order to demonstrate that the quantum states did play a secondary role in the prior analysis of the effect of pre- and post-selection on the conditional average, we depict the exact same situation as in Fig. 6.1 for finite detuning in Fig 6.7. In Fig. 6.7 (a) we show the pure quantum contribution to the conditonal average at the exact same conditions where Fig. 6.1 (a) has been calculated for. The conditional average depicted in Fig. 6.7 (b) is equivalent to the one depicted in 6.1 (a), where all contributions to the conditional average have been taken into account. In Fig. 6.7 (c) we show the situation where the conditional average was calculated by only considering the classical part of the CF. However, the quantum contribution turns out to be completely overshadowed by the classical features, as they are about two orders of magnitude smaller in this parameter regime. At much lower temperatures the quantum corrections may become noticeable as demonstrated in Fig. 6.8.

6.4. Conclusion

In this chapter we studied the effect of the pre- and post-selection of states of the TLS on the first two conditional cumulants of the dissipated energy. We found that not only the choice of initial and final states but additionally driving the TLS off resonance yields interesting and rich results.

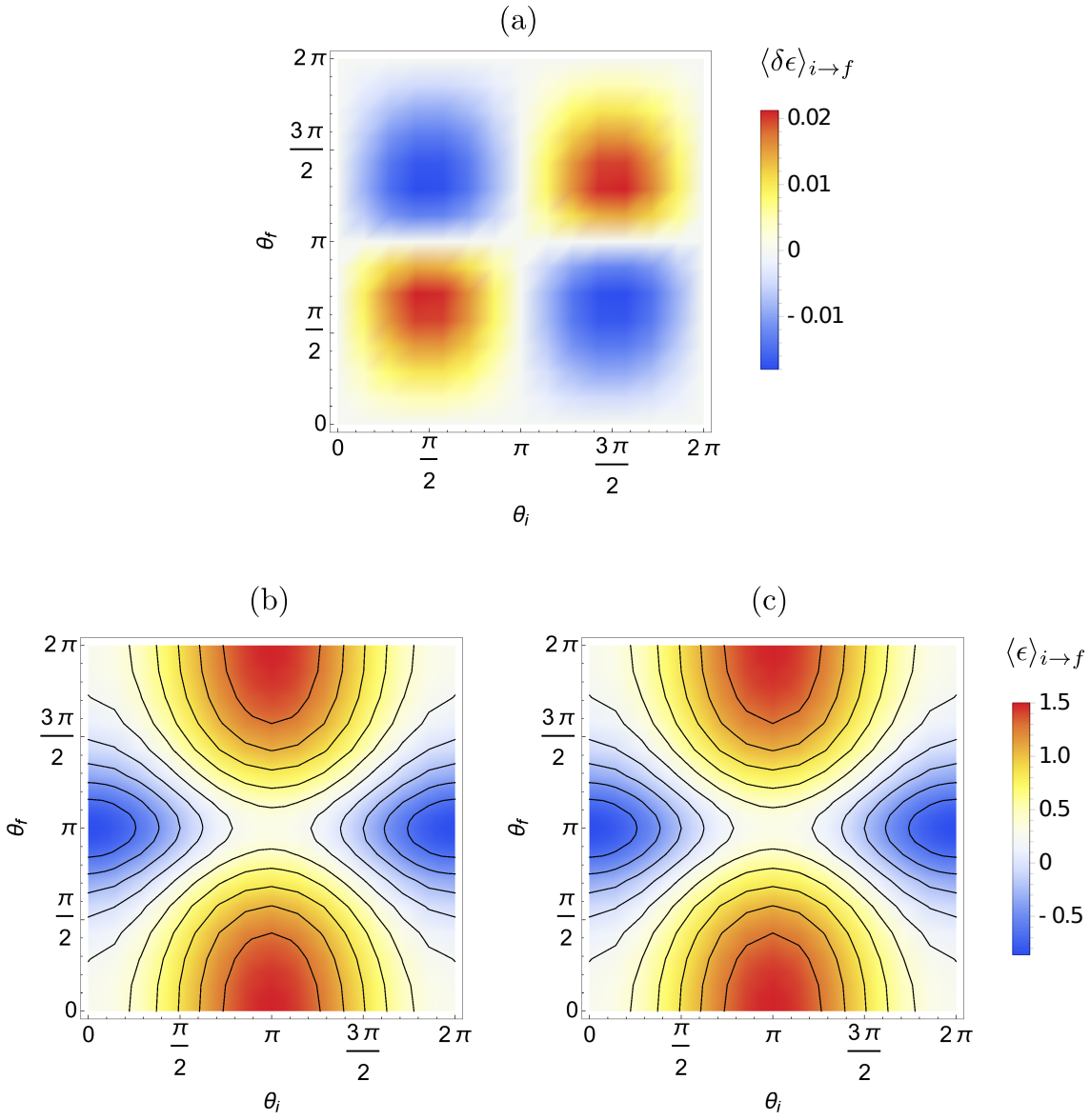

Figure 6.7.: Contribution of the coherences to the conditional average as a function of the pre- and post-selection angles for finite detuning $\Delta = 0.2\omega$. In panel (a) the bare quantum contribution is depicted. Panel (b) shows the situation where the quantum corrections have been taken into account to compute the total conditional average (cf. Fig. 6.1). The conditional average shown panel (c) has been calculated by only considering the classical part of the CF. As indicated by the different plot legends, the quantum signatures are suppressed by two orders of magnitude.

The average heat current $\lim_{\tau\to\infty}\langle\epsilon_\tau\rangle_{i\to f}/\tau$ is independent of choice of the pre- and post selection and is only sensitive to the detuning of the drive. As expected, the heat current becomes maximal when the driving is resonant. For finite detuning and an energetically unfavorable choice of pre- and post-selected system states, our analysis shows that the conditional average becomes negative at times of order of the relaxation times above a crossover temperature T_0. Further analysis shows that this temperature tends to diverge as a function of the driving time. Thus, for a long enough driving time the system has to dissipate energy to the bath independent of the temperature of the bath.

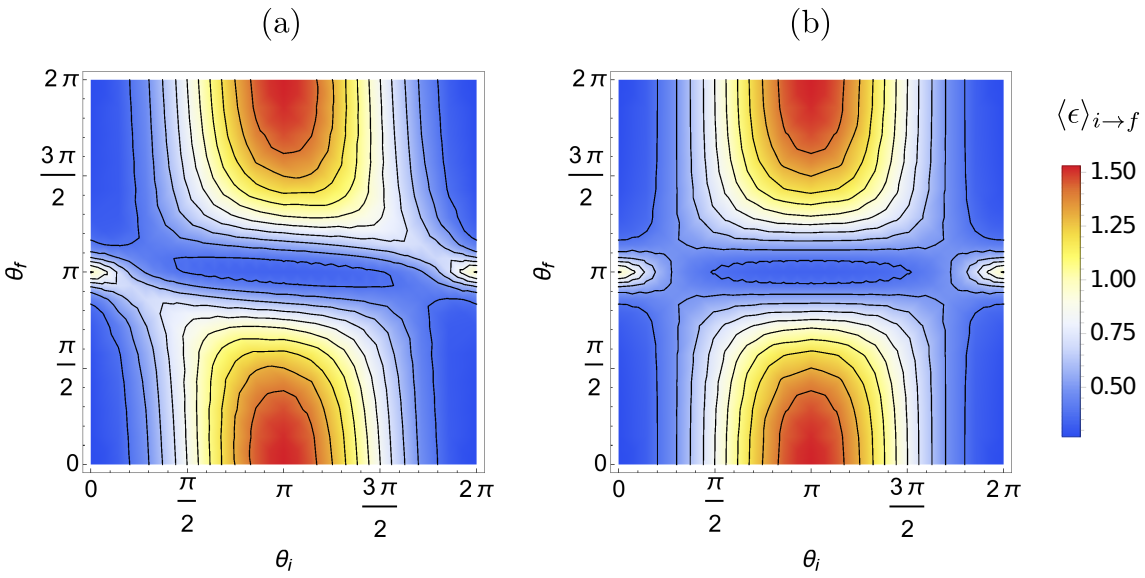

Figure 6.8.: Contribution of the quantum corrections to the conditional average at low temperatures. In panel (a) we show the conditional average of the dissipated energy where the quantum contributions are fully included. In panel (b) the quantum corrections are dropped. The plots are evaluated in the same parameter regime as in Fig. 6.1 except that the temperature is much lower, i.e. $T = 0.1\omega$.

Furthermore we find that the state selection manifests itself mostly in a time-independent contribution which turns out to be sensitive to the detuning. In the vicinity of the $|e\rangle \to |g\rangle$ transition a detailed analysis shows that the increase of detuning favors a distinct transition rate and, therefore, a distinct energy emission $\Omega + \omega$. Consequently, this causes a suppression of the conditional noise.

As the effect is time-independent, it may be most easily detectable after long driving times $\tau \gg \Gamma_{\mathrm{rel}}^{-1}$ (as a small pre- and post-selection dependent correction to the selection independent contribution). However, even at times of order of relaxation times, $\tau \sim \Gamma_{\mathrm{rel}}^{-1}$, the selection dependent contribution may dominate.

We further show that the quantum contributions to the conditional average play a minor role on the effect of pre- and post-selection in the parameter regime of study. However, the quantum features become largest in the vicinity of the pre- and post-selected states of the system with maximal coherence and at a driving time of order of the dephasing time Γ_{φ}^{-1}.

7. A weak measurement proposal and the connection to the conditional average

The concept of weak measurements was firstly proposed by Aharonov, Albert and Vaidman in 1987 [34]. It provided a new interpretation for the outcome of a quantum measurement. Using a distinct initial and final state selection of the measured system, very peculiar but also very improbable measurement outcomes were to appear: the *weak values*. There are several theoretical generalizations and studies [87, 88, 89, 90] on the topic of weak values. Additionally, they have been observed experimentally [91]. Interestingly, the weak value of an observable can in general be complex and larger than the expectation value of the observable itself. Hence, the concept of weak measurements turns out to be useful in many different ways. As an example, the weak measurement may be used as an amplification mechanism [36] or allows for the direct detection of the wave function of the system [37].

As the name indicates, the weak measurement approach is in contrast to a strong measurement. The strong measurement, as proposed by von Neumann [75] consists of a quantum mechanical measurement apparatus which is a quantum mechanical system itself. The measurement apparaturs is coupled to the observable $\mathcal{A}$ of the system of interest. For an ideal strong measurement, the outcome of the measurement is an eigenvalue a_j of the measured observable $\mathcal{A}$. As a consequence, the system will be in the corresponding eigenstate of that eigenvalue after the measurement has been performed. Consequently, the system has been strongly disturbed by the measurement.

The idea behind the weak measurement is to either modify the coupling between the system and the detector in a way that the system is weakly disturbed or to prepare the detector in an uncertain state. We will clarify below what is meant by this preparation of the detector. The weakness of the measurement guarantees that the system is only weakly disturbed by the measurement. On the other hand the output does not necessarily provide much information about the state of the system.

In this chapter we propose an extension to the existing concept of weak measurements. We will consider the weak continuous measurement of a driven open quantum system. In the following, we suggest the weak measurement of the energy current, which transfers the energy exchanged between the system and the bath. Using the driven TLS, we show that the weak value of the energy current turns out to be a complex oscillating quantity. Yet, we will show that the outcome is related to the conditional average of the dissipated energy by integrating the weak value over the measurement time.

Before we derive the continuous weak measurement approach, we will provide a brief detour to introduce the concept of weak measurements. We will also discuss the outcome of a weak measurement, the weak value.

7.1. Weak measurements and weak values

This section provides a brief introduction to the concept of weak measurements. We will briefly review the pioneering considerations by Aharonov, Albert and Vaidman [34]. We further clarify the circumstances in which the outcome of a weak measurement may become a weak value, i.e. discuss the necessary conditions of the detector.

7.1.1. The weak measurement and weak values

In principle, a quantum mechanical measurement as proposed by von Neumann requires a detector, which is a quantum mechanical system itself [75]. Concerning the measurement process itself, there are a few requirements necessary to the measurement [35]. At first, the measurement will last for some measurement time τ_M. During this measurement time the system and the detector are coupled, whereas, before and after the measurement both systems are decoupled and independent. However, there is no restriction to the duration of the measurement, but in some situations an *impulsive* measurement, i.e. a measurement with a very short measurement time, may be desirable. Secondly, the measurement causes a deflection of the meter which is correlated to the measured observable of the system. Furthermore, the measured observable is not changed by the measurement.

Keeping this in mind, one is able to write down a quite general system detector Hamiltonian

$$\hat{H} = \hat{H}_S + \hat{H}_M + \hat{H}_{SM}, \tag{7.1}$$

where $\hat{H}_{S/M}$ are the free system / detector Hamiltonians. They are coupled via

$$\hat{H}_{SM} = g(t)\mathcal{A}P_M, \tag{7.2}$$

where $g(t)$ is the coupling function with $\int_0^{\tau_M} dt\, g(t) = g_0$ and $\mathcal{A}$ denotes the observable of interest. The observable $\mathcal{A}$ is coupled to the detector operator P_M, which could, for example, be the momentum of the detector. There is a conjugate operator Q_M to P_M with the commutation relation $[Q_M, P_M] = i$. This will be crucial for the measurement as we illustrate in the following. The detector itself is prepared in a known initial state of Q_M. From the Heisenberg equation of motion follows that the operator Q_M evolves according to

$$\begin{aligned} Q_M(\tau_M) - Q_M(0) &= \int_0^{\tau_M} dt \frac{dQ_M}{dt} \\ &= i\int_0^{\tau_M} dt[\hat{H}_M, Q_M] + g_0\mathcal{A}. \end{aligned} \tag{7.3}$$

One immediately sees that for an impulsive measurement ($\tau_M \to 0$, but finite g_0) the change of Q_M is determined by $g_0\mathcal{A}$, i.e. it corresponds to the measured observable of interest. From the structure of Eq. (7.2) one immediately sees that by choosing a very small coupling constant $g_0 \ll 1$, the measurement can, in principle, be weak.

Yet, there is another possibility to manipulate the strength of the measurement as we will discuss in the following. The discussion will be made in the context of pre- and post-selected ensembles [35]. Consequently, the system has been initially prepared in a distinct state $|i\rangle$. After the measurement has been performed, a distinct final state $|f\rangle$ is post-selected. For example, this may be achieved by a measurement protocol as presented in Ch. 2.3.

In what follows, the measurement is supposed to be impulsive, i.e. the internal dynamics of the meter may be discarded. The corresponding system-detector coupling is set to $g_0 = 1$. The initial state of the meter is given by

$$\phi_{\text{in}}(Q_M) = \frac{1}{(\varepsilon^2\pi)^{-1/4}} e^{-\frac{Q_M^2}{2\varepsilon^2}}, \tag{7.4}$$

which is chosen to be Gaussian distributed. Hence, the uncertainty is given by $\Delta Q_M = \varepsilon/\sqrt{2}$. Note that ε may be used to determine the strength of the measurement: A small ε corresponds to a strong measurement where the distribution of Q_M of the initial state of the detector is quite well known. In the limit of $\varepsilon \to 0$, the initial state is known exactly which corresponds to an ideal measurement. In the opposite case of large ε, the uncertainty of Q_M is large. This implies a small uncertainty for the coupling observable $\Delta P_M = 1/(\sqrt{2}\varepsilon)$ such that P_M can generally chosen to be small. Consequently, the measurement for large ε can be considered as weak.

The combined state of the system and of the meter evolves according to the time evolution operator $U = \exp[-i\mathcal{A}P_M]$. Considering a large ε, the time evolution operator can be expanded in powers of P_M. Taking the post-selection into account, one arrives at [34, 35]

$$\begin{aligned}
\langle f|e^{-i\mathcal{A}P_M}|i\rangle\phi_{\text{in}}(Q_M) &\approx \langle f|\left(1 - \mathcal{A}P_M\right)|i\rangle\phi_{\text{in}}(Q_M) \\
&= \langle f|i\rangle\left(1 - i\frac{\langle f|\mathcal{A}|i\rangle}{\langle f|i\rangle}P_M\right)\phi_{\text{in}}(Q_M) \\
&\approx \langle f|i\rangle e^{-i\mathcal{A}_W P_M}\phi_{\text{in}}(Q_M),
\end{aligned} \tag{7.5}$$

where the weak value of $\mathcal{A}$ is defined as

$$\mathcal{A}_W \equiv \frac{\langle f|\mathcal{A}|i\rangle}{\langle f|i\rangle}. \tag{7.6}$$

Since Q_M and P_M are conjugate variables, the matrix exponent in the last line of Eq. (7.5) gives the deflection of the state of the meter, i.e.

$$\phi_{\text{fin}}(Q_M) \approx \phi_{\text{in}}(Q_M - \mathcal{A}_W). \tag{7.7}$$

Consequently, the initial state of the meter is shifted by the weak value $\mathcal{A}_W$.

The concept of weak measurements and weak values has been considered for mixed states as well. The weak value in this case was derived in [92, 87] as

$$\mathcal{A}_{W,\rho} = \frac{\langle f|\mathcal{A}\rho|i\rangle}{\langle f|\rho|i\rangle}, \tag{7.8}$$

where the system is described by a density operator ρ rather than a pure state $|\Psi\rangle$.

7.1.2. A gedanken experiment: The weak measurement of a spin 1/2 particle

To provide an illustrative example for the weak measurement, we review the gedanken experiment proposed by Aharonov, Albert and Vaidman [34]. They considered the weak measurement of a spin 1/2 particle with an additional pre- and post-selection of the spin states. In a modified Stern-Gerlach experiment the particle beam is prepared in such a way that the orientation of the spin is along a certain direction ξ in the $\hat{x}z$-plane (cf. Fig 7.1). Consequently, the pre-selected state is given by $|\uparrow_\xi\rangle$, which is characterized by the angle α with respect to the $\hat{x}$-direction. The beam passes through a first measurement apparatus which weakly measures the σ_z component of the spin. The weak measurement of the σ_z

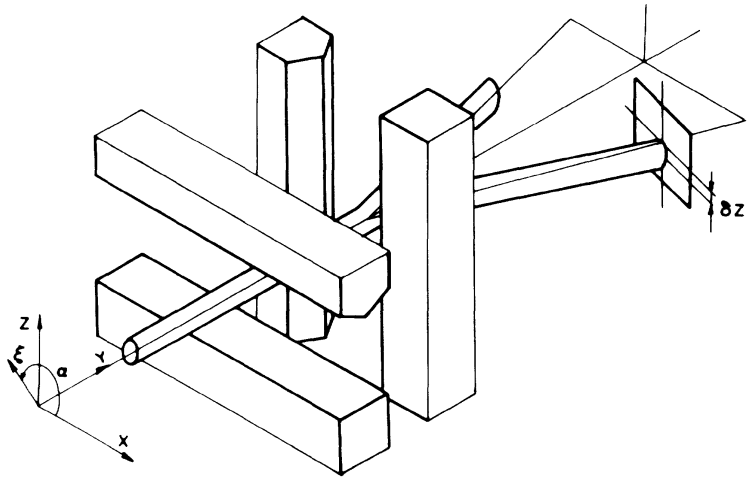

Figure 7.1.: Sketch for the experimental setup regarding to a weak measurement, taken from [34]. The content of the picture as well as the experiment are discussed in the main text.

component makes the initial wave function to separate spatially into two parts connected to the σ_z value. Finally, the beam is guided through a second measurement device which strongly measures the σ_x component. However, only states which finally were measured in the $|\uparrow_x\rangle$ state are kept for the measurement. Due to the weak measurement of the σ_z component, the deflection visible on the detector is correlated to the weak value of σ_z

$$\sigma_{z,W} = \frac{\langle\uparrow_x |\sigma_z| \uparrow_\xi\rangle}{\langle\uparrow_x | \uparrow_\xi\rangle} = \tan\frac{\alpha}{2}, \tag{7.9}$$

which can, in principle, be larger than the expectation value of σ_z.

7.2. Weak measurement for the driven open quantum system

Analogous to previous works [34], we consider the weak measurement of the dissipative energy current $\hat{I}_\epsilon \equiv -i[H_B, H_I]$ of a driven open system. The time-dependent Hamiltonian is given by

$$\hat{H}(t) = \hat{H}_S(t) + \hat{H}_B + \hat{H}_I + \hat{H}_{SM}, \tag{7.10}$$

where $\hat{H}_S(t)$ denotes the Hamiltonian of the driven system and the bath is represented by $\hat{H}_B$. The system-bath coupling is denoted by $\hat{H}_I = AB$ with system (bath) operators A (B). The coupling to the meter is denoted by $\hat{H}_{SM} = g\hat{I}_\epsilon P_M$, where P_M is the momentum operator of the measuring device. Note that in the general situation, the weakly monitored observable may be a pure system (or bath) observable or (as in our case) any arbitrary combination of system plus bath observable. The free Hamiltonian of the meter will be neglected in our approach. The setup is depicted in Fig. 7.2. The dimensionless coupling between system and measuring device $g \ll 1$ is supposed to be small.

The measurement protocol is organized as follows. The system S is prepared at time $t = 0$ in the initial state $|i\rangle$ with a strong projective measurement. At the same time the driving begins. At time $t = \tau$, the system is again strongly measured and projected onto the desired final state $|f\rangle$. During the driving, the measurement device weakly measures the desired observable $\hat{I}_\epsilon$ continuously.

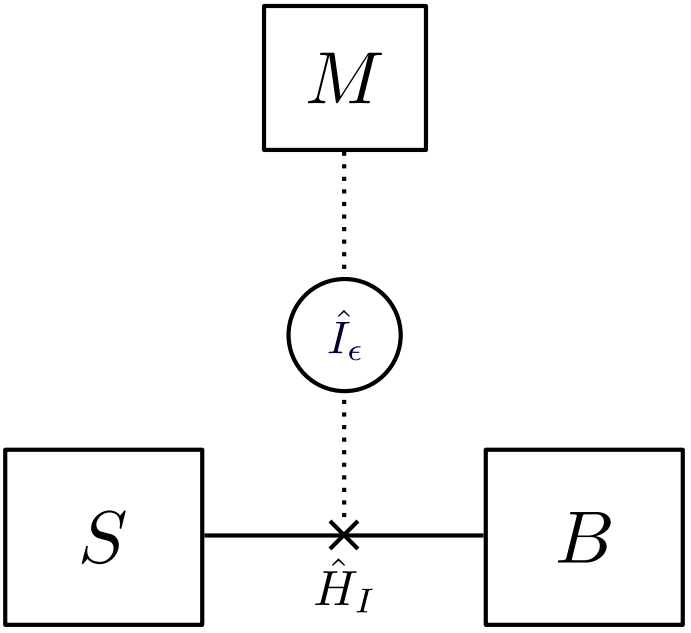

Figure 7.2.:]
Sketch of the measurement setup. The system S is coupled to the bath via $\hat{H}_I$. The detector is weakly monitoring the dissipated energy current $\hat{I}_\epsilon$.

We evaluate the reduced density matrix of the meter, which is defined as

$$\rho_M^f(\tau) \equiv \mathrm{Tr}_{SB}\left[P_f \rho(\tau)\right] \ , \tag{7.11}$$

where $P_f = |f\rangle\langle f|$ is the projector on the final (postselected) state of the system and $\rho(\tau)$ is the density matrix of the whole system including the meter. For the latter we obtain

$$\rho(\tau) = U_{SBM}(\tau,0)\rho_{SB}^i \rho_M U_{SBM}^\dagger(\tau,0) \ . \tag{7.12}$$

Here the initial density matrix of the system with the bath and of the meter is assumed to factorize. The density operator evolves according to the full time evolution operator $U_{SBM}(\tau,0)$, see Eqs. (7.17)-(7.21). Next, we expand the time evolution operator $U_{SBM(\tau,0)}$ in powers of the system-meter coupling g to obtain

$$\rho_M^f(\tau) \approx \mathcal{P}_f(\tau)(\tau)\, e^{-ig\int_0^\tau dt \hat{I}_{\epsilon,W}(t) P_M} \rho_M e^{ig\int_0^\tau dt \hat{I}_{\epsilon,W}^\dagger(t) P_M}. \tag{7.13}$$

Here

$$\begin{aligned}\mathcal{P}_f(\tau) &= \mathrm{Tr}_{SB}\left[P_f U_{SB}(\tau,0)\rho_{SB}^i U_{SB}^\dagger(\tau,0)\right] \\ &= \mathrm{Tr}_{SB}\left[P_f^H(\tau)\rho_{SB}^i\right]\end{aligned} \tag{7.14}$$

is the conditional probability to obtain the desired final state of the system given it was prepared in $|i\rangle$. The resulting deflection of the meter in first order system-detector coupling g is given by the integral $g\int_0^\tau dt \hat{I}_{\epsilon,W}(t)$, where

$$\hat{I}_{\epsilon,W}(t) = \frac{\mathrm{Tr}_{SB}\left[P_f U_{SB}(\tau,t)\hat{I}_\epsilon U_{SB}(t,0)\rho_{SB}^i U_{SB}^\dagger(\tau,0)\right]}{P_S^f(\tau)}. \tag{7.15}$$

We rewrite Eq. (7.15) to finally obtain

$$\hat{I}_{\epsilon,W}(t) = \frac{\mathrm{Tr}_{SB}\left[P_f^H(\tau)\hat{I}_\epsilon^H(t)\rho_{SB}^i\right]}{\mathrm{Tr}_{SB}\left[P_f^H(\tau)\rho_{SB}^i\right]} \ , \tag{7.16}$$

where the superscript H denotes the Heisenberg picture. We note that Eq. (7.16) has a structure similar to the weak value for the mixed state (7.8).

7.3. The connection between the weak value and the conditional average of dissipated energy

In this section we will derive a connection between Eq. (7.16) and the strong measurement approach which is used in the context of the FCS. We will demonstrate two properties. Firstly, we will show that both measurement approaches yield the same result for the dissipated energy. Secondly, we will show that the outcome of the weak value approach, i.e. the time integral of Eq. (7.16) is real, which may not be obvious by Eq. (7.16) itself. It is useful to introduce all the necessary time evolution operators

$$U_{SBM}(t,0) = U_{SB}(t,0)S(t,0)\ , \tag{7.17}$$

$$S(t,0) = \mathcal{T}\exp\left(-i\int_0^t dt'\,\hat{H}^H_{SM}(t')\right) = \mathcal{T}\exp\left(-i\int_0^t dt'\,U^\dagger_{SB}(t')\hat{H}_{SM}U_{SB}(t')\right)\ , \tag{7.18}$$

$$U_{SB}(t,0) = U_0(t,0)W(t,0)\ , \tag{7.19}$$

$$U_0(t,0) = U_{0,S}(t,0)U_{0,B}(t,0)\ , \tag{7.20}$$

$$W(t) = \mathcal{T}\exp\left(-i\int_0^t dt'\,\hat{H}^W_I(t')\right) = \mathcal{T}\exp\left(-i\int_0^t dt'\,U^\dagger_0(t')\hat{H}_I U_0(t')\right). \tag{7.21}$$

Here, $U_{SBM}(t,0)$ is the full time evolution operator with respect to system, bath and measuring device. It can be split into the product of $U_{SB}(t,0)$, determining the evolution of system plus bath, and $S(t,0)$ being the time-ordered exponent of the interaction between system bath and measurement device. The operator $U_{SB}(t,0)$ itself can again be decomposed into the free evolution of system and bath $U_0(t,0)$ and the interaction between system and bath $W(t,0)$. The transformed Hamiltonians for the time ordered product in the exponent are labeled by W (interaction between full system plus measuring device) and I (interaction between system and bath). We keep in mind that the time evolution operator for two different time arguments reads

$$U_{SBM}(t,t_0) = U_{SB}(t,0)S(t,t_0)U^\dagger_{SB}(t_0,0). \tag{7.22}$$

Similarly, the relation (7.22) holds for $U_{SB}(t,t_0)$ by replacing $U_{SB}(t,t') \to U_0(t,t')$ and $S(t,t_0) \to W(t,t_0)$.

7.3.1. Full counting statistics approach

In this section we describe the FCS approach to the problem. The method of FCS has been introduced in Ch. 4. In a first approach we briefly rederive the CF using the two-point-measurement approach, cf. Ch. 4.2 and Ref. [12] We have

$$\begin{aligned}\chi_\tau(\lambda, f|i) &= \mathrm{Tr}_{SB}\left[P_f e^{iH_B\lambda/2}U_{SB}(\tau,0)e^{-iH_B\lambda/2}\rho_0 e^{-iH_B\lambda/2}U^\dagger_{SB}(\tau,0)e^{iH_B\lambda/2}\right]\\ &= \mathrm{Tr}_{SB}\left[P_f e^{iH_B\lambda}U_{SB}(\tau,0)e^{-iH_B\lambda}\rho_0 U^\dagger_{SB}(\tau,0)\right],\end{aligned} \tag{7.23}$$

where we used $[H_B, P_f] = [H_B, \rho_0] = 0$ in the second line. Taking the derivative with respect to λ at $\lambda = 0$ gives

$$\begin{aligned}\frac{1}{i}\partial_\lambda\chi_\tau(\lambda, f|i)|_{\lambda=0} &= \mathrm{Tr}_{SB}\left[P_f H_B U_{SB}(\tau,0)\rho_0 U^\dagger_{SB}(\tau,0)\right]\\ &\quad - \mathrm{Tr}_{SB}\left[P_f U_{SB}(\tau,0)H_B\rho_0 U^\dagger_{SB}(\tau,0)\right]\\ &= \mathrm{Tr}_{SB}\left[P_f\left[H_B, U_{SB}(\tau,0)\right]\rho_0 U^\dagger_{SB}(\tau,0)\right].\end{aligned} \tag{7.24}$$

Similarly we can write

$$\begin{aligned}\frac{1}{i}\partial_\lambda \chi_\tau(\lambda, f|i)|_{\lambda=0} &= \mathrm{Tr}_{SB}\left[P_f U_{SB}(\tau,0)\rho_0\left[U_{SB}^\dagger(\tau,0), H_B\right]\right] \\ &= \left(\mathrm{Tr}_{SB}\left[P_f\left[H_B, U_{SB}(\tau,0)\right]\rho_0 U_{SB}^\dagger(\tau,0)\right]\right)^\dagger . \end{aligned} \tag{7.25}$$

This imposes that the derivative must be real. To evaluate the commutator, we introduce

$$t_n = \Delta t n, \qquad \Delta t = \frac{t}{N}, \tag{7.26}$$

which enables us to rewrite the time-evolution operator as

$$U_{SB}(t,t_0) = \lim_{N\to\infty} U_{SB}(t_N, t_{N-1}) U_{SB}(t_{N-1}, t_{N-2}) ... U_{SB}(t_1, t_0). \tag{7.27}$$

Consequently, the commutator yields

$$[H_B, U_{SB}(\tau,0)] = \lim_{N\to\infty} \left([H_B, U_N]U_{N-1}...U_0 + U_N[H_B, U_{N-1}]...U_0 + ... + U_N...U_1[H_B, U_0]\right), \tag{7.28}$$

where $U_N \equiv U_{SB}(t_N, t_{N-1})$. Each commutator in Eq. (7.28) is approximated as

$$[H_B, U_N] \approx -i\Delta t[H_B, H] = \Delta t \hat{I}_\epsilon \ , \tag{7.29}$$

which finally enables us to rewrite Eq. (7.28)

$$\begin{aligned}[H_B, U_{SB}(\tau,0)] &= \int_0^\tau U_{SB}(\tau,t)\hat{I}_\epsilon U_{SB}(t,0) \\ &= U_{SB}(\tau,0)\int_0^\tau dt \hat{I}_\epsilon^H(t). \end{aligned} \tag{7.30}$$

Inserting the integral representation of the commutator Eq. (7.30) into the derivative of the CF, Eq. (7.24) yields

$$\frac{1}{i}\partial_\lambda \chi_\tau(\lambda, f|i)|_{\lambda=0} = \int_0^\tau dt\, \mathrm{Tr}_{SB}\left[P_f^H(\tau)\hat{I}_\epsilon^H(t)\rho_0\right]. \tag{7.31}$$

Consequently, the conditional average of the dissipated energy is obtained as

$$\begin{aligned}\langle \epsilon_\tau \rangle_{i\to f} &= \partial_{i\lambda} \ln \chi_\tau(\lambda, f|i)|_{\lambda=0} \\ &= \frac{\int_0^\tau dt\, \mathrm{Tr}_{SB}\left[P_f^H(\tau)\hat{I}_\epsilon^H(t)\rho_0\right]}{\mathrm{Tr}_{SB}\left[P_f^H(\tau)\rho_0\right]} \\ &= \int_0^\tau dt\, \frac{\langle P_f^H(\tau)\hat{I}_\epsilon^H(t)\rangle}{\langle P_f^H(\tau)\rangle}. \end{aligned} \tag{7.32}$$

With Eq. (7.32) a connection between the conditional average as derived by the FCS approach and the above proposed weak measurement scheme in Ch. 7.2 is established. The FCS calculations result in the integral of the weak value Eq. (7.16). To convince ourselves that the proposed weak measurement scheme is indeed self-consistent, we may check if the integral over the weak value indeed appears to be real-valued.

7.3.2. Proof that Eq. (7.32) is real

In the following we show that the integral of $\int_0^\tau dt \mathrm{Tr}_{SB}\left[P_f^H(\tau)\hat{I}_\epsilon^H(t)\rho_0\right]$ is real-valued. We rewrite

$$\begin{aligned}\int_0^\tau dt \mathrm{Tr}_{SB}\left[P_f^H(\tau)\hat{I}_\epsilon^H(t)\rho_0\right] &= \mathrm{Tr}_{SB}\left[U_{SB}^\dagger(\tau,0)P_f\int_0^\tau dt\, U_{SB}(\tau,t)\hat{I}_\epsilon U_{SB}(t,0)\rho_0\right] \\ &= \mathrm{Tr}_{SB}\left[U_{SB}^\dagger(\tau,0)P_f[H_B,U_{SB}(\tau,0)]\rho_0\right] \\ &= \mathrm{Tr}_{SB}\left[[U_{SB}^\dagger(\tau,0),H_B]P_f U_{SB}(\tau,0)\rho_0\right], \end{aligned} \tag{7.33}$$

where we used Eq. (7.30). Consequently, we obtain

$$\begin{aligned}[U^\dagger(\tau,0),H_B] &= ([H_B,U(\tau,0)])^\dagger \\ &= \int_0^\tau dt\, U^\dagger(t,0)I_\epsilon U^\dagger(\tau,t), \end{aligned} \tag{7.34}$$

which finally provides the identity

$$\begin{aligned}\int_0^\tau dt\, \mathrm{Tr}_{SB}\left[P_f^H(\tau)\hat{I}_\epsilon^H(t)\rho_0\right] &= \int_0^\tau dt\, \mathrm{Tr}_{SB}\left[\hat{I}_\epsilon^H(t)P_f^H(\tau)\rho_B\right] \\ &= \left(\int_0^\tau dt\, \mathrm{Tr}_{SB}\left[P_f^H(\tau)\hat{I}_\epsilon^H(t)\rho_0\right]\right)^* . \end{aligned} \tag{7.35}$$

So far we have established a connection between the proposed continuous weak measurement scheme in Ch. 7.2 and the FCS approach. The equivalence is independent of the duration of the measurement (a longer drive demands that the system meter coupling g must be arbitrary small) and independent of the coupling between system and bath. We further showed that the integral over the weak value with respect to the duration of the measurement time is real which is not obvious by the general structure of $\hat{I}_{\epsilon,W}(t)$.

7.4. Continuous weak measurement of the energy current dissipated by the driven TLS

In this section we explicitly calculate the weak value Eq. (7.16) of the energy current $\hat{I}_\epsilon$. The calculation is carried using the circularly polarized driven TLS. For convenience, we provide again the Hamiltonian Eq. (5.48),

$$\hat{H}(t) = \hat{H}_{TLS}(t) + \hat{H}_I(\vartheta = 0) + \hat{H}_B, \tag{7.36}$$

containing, inter alia, the Hamiltonian $\hat{H}_{TLS}(t)$ of the circularly polarized driven TLS. The analysis is carried out for the transversal system bath coupling $\hat{H}_I(\vartheta = 0) = \sigma_x B$. Consequently, the energy current of the dissipated energy to our problem is obtained as

$$\hat{I}_\epsilon = \sigma_x \hat{I}_B, \tag{7.37}$$

where $\hat{I}_B = -i[\hat{H}_B, B]$. At first, we present and discuss the weak value of the energy current of the dissipated energy in the subsequent section.

7.4.1. Weak value of the energy current

In order to calculate the weak value of the dissipative energy current, it is convenient to analyze the numerator and the denominator of the weak value Eq. (7.16) separately. We start with the analysis of the numerator $\langle P^H(\tau)I^H(t)\rangle$. We make use of the quantum

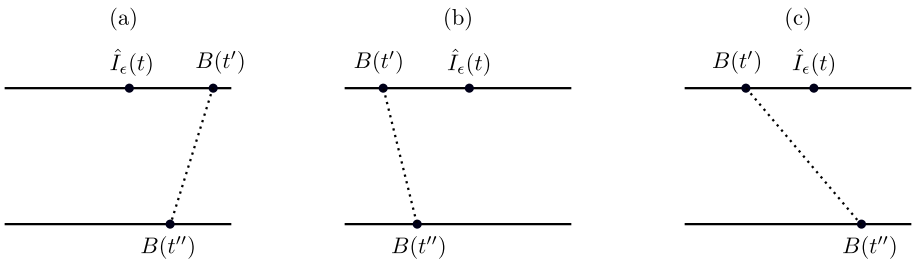

Figure 7.3.: Exemplary sketch for diagrams contributing due to the quantum regression approximation. Type (a) and (b) diagrams show allowed contractions of bath operators whereas type (c) diagrams are discarded.

regression approximation [93, 94, 95]. This approximation is a powerful tool for analyzing multi-time correlation functions. It states that, with respect to time ordered correlation functions, the earlier operator can be considered to be the initial density operator to the latter operator. Considering the dynamics of an open system, the quantum regression approximation results in the discarding of certain diagrams as depicted in Fig. 7.3. We rewrite the numerator of Eq. (7.16)

$$\begin{aligned}\langle P_f^H(\tau)\hat{I}_\epsilon^H(t)\rangle =& \mathrm{Tr}_{SB}\Big[P_f U_{SB}(\tau,t_>)U_{SB}(t_>,t)\hat{I}_\epsilon U_{SB}(t,t_<)U_{SB}(t_<,0)\rho_S^i\rho_B U_{SB}^\dagger(\tau,0)\Big]\\ \approx& \mathrm{Tr}_{SB}\Bigg[P_f U_{SB}(\tau,t_>)\underbrace{U_{SB}(t_>,t)\hat{I}_\epsilon U_{SB}(t,t_<)\rho_S(t_<)\rho_B U_{SB}^\dagger(t_>,t_<)}_{\rho_S(t_>)\rho_B}U_{SB}^\dagger(\tau,t_>)\Bigg]\\ \approx& \mathrm{Tr}_{SB}\Big[Pe^{\mathcal{L}(\tau-t_>)}U_{SB}(t_>,t)\hat{I}_\epsilon U_{SB}(t,t_<)\rho_B e^{\mathcal{L}t_<}\rho_S^i\Big],\end{aligned} \tag{7.38}$$

where we used the quantum regression approximation in the last line. Consequently, the initial density operator evolves dissipatively in time until the energy is exchanged with the bath via the energy current $\hat{I}_\epsilon$ is measured. After the measurement of the dissipative energy current has taken place, the system again evolves dissipatively until it is projected onto the desired final state. The dissipative time evolution in the intervals $[0,t_<]$ and $[t_>,\tau]$ is described by the super operator $\mathcal{L}$, which has been derived previously in Ch. 5, Eq. (5.54). The operator $\hat{I}_\epsilon$ itself contains a system bath coupling Hamiltonian $\hat{H}_I$. Hence, the zeroth contribution $\langle\hat{I}_\epsilon\rangle = 0$ will vanish as we are considering a bath in thermal equilibrium. Consequently, we expand $\hat{I}^H(t)$ in the vicinity of t, i.e. inbetween the times $t_<$ and $t_<$, diagrammatically (see Ch. 3.3) with respect to the applied protocol, in lowest order non-vanishing contributions. Hence, we rewrite

$$\begin{aligned}\hat{I}_\epsilon(t) &= U_{SB}^\dagger(t,0)\hat{I}_\epsilon U_{SB}(t,0)\\ &= U_{SB}^\dagger(t_>,0)U_{SB}(t_>,t)\hat{I}_\epsilon U_{SB}(t,t_<)U_{SB}(t_<,0),\end{aligned} \tag{7.39}$$

where $t_> > t' > t$ and, $t <, t' < t_<$ denote the times between which a contraction of $\hat{I}_\epsilon(t)$ and $\hat{H}_I(t')$ appears. Considering the dissipative time evolution in a rigorous manner, we expand $U_{SB}(t_>,t)\hat{I}_\epsilon U_{SB}(t,t_<)$ in Eq. (7.38) in the system-bath coupling, obtaining

$$\begin{aligned}\langle P_f^H(\tau)\hat{I}_\epsilon^H(t)\rangle \approx& \mathrm{Tr}_{SB}\left[P_f e^{\mathcal{L}\tau}(-i)\int_t^{t_>}dt' e^{-\mathcal{L}t'}\hat{H}_I^I(t')\hat{I}_\epsilon^I(t)\rho_B e^{\mathcal{L}t}\rho_S^i\right]\\ &+\mathrm{Tr}_{SB}\left[P_f e^{\mathcal{L}(\tau-t)}\hat{I}_\epsilon^I(t)(-i)\int_{t_<}^{t}dt'\hat{H}_I^I(t')\rho_B e^{\mathcal{L}t'}\rho_S^i\right]\\ \approx& \mathrm{Tr}_S\left[P_f e^{\mathcal{L}(\tau-t)}\hat{I}_{\mathrm{diss}}(t)e^{\mathcal{L}t}\rho_S^i\right],\end{aligned} \tag{7.40}$$

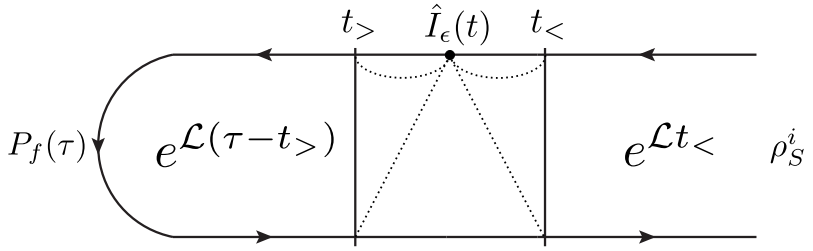

Figure 7.4.: Sketch of the Keldysh contour of the problem. The density matrix evolves according to $\mathcal{L}$ until the energy is exchanged between system and bath via the energy current operator $\hat{I}_\epsilon$. After the energy exchange has taken place, the system again evolves according to $\mathcal{L}$.

where

$$\begin{aligned}\hat{I}_{\rm diss}(t) &= -i{\rm Tr}_B\left[\int_0^\infty ds\ e^{-\mathcal{L}s}\hat{H}_I^I(s)\hat{I}_\epsilon^I(t)\rho_B + \int_{-\infty}^0 ds\ \hat{I}(t)\hat{H}_I^I(s)e^{\mathcal{L}s}\rho_B\right]\ , \\ &\approx -i{\rm Tr}_B\left[\int_0^\infty ds\ \hat{H}_I^I(s)\hat{I}_\epsilon^I(t)\rho_B + \int_{-\infty}^0 ds\ \hat{I}(t)\hat{H}_I^I(s)\rho_B\right]\ , \end{aligned} \tag{7.41}$$

is the first order expansion of $\hat{I}_\epsilon^H(t)$ in system bath coupling in the vicinity of t. In the second line of Eq. (7.41) we used the fact that the contributions of the super operator $\mathcal{L}$ are negligibly small. This is explained as follows. In the expansion of the superoperator $\hat{I}_{\rm diss}(t)$ there appear bath correlation functions $C_{BI}(s) \equiv \langle B(s)\hat{I}_B(0)\rangle$. These correlation functions $C_{BI}(s) = \langle B(s)\hat{I}_B(0)\rangle$ decay on a time scale determined by the bath correlation time τ_B. However, the super operator $\mathcal{L}$ becomes influential at timescales of $1/\Gamma_{\rm rel} \gg \tau_B$, where the the bath correlation functions have already decayed. Hence the influence of $\mathcal{L}$ in the integrals of Eq. (7.41) are negligibly small and the corresponding integrals are evaluated neglecting the exponential functions $e^{\pm\mathcal{L}s}$. The time evolution of that problem is depicted on a Keldysh contour in Fig 7.4. The explicit calculation of $\hat{I}_{\rm diss}(t)$, including the matrix elements of $\hat{I}_{\rm diss}(t)$, is carried out in the appendix C. The matrix elements of the current operator $\hat{I}_{\rm diss}(t)$ turn out to be complex oscillating functions. Consequently, the quantity $\langle P_f^H(\tau)\hat{I}_\epsilon^H(t)\rangle$ in general turns out to be a complex oscillating function.

So far, we have evaluated the numerator of Eq. (7.16). In what follows, we will briefly discuss the denominator, i.e. the transition probability to $\mathcal{P}_\tau(f|i)$ for the system to found in the final state $|f\rangle$, given it has been prepared in the state $|i\rangle$. To determine the transition probability, we make use of the CF obtained by the FCS approach in Ch. 5.2.3. Recalling Eq. (6.19) we have

$$= \mathcal{P}_\tau^{cl}(f|i) + \delta\mathcal{P}_\tau(f|i). \tag{7.42}$$

where

$$\mathcal{P}_\tau^{x,cl}(f|i) = \chi_\tau^{x,cl}(0,f|i) = \frac{\Gamma_{\rm rel} + \cos\theta_f(\Gamma_{ge}-\Gamma_{eg}) + e^{-\Gamma_{\rm rel}t}\cos\theta_f(\cos\theta_i\Gamma_{\rm rel} - \Gamma_{ge}+\Gamma_{eg})}{2\Gamma_{\rm rel}}, \tag{7.43}$$

is the classical part of the transition probability, which only depends on the dynamics of the populations of the density operator. For convenience, the quantum part is given by

$$\delta\mathcal{P}_\tau^x(f|i) = \delta\chi_\tau^x(0,f|i) = \frac{1}{2}\cos(\Omega t)\ \sin\theta_i\sin\theta_f e^{-\Gamma_\varphi(0)t}. \tag{7.44}$$

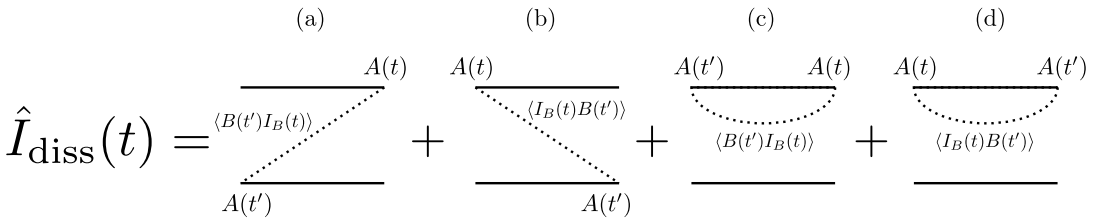

Figure 7.5.: Lowest order diagrams contributing to the super operator $\hat{I}_{\rm diss}(t)$.

As we see from the transition probability, the information about the initially prepared system state is lost due to dephasing and relaxation processes induced by the bath. The bath tends to relax the system towards its thermal equilibrium state, where all the information from the initial state is lost. The expected behavior is reflected by the transition probability Eq. (7.42) at times $\tau \gg \Gamma_{\rm rel}^{-1}$, which is dominated by the time-independent part of Eq. (7.43)

$$\mathcal{P}^{x,cl}_{\tau\gg 1/\Gamma_{\rm rel}} \approx \frac{1}{2} + \cos\theta_f \frac{\Gamma_{ge} - \Gamma_{eg}}{2\Gamma_{\rm rel}}, \tag{7.45}$$

which is independent of the choice of the initial state and the final state selection is taken with respect to the steady state, $(\Gamma_{ge} - \Gamma_{eg})/\Gamma_{\rm rel}$ of the driven TLS.

Hence, in order to achieve an outcome in the spirit of a weak value, where the transition probability between the pre- and post-selected states of the system remains small, the driving time τ should be chosen in the vicinity of the characteristic relaxation times $\Gamma_{\rm rel}^{-1}$ and $\Gamma_{\varphi}^{-1}(0)$ of the system.

7.4.2. Comparison with the FCS result

In this section we want to compare the results of the previous section with the results obtained by the FCS calculation carried out in Ch. 5. We were able to check with the help of Mathematica that

$$\int_0^\tau dt\, {\rm Tr}_S \left[P_f e^{\mathcal{L}(\tau-t)} \hat{I}_{\rm diss}(t) e^{\mathcal{L}t} \rho_S^i \right] \approx \partial_{i\lambda}\, \chi_\tau(\lambda, f|i)|_{\lambda=0}\,, \tag{7.46}$$

is fulfilled. For the subsequent discussion it is convenient to split the dissipative energy current into two parts,

$$\hat{I}_{\rm diss}(t) = \hat{I}^0_{\rm diss}(t) - \hat{I}^{\rm osc}_{\rm diss}(t), \tag{7.47}$$

where

$$\hat{I}^0_{\rm diss}(t) = \begin{pmatrix} I_{gg\leftarrow gg}(t) & I_{gg\leftarrow ee}(t) & 0 & 0 \\ I_{ee\leftarrow gg}(t) & I_{ee\leftarrow ee}(t) & 0 & 0 \\ 0 & 0 & I_{eg\leftarrow eg}(t) & I_{eg\leftarrow ge}(t) \\ 0 & 0 & I_{ge\leftarrow eg}(t) & I_{ge\leftarrow ge}(t) \end{pmatrix}, \tag{7.48}$$

and

$$\hat{I}^{\rm osc}_{\rm diss}(t) = \begin{pmatrix} 0 & 0 & I_{gg\leftarrow eg}(t) & I_{gg\leftarrow ge}(t) \\ 0 & 0 & I_{ee\leftarrow eg}(t) & I_{ee\leftarrow ge}(t) \\ I_{eg\leftarrow gg}(t) & I_{eg\leftarrow ee}(t) & 0 & 0 \\ I_{ge\leftarrow gg}(t) & I_{ge\leftarrow ee}(t) & 0 & 0 \end{pmatrix}. \tag{7.49}$$

Both contributions Eqs. (7.48) and (7.49) to the energy current contain complex oscillating functions, oscillating with frequencies of order of the driving frequency ω. We keep in mind that the quantity obtained by the integral of the current has the dimension of energy. Consequently, the leading contributions with respect to the driving time are proportional to the heat current times the driving time τ. The integration of any oscillating function contained in Eqs. (7.48) and (7.49), needed to evaluate Eq. (7.46), results in contributions containing a prefactor $\sim \omega^{-1}$. However, constant contributions to the matrix elements exist, which will receive a prefactor of $\Gamma_{\mathrm{rel}}^{-1}$ from the integration. In our analysis the system is weakly coupled to the bath, hence $\Gamma_{\mathrm{rel}} \ll \omega$. Consequently, the fast oscillating complex contributions to Eq. (7.40) are strongly suppressed after the integration over the driving time has been performed. In particular, all the contributions ascribed to the part of the energy current $\hat{I}_{\mathrm{diss}}^{\mathrm{osc}}(t)$ become insignificant after the integration.

Considering the contributions of $\hat{I}_{\mathrm{diss}}^{0}(t)$ the non-oscillating real contributions remain, providing the the result as obtained by the FCS approach. Interestingly, the only remaining matrix elements contributing to the conditional average are processes corresponding to diagrams of type (a) and (b) in Fig. 7.5. On a technical level this looks rather similar to the FCS approach. Reminding the derivation of the CF in Ch. 5.2.1, the counting field of the dissipated energy was affecting the bath correlation functions equivalent to type (a) and (b) diagrams.

7.5. Conclusion

This chapter provided an alternative way to investigate the energy dissipation. Rather than in the well known FCS approaches we presented a generalization of the weak measurement protocol [34]. We proposed a weak measurement of the energy current $\hat{I}_{\epsilon}$ including the pre- and the post-selection of the states of the system. Using a diagrammatic expansion of the energy current, we were able to determine its weak value. Our findings show that the resulting quantity is a complex oscillating function. Despite its complicated structure we could show that the conditional average of the dissipated energy is obtained by integrating the weak value in time.

8. Conclusion

In this thesis we have investigated the statistics of energy dissipated by a periodically driven TLS. We proposed a measurement scheme, where not only the energy exchange between system and bath is considered but, in addition, the system undergoes two strong measurements before and after the drive is applied. These two strong measurements are fixing the initial and final state of the TLS. Consequently, the energy exchange between the system and the bath does not only depend on the duration of the drive but also on the difference of the energy expectation values with respect to the choice of the pre- and post-selected states of the TLS.

In Ch. 5 we elaborated upon the necessary framework to calculate the statistics of energy dissipated by a driven TLS. We extended and adjusted the existing formalisms concerning energy exchange statistics [12, 83] to our model and derived the CF of dissipated energy using a master equation in full secular approximation. Further analysis showed that the energy received from the driving source can only be transfered to the bath if the system-bath coupling contains a transverse coupling element. Nevertheless, we studied both limits of pure longitudinal and transverse system-bath couplings. In both situations we were capable of computing the full conditional probability distribution of the dissipated energy considering the pre- and post-selection of states of TLS. In the limits of our model, i.e. in full secular approximation, it turned out that the conditional probability distributions of dissipated energy split into a classical part, which is fully characterized by the dynamics of the populations of the TLS and a quantum part, which is solely depending on the dynamics of the coherences. Depending on the choice of pre- and post-selected states of the TLS, these quantum corrections significantly changed the structure of the conditional probability distribution function. Furthermore, our results were in agreement with the quantum version of the detailed fluctuation relation [33].

The results obtained for the distribution function led to the question as to whether the quantum signatures were visible when considering the conditional average of dissipated energy rather than the conditional distribution function. This was primarily motivated by the fact that the conditional average of dissipated energy may be more easily accessible in an experiment. Consequently we studied the effect of pre- and post-selection of states of the TLS on the first two conditional cumulants of the dissipated energy in Ch. 6. Considering the conditional average of the dissipated energy, we found that the pre- and post-selection as well as the character of the drive, i.e. whether the system was driven in resonance or off resonance, significantly affected the results. The most pronounced features with respect to the state selection were attributed to a time-independent contribution which turned out

to be sensitive to the detuning. Subsequently, we carried out an analysis of the conditional noise. Similar to the conditional average, the overall dependency on the pre- and post-selection could be mostly attributed to a time-independent contribution. Considering the off-resonant drive, one particular set of pre- and post-selected system states, namely the $|e\rangle \to |g\rangle$ selection, showed quite an interesting property. The conditional average of dissipated energy exhibited a maximum while the noise simultaneously was suppressed. We found that the pre- and post-selection tend to favor a certain matrix element connecting the excited- and the ground-state populations of the associated density operator. This particular matrix element contains two competing transitions. The detuning generates an asymmetry in favor of the transition corresponding to maximal energy dissipation. Consequently, the preference of one particular transition was reflected in the simultaneous suppression of noise.

Considering the quantum contributions to the conditional average, we found that quantum features were still detectable in our analysis. However, in the parameter regime we investigated, they were strongly overshadowed by contributions which were of classical origin.

In Ch. 7 we approached the problem from a quite different point of view. We proposed to weakly measure the dissipative energy current $\hat{I}_\epsilon$ rather than the energy exchanged between the TLS and the bath. Hence, we derived a generalization of the weak measurement scheme in the spirit of the pioneering work by Aharonov, Albert and Vaidman [34], suitable to the problem of energy dissipation. We convinced ourselves that the deflection appearing on the ancillary measurement device, i.e. the time integral of the weak value of the heat current, is indeed equivalent to the conditional average of dissipated energy. Considering the weak value in the context of the driven TLS, we were able to show that the resulting quantity is a complex oscillating function. Furthermore, we checked if the integral of the weak value over the driving time is equivalent to the previously obtained results obtained by the FCS technique. In what we found the weak measurement approach turned out to be self-consistent up to negligibly small contributions.

Within the work at hand we were able to show that an additional manipulation of the system, namely the pre- and post-selection of states, may be a valuable tool to detect quantum effects appearing in the context of energy dissipation. What are the next steps to be done? At least from an experimental point of view, it seems to be less demanding to measure the conditional average of the dissipated energy rather than the distribution function. As it turned out, the investigation of the statistics of the energy, dissipated by a driven TLS, is a non-trivial task. A variety of parameters, i.e. the pre- and post-selection of states, the detuning, the driving time and the temperature, act in combination, providing a rich area of interesting physics. Hence, looking in a different parameter regime, e.g. a variation of temperature and driving time, could provide further insight into the problem. Furthermore, going beyond secular approximation may be an insightful approach to the problem. However, in this case the distinct separation between classical and quantum contributions may no longer be possible.

Within this work a consideration of the detector back-action [96] has not been taken into account, i.e. the measurement process itself could perturb the system and modify the results. In a recent experiment on the fluctuation relations in a double quantum dot [97, 17], it was recognized that the detector back-action changed the obtained results in a significant way. Hence, the concept of a weak measurement seems to provide an appealing tool in this context. One could consider using the weak measurement approach to amplify the quantum features by elaborating a clever measurement protocol while minimally disturbing the system of interest. As the weak value of the energy current turned out to be an interesting but challenging quantity, it requires further investigations.

In conclusion, this thesis has offered novel perspectives to the research field of fluctuation relations and thermodynamics towards the quantum regime. The concept of pre- and post-selection provides a valuable tool in the search for quantum signatures in the context of energy dissipation.

Danksagung

Viele Menschen haben mich während der Anfertigung dieser Arbeit in vielfältiger Art und Weise unterstützt. Dafür möchte ich mich bedanken. Allen voran danke ich Prof. Alexander Shnirman, für die exzellente Betreuung meiner Arbeit, zahlreiche ergiebige Diskussionen, sowie für die Unterstützung bei der Umsetzung meiner Ideen.

Ein ganz großes Dankeschön geht an Boris Narozhny, zum einen für die Übernahme des Korreferats, insbesondere aber auch für aufklärende Diskussionen.

A special thanks goes to Prof. Yasuhiro Utsumi for various reasons, namely the numerous fruitful discussions and the effort he spent on our joint collaborations. I also want to thank him for the invitation to his University in Japan and for the exquisite hospitality during my stay.

Des Weiteren möchte ich die unglaublich tolle Arbeitsatmosphäre des TKM hervorheben. Insbesondere bedanken möchte ich mich bei meinen Büromitbewohnern Pablo und Billa, die jederzeit für Diskussionen jedweder Art zur Verfügung standen. Neben meinen Büromitbewohnern habe ich auch mit vielen anderen (auch ehemaligen) Institutsmitgliedern über wissenschaftliche Probleme diskutiert und möchte mich deshalb bei Nicolas Vogt, Mathias Scheurer, Pia Gagel, Nikolaos Kainaris, Elio König, Ingo Kamleitner, Tobias Sproll, Michael Schneider und Christian Seiler bedanken. Ein besonderer Dank geht an Ulf, mit dem ich auch über Themen weit über die Physik hinaus mit Freude habe diskutieren dürfen. Darüber hinaus haben Janina Klier, Julia Link, Mareike Hoyer, Matthias Bard, Patrik Hlobil, Tim Ludwig und Markus Klug meine Zeit am TKM bereichert. Ein großer Dank geht an Andreas Poenicke, der immer mit Rat und Tat zur Seite stand, wenn ich Probleme mit meinem Computer hatte.

Außerhalb des TKM möchte mich auch bei Jürgen Lisenfeld, Sebastian Zanker, Michael Marthaler, Christian Karlewski und Gerd Schön für bereichernde Diskussionen rund um die Physik bedanken.

Ich bedanke mich auch bei Linda, Pablo, Mathias, Paddl, Niko und Billa für das Gegenlesen meiner Arbeit.

Zu guter Letzt möchte ich mich bei meinen Eltern, meiner Schwester Isabel sowie meiner Freundin Anja bedanken. Ohne ihre Unterstützung wäre die Fertigstellung dieser Arbeit nicht möglich gewesen.

Bibliography

[1] Chad Rigetti, Jay M. Gambetta, Stefano Poletto, B. L. T. Plourde, Jerry M. Chow, A. D. Córcoles, John A. Smolin, Seth T. Merkel, J. R. Rozen, George A. Keefe, Mary B. Rothwell, Mark B. Ketchen, and M. Steffen. Superconducting qubit in a waveguide cavity with a coherence time approaching 0.1 ms. *Phys. Rev. B*, 86:100506, Sep 2012.

[2] R. Barends, J. Kelly, A. Megrant, D. Sank, E. Jeffrey, Y. Chen, Y. Yin, B. Chiaro, J. Mutus, C. Neill, P. O'Malley, P. Roushan, J. Wenner, T. C. White, A. N. Cleland, and John M. Martinis. Coherent josephson qubit suitable for scalable quantum integrated circuits. *Phys. Rev. Lett.*, 111:080502, Aug 2013.

[3] Albert Einstein. Über die von der molekularkinetischen theorie der wärme geforderte bewegung von in ruhenden flüssigkeiten suspendierten teilchen. *Annalen der Physik. - Berlin*, (4(1905)):549 – 560, 1905.

[4] William Sutherland. Lxxv. a dynamical theory of diffusion for non-electrolytes and the molecular mass of albumin. *Philosophical Magazine Series 6*, 9(54):781–785, 1905.

[5] J. B. Johnson. Thermal agitation of electricity in conductors. *Phys. Rev.*, 32:97–109, Jul 1928.

[6] H. Nyquist. Thermal agitation of electric charge in conductors. *Phys. Rev.*, 32:110–113, Jul 1928.

[7] Herbert B. Callen and Theodore A. Welton. Irreversibility and generalized noise. *Phys. Rev.*, 83:34–40, Jul 1951.

[8] G. N. Bochkov and Yu. E. Kuzovlev. General theory of thermal fluctuations in nonlinear systems. *Zh. Eksp. Teor. Fiz.*, 72:238, 1977. [Sov. Phys. JETP 45, 125 (1977)].

[9] C. Jarzynski. Nonequilibrium equality for free energy differences. *Phys. Rev. Lett.*, 78:2690–2693, Apr 1997.

[10] Gavin E. Crooks. Entropy production fluctuation theorem and the nonequilibrium work relation for free energy differences. *Phys. Rev. E*, 60:2721–2726, Sep 1999.

[11] Michele Campisi, Peter Hänggi, and Peter Talkner. *Colloquium* : Quantum fluctuation relations: Foundations and applications. *Rev. Mod. Phys.*, 83:771–791, Jul 2011.

[12] Massimiliano Esposito, Upendra Harbola, and Shaul Mukamel. Nonequilibrium fluctuations, fluctuation theorems, and counting statistics in quantum systems. *Rev. Mod. Phys.*, 81:1665–1702, Dec 2009.

[13] Udo Seifert. Stochastic thermodynamics, fluctuation theorems and molecular machines. *Reports on Progress in Physics*, 75(12):126001, 2012.

[14] G. M. Wang, E. M. Sevick, Emil Mittag, Debra J. Searles, and Denis J. Evans. Experimental demonstration of violations of the second law of thermodynamics for small systems and short time scales. *Phys. Rev. Lett.*, 89:050601, Jul 2002.

[15] Jan Liphardt, Sophie Dumont, Steven B. Smith, Ignacio Tinoco, and Carlos Bustamante. Equilibrium information from nonequilibrium measurements in an experimental test of jarzynski's equality. *Science*, 296(5574):1832–1835, 2002.

[16] Collin D., Ritort F., Jarzynski C., Smith S. B., Tinoco I. , and Bustamante C. Verification of the Crooks fluctuation theorem and recovery of RNA folding free energies. *Nature*, 437(7056):231–234, sep 2005. 10.1038/nature04061.

[17] Y. Utsumi, D. S. Golubev, M. Marthaler, K. Saito, T. Fujisawa, and Gerd Schön. Bidirectional single-electron counting and the fluctuation theorem. *Phys. Rev. B*, 81:125331, Mar 2010.

[18] B. Küng, C. Rössler, M. Beck, M. Marthaler, D. S. Golubev, Y. Utsumi, T. Ihn, and K. Ensslin. Irreversibility on the level of single-electron tunneling. *Phys. Rev. X*, 2:011001, Jan 2012.

[19] Koski J. V. and Sagawa T. and Saira O-P. and Yoon Y. and Kutvonen A. and Solinas P. and Mottonen M. and Ala-Nissila T. and Pekola J. P. Distribution of entropy production in a single-electron box. *Nat Phys*, 9(10):644–648, 2013.

[20] Shuji Nakamura, Yoshiaki Yamauchi, Masayuki Hashisaka, Kensaku Chida, Kensuke Kobayashi, Teruo Ono, Renaud Leturcq, Klaus Ensslin, Keiji Saito, Yasuhiro Utsumi, and Arthur C. Gossard. Fluctuation theorem and microreversibility in a quantum coherent conductor. *Phys. Rev. B*, 83:155431, Apr 2011.

[21] Tameem Albash, Daniel A. Lidar, Milad Marvian, and Paolo Zanardi. Fluctuation theorems for quantum processes. *Phys. Rev. E*, 88:032146, Sep 2013.

[22] Tiago B. Batalhão, Alexandre M. Souza, Laura Mazzola, Ruben Auccaise, Roberto S. Sarthour, Ivan S. Oliveira, John Goold, Gabriele De Chiara, Mauro Paternostro, and Roberto M. Serra. Experimental reconstruction of work distribution and study of fluctuation relations in a closed quantum system. *Phys. Rev. Lett.*, 113:140601, Oct 2014.

[23] Michele Campisi, Ralf Blattmann, Sigmund Kohler, David Zueco, and Peter Hänggi. Employing circuit qed to measure non-equilibrium work fluctuations. *New Journal of Physics*, 15(10):105028, 2013.

[24] R. Dorner, S. R. Clark, L. Heaney, R. Fazio, J. Goold, and V. Vedral. Extracting quantum work statistics and fluctuation theorems by single-qubit interferometry. *Phys. Rev. Lett.*, 110:230601, Jun 2013.

[25] L. Mazzola, G. De Chiara, and M. Paternostro. Measuring the characteristic function of the work distribution. *Phys. Rev. Lett.*, 110:230602, Jun 2013.

[26] Peter Talkner, Eric Lutz, and Peter Hänggi. Fluctuation theorems: Work is not an observable. *Phys. Rev. E*, 75:050102, May 2007.

[27] J P Pekola, P Solinas, A Shnirman, and D V Averin. Calorimetric measurement of work in a quantum system. *New Journal of Physics*, 15(11):115006, 2013.

[28] F. W. J. Hekking and J. P. Pekola. Quantum jump approach for work and dissipation in a two-level system. *Phys. Rev. Lett.*, 111:093602, Aug 2013.

[29] Andrey V. Timofeev, Meri Helle, Matthias Meschke, Mikko Möttönen, and Jukka P. Pekola. Electronic refrigeration at the quantum limit. *Phys. Rev. Lett.*, 102:200801, May 2009.

[30] S. Gasparinetti, K. L. Viisanen, O.-P. Saira, T. Faivre, M. Arzeo, M. Meschke, and J. P. Pekola. Fast electron thermometry for ultrasensitive calorimetric detection. *Phys. Rev. Applied*, 3:014007, Jan 2015.

[31] O.-P. Saira, M. Zgirski, K. L. Viisanen, D. S. Golubev, and J. P. Pekola. Dispersive thermometry with a josephson junction coupled to a resonator. *Phys. Rev. Applied*, 6:024005, Aug 2016.

[32] J. Govenius, R. E. Lake, K. Y. Tan, and M. Möttönen. Detection of zeptojoule microwave pulses using electrothermal feedback in proximity-induced josephson junctions. *Phys. Rev. Lett.*, 117:030802, Jul 2016.

[33] C. Jarzynski. Hamiltonian derivation of a detailed fluctuation theorem. *Journal of Statistical Physics*, 98(1):77–102, 2000.

[34] Yakir Aharonov, David Z. Albert, and Lev Vaidman. How the result of a measurement of a component of the spin of a spin- *1/2* particle can turn out to be 100. *Phys. Rev. Lett.*, 60:1351–1354, Apr 1988.

[35] Yakir Aharonov and Daniel Rohrlich. *Quantum paradoxes : quantum theory for the perplexed*. Physics textbook. Wiley-VCH, Weinheim [u.a.], 2005.

[36] Onur Hosten and Paul Kwiat. Observation of the spin hall effect of light via weak measurements. *Science*, 319(5864):787–790, 2008.

[37] Lundeen Jeff S., Sutherland Brandon, Patel Aabid, Stewart Corey, and Bamber Charles. Direct measurement of the quantum wavefunction. *Nature*, 474(7350):188–191, jun 2011. 10.1038/nature10120.

[38] Matteo [Hrsg.] Paris, editor. *Quantum state estimation*. Lecture notes in physics ; 649. Springer, Berlin, 2004.

[39] Floquet. Sur les équations différentielles linéaires à coefficients périodiques. *Annales scientifiques de l'École Normale Supérieure, Sér. 2, 12, 1883*, 1883.

[40] Leonid S. Levitov, Hyunwoo Lee, and Gordey B. Lesovik. Electron counting statistics and coherent states of electric current. *Journal of Mathematical Physics*, 37(10):4845–4866, 1996.

[41] J.J. Sakurai and S.F. Tuan. *Modern quantum mechanics*. Addison-Wesley Pub. Co., 1994.

[42] A. J. Leggett, S. Chakravarty, A. T. Dorsey, Matthew P. A. Fisher, Anupam Garg, and W. Zwerger. Dynamics of the dissipative two-state system. *Rev. Mod. Phys.*, 59:1–85, Jan 1987.

[43] Milena Grifoni and Peter Hänggi. Driven quantum tunneling. *Physics Reports*, 304(5-6):229 – 354, 1998.

[44] Walther Gerlach and Otto Stern. Das magnetische moment des silberatoms. *Zeitschrift für Physik*, 9(1):353–355, 1922.

[45] Yuriy Makhlin, Gerd Schön, and Alexander Shnirman. Quantum-state engineering with josephson-junction devices. *Rev. Mod. Phys.*, 73:357–400, May 2001.

[46] J. Q. You and Franco Nori. Superconducting circuits and quantum information. *Physics Today*, 58(11):42, November 2005.

[47] P. w. Anderson, B. I. Halperin, and c. M. Varma. Anomalous low-temperature thermal properties of glasses and spin glasses. *Philosophical Magazine*, 25(1):1–9, 1972.

[48] W A Phillips. Two-level states in glasses. *Reports on Progress in Physics*, 50(12):1657, 1987.

[49] Anatole Abragam. *The principles of nuclear magnetism*. International series of monographs on physics ; 32. Oxford Univ. Pr., Oxford [u.a.], repr. edition, 2011.

[50] Michael A. Nielsen and Isaac L. Chuang. *Quantum computation and quantum information*. Cambridge Univ. Press, Cambridge [u.a.], 9. print. edition, 2007.

[51] L. J. Geerligs, V. F. Anderegg, P. A. M. Holweg, J. E. Mooij, H. Pothier, D. Esteve, C. Urbina, and M. H. Devoret. Frequency-locked turnstile device for single electrons. *Phys. Rev. Lett.*, 64:2691–2694, May 1990.

[52] L. J. Geerligs, S. M. Verbrugh, P. Hadley, J. E. Mooij, H. Pothier, P. Lafarge, C. Urbina, D. Estève, and M. H. Devoret. Single cooper pair pump. *Zeitschrift für Physik B Condensed Matter*, 85:349–355, 1991. 10.1007/BF01307630.

[53] Lisenfeld Jürgen, Grabovskij Grigorij J., Müller Clemens, Cole Jared H., Weiss Georg, and Ustinov Alexey V. Observation of directly interacting coherent two-level systems in an amorphous material. *Nature Communications*, 6:6182, feb 2015.

[54] Thomas Dittrich, editor. *Quantum transport and dissipation*. Wiley-VCH, Weinheim [u.a.], 1998.

[55] I. I. Rabi. Space quantization in a gyrating magnetic field. *Phys. Rev.*, 51:652–654, Apr 1937.

[56] V Bouchiat, D Vion, P Joyez, D Esteve, and M H Devoret. Quantum coherence with a single cooper pair. *Physica Scripta*, 1998(T76):165, 1998.

[57] K. W. Lehnert, K. Bladh, L. F. Spietz, D. Gunnarsson, D. I. Schuster, P. Delsing, and R. J. Schoelkopf. Measurement of the excited-state lifetime of a microelectronic circuit. *Phys. Rev. Lett.*, 90:027002, Jan 2003.

[58] Jens Koch, Terri M. Yu, Jay Gambetta, A. A. Houck, D. I. Schuster, J. Majer, Alexandre Blais, M. H. Devoret, S. M. Girvin, and R. J. Schoelkopf. Charge-insensitive qubit design derived from the cooper pair box. *Phys. Rev. A*, 76:042319, Oct 2007.

[59] Jürgen Lisenfeld, Grigorij J Grabovskij, Clemens Müller, Jared H Cole, Georg Weiss, and Alexey V Ustinov. Observation of directly interacting coherent two-level systems in an amorphous material. *Nature communications*, 6, 2015.

[60] Philip Wollfarth, Yasuhiro Utsumi, and Alexander Shnirman. Analysis of the conditional average and conditional variance of dissipated energy in the driven spin-boson model, 2016.

[61] H.P. Breuer and F. Petruccione. *The theory of open quantum systems*. Oxford University Press, 2007.

[62] L. V. Keldysh. Diagram technique for nonequilibrium processes. *Zh. Eksp. Teor. Fiz.*, 47:1515, 1965.

[63] Herbert Schoeller and Gerd Schön. Mesoscopic quantum transport: Resonant tunneling in the presence of a strong coulomb interaction. *Phys. Rev. B*, 50:18436–18452, Dec 1994.

[64] R. K. Wangsness and F. Bloch. The dynamical theory of nuclear induction. *Phys. Rev.*, 89:728–739, Feb 1953.

[65] F. Bloch. Dynamical theory of nuclear induction. ii. *Phys. Rev.*, 102:104–135, Apr 1956.

[66] F. Bloch. Generalized theory of relaxation. *Phys. Rev.*, 105:1206–1222, Feb 1957.

[67] Alfred G Redfield. On the theory of relaxation processes. *IBM Journal of Research and Development*, 1(1):19–31, 1957.

[68] K. Blum. *Density matrix theory and applications*. Physics of atoms and molecules. Plenum Press, 1996.

[69] G. Lindblad. On the generators of quantum dynamical semigroups. *Communications in Mathematical Physics*, 48(2):119–130, 1976.

[70] Robert W. Fuller Frederick W. Byron. *Mathematics of classical and quantum physics*. Dover Publications, 1992.

[71] Yuriy Makhlin, Gerd Schön, and Alexander Shnirman. Dissipative effects in josephson qubits. *Chemical Physics*, 296(2-3):315 – 324, 2004. The Spin-Boson Problem: From Electron Transfer to Quantum Computing ... to the 60th Birthday of Professor Ulrich Weiss.

[72] E. Paladino, Y. M. Galperin, G. Falci, and B. L. Altshuler. $\mathbf{1/f}$ noise: Implications for solid-state quantum information. *Rev. Mod. Phys.*, 86:361–418, Apr 2014.

[73] Macroscopic quantum coherence and quantum computing : [proceedings of the international workshop on macroscopic quantum coherence and computing; mqc 2 istituto italiano per gli studi filosofici, held june 14 - 17, 2000, in naples, italy]. New York [u.a.], 2001. Kluwer Academic/Plenum Publishers. Includes bibliographical references and index.

[74] YuV. Nazarov and M. Kindermann. Full counting statistics of a general quantum mechanical variable. *The European Physical Journal B - Condensed Matter and Complex Systems*, 35:413–420, 2003. 10.1140/epjb/e2003-00293-1.

[75] John Von Neumann. *Mathematische Grundlagen der Quantenmechanik*. Die Grundlehren der mathematischen Wissenschaften in Einzeldarstellungen ; 38. Springer, Berlin, 1932. Mit 4 Abb.

[76] E. Wigner. On the quantum correction for thermodynamic equilibrium. *Phys. Rev.*, 40:749–759, Jun 1932.

[77] W. Belzig and Yu. V. Nazarov. Full counting statistics of electron transfer between superconductors. *Phys. Rev. Lett.*, 87:197006, Oct 2001.

[78] Pekola Jukka P. Towards quantum thermodynamics in electronic circuits. *Nat Phys*, 11(2):118–123, feb 2015.

[79] G N Bochkov and Yu E Kuzovlev. Fluctuation-dissipation relations. achievements and misunderstandings. *Physics-Uspekhi*, 56(6):590, 2013.

[80] Keiji Saito and Yasuhiro Utsumi. Symmetry in full counting statistics, fluctuation theorem, and relations among nonlinear transport coefficients in the presence of a magnetic field. *Phys. Rev. B*, 78:115429, Sep 2008.

[81] O.-P. Saira, Y. Yoon, T. Tanttu, M. Möttönen, D. V. Averin, and J. P. Pekola. Test of the jarzynski and crooks fluctuation relations in an electronic system. *Phys. Rev. Lett.*, 109:180601, Oct 2012.

[82] Philip Wollfarth, Alexander Shnirman, and Yasuhiro Utsumi. Distribution of energy dissipated by a driven two-level system. *Phys. Rev. B*, 90:165411, Oct 2014.

[83] S Gasparinetti, P Solinas, A Braggio, and M Sassetti. Heat-exchange statistics in driven open quantum systems. *New Journal of Physics*, 16(11):115001, 2014.

[84] B. R. Mollow. Power spectrum of light scattered by two-level systems. *Phys. Rev.*, 188:1969–1975, Dec 1969.

[85] Ata Ulhaq, Stefanie Weiler, Chiranjeeb Roy, Sven Marcus Ulrich, Michael Jetter, Stephen Hughes, and Peter Michler. Detuning-dependent mollow triplet of a coherently-driven single quantum dot. *Opt. Express*, 21(4):4382–4395, Feb 2013.

[86] A. P. Saiko, R. Fedaruk, and S. A. Markevich. Detuning-dependent narrowing of mollow triplet lines of driven quantum dots. *Journal of Experimental and Theoretical Physics*, 118(4):655–661, 2014.

[87] Jeff S. Lundeen and Charles Bamber. Procedure for direct measurement of general quantum states using weak measurement. *Phys. Rev. Lett.*, 108:070402, Feb 2012.

[88] J. Dressel and A. N. Jordan. Significance of the imaginary part of the weak value. *Phys. Rev. A*, 85:012107, Jan 2012.

[89] Alessandro Romito and Yuval Gefen. Weak measurement of cotunneling time. *Phys. Rev. B*, 90:085417, Aug 2014.

[90] Justin Dressel, Mehul Malik, Filippo M. Miatto, Andrew N. Jordan, and Robert W. Boyd. *Colloquium* : Understanding quantum weak values: Basics and applications. *Rev. Mod. Phys.*, 86:307–316, Mar 2014.

[91] Dawei Lu, Aharon Brodutch, Jun Li, Hang Li, and Raymond Laflamme. Experimental realization of post-selected weak measurements on an nmr quantum processor. *New Journal of Physics*, 16(5):053015, 2014.

[92] H. M. Wiseman. Weak values, quantum trajectories, and the cavity-qed experiment on wave-particle correlation. *Phys. Rev. A*, 65:032111, Feb 2002.

[93] Melvin Lax. Formal theory of quantum fluctuations from a driven state. *Phys. Rev.*, 129:2342–2348, Mar 1963.

[94] Crispin W. Gardiner and Peter Zoller. *Quantum noise : a handbook of Markovian and non-Markovian quantum stochastic methods with applications to quantum optics.* Springer series in synergeticsSpringer complexity. Springer, Berlin, 3. ed. edition, 2004. Pp. : EUR 96.25 (freier Pr.), ca. sfr 152.50 (freier Pr.).

[95] S Swain. Master equation derivation of quantum regression theorem. *Journal of Physics A: Mathematical and General*, 14(10):2577, 1981.

[96] M. Hatridge, S. Shankar, M. Mirrahimi, F. Schackert, K. Geerlings, T. Brecht, K. M. Sliwa, B. Abdo, L. Frunzio, S. M. Girvin, R. J. Schoelkopf, and M. H. Devoret. Quantum back-action of an individual variable-strength measurement. *Science*, 339(6116):178–181, 2013.

[97] Toshimasa Fujisawa, Toshiaki Hayashi, Ritsuya Tomita, and Yoshiro Hirayama. Bidirectional counting of single electrons. *Science*, 312(5780):1634–1636, 2006.

List of Figures

List of publications

1. **Full counting statistics applied to dissipative Cooper pair pumping**
   P. Wollfarth, I. Kamleitner, A. Shnirman
   Phys. Rev. B **87**, 064511 (2013).
2. **Distribution of energy dissipated by a driven two-level system**
   Philip Wollfarth, Alexander Shnirman, Yasuhiro Utsumi
   Phys. Rev. B **90**, 165411 (2014)
3. **Analysis of the conditional average and conditional variance of dissipated energy in the driven spin-boson model**
   Philip Wollfarth, Yasuhiro Utsumi, Alexander Shnirman
   Preprint on arXiv:1610.02697 (2016)

Appendix

A. Quantum version of the detailed fluctuation relation

Within this appendix we demonstrate the quantum version of the detailed fluctuation relation[33]. We will need the anti-unitary time reversal operator Θ[41]. With $\Theta|n\rangle = |\bar{n}\rangle$ we have

$$\langle n|n'\rangle = \langle \bar{n}'|\bar{n}\rangle \tag{A.1}$$

$$\Theta\left(a|n\rangle + b|n'\rangle\right) = a^*|\bar{n}\rangle + b^*|\bar{n}'\rangle, \tag{A.2}$$

with a and b being complex numbers. From the two above equations follows

$$\langle n|O|n'\rangle = \langle \bar{n}'|\Theta O^\dagger \Theta^{-1}|\bar{n}\rangle \tag{A.3}$$

$$\Theta U(\tau,0)\Theta^{-1} = U_B(0,\tau) \tag{A.4}$$

$$\Theta \hat{H}_B \Theta^{-1} = \hat{H}_B \tag{A.5}$$

$$\Theta P_f \Theta^{-1} = P_f, \tag{A.6}$$

$$\Theta \rho_S^i \Theta^{-1} = \rho_S^i, \tag{A.7}$$

which will be useful in the following. We write the generating function as

$$\begin{aligned}
\chi_\tau(\lambda, f|i) &= \mathrm{Tr}\left[P_f e^{i\lambda\hat{H}_B} U(\tau,0) e^{-i\lambda\hat{H}_B}\rho_S^i\rho_B U^\dagger(\tau,0)\right] \\
&= \mathrm{Tr}\Big[(\Theta U(\tau,0)\Theta^{-1})(\Theta\rho_B\Theta^{-1})(\Theta\rho_S^i\Theta^{-1})(\Theta e^{i\lambda\hat{H}_B}\Theta^{-1}) \\
&\times (\Theta U^\dagger(\tau,0)\Theta^{-1})(\Theta e^{-i\lambda\hat{H}_B}\Theta^{-1})(\Theta P_F\Theta^{-1})\Big] \\
&= \mathrm{Tr}\left[U_B(0,\tau)\rho_B\rho_S^i e^{-i\lambda\hat{H}_B} U_B^\dagger(0,\tau) e^{i\lambda\hat{H}_B} P_f\right] \\
&= \mathrm{Tr}\left[P_i e^{i(-\lambda+i\beta)\hat{H}_B} U_B(\tau,0) e^{-i(-i\lambda+i\beta)\hat{H}_B}\rho_S^f\rho_B U_B^\dagger(\tau,0)\right] \\
&= \chi_{\tau,B}(-\lambda+i\beta, i|f),
\end{aligned} \tag{A.8}$$

where we used the fact that the bath is in thermal equilibrium, i.e. the density operator $\rho_B = e^{-\beta H_B}/Z_B$ of the bath does not change. Performing the inverse Fourier transform

$$\mathcal{P}_\tau(\epsilon, f|i) = \frac{1}{2\pi}\int d\lambda\, e^{-i\lambda\epsilon}\chi_\tau(\lambda, f|i), \tag{A.9}$$

we immediately find the desired equality

$$\frac{\mathcal{P}_\tau(\epsilon, f|i)}{\mathcal{P}_{\tau,B}(-\epsilon, i|f)} = e^{\beta\epsilon}. \tag{A.10}$$

B. Analytic result for the Quantum correction of probability densities

In the following, we sometimes use $\epsilon' = \epsilon/\omega$ and $\lambda' = \lambda\omega$. We now focus on the calculation of the corrections due to the coherences

$$\delta\chi_\tau(\lambda, f|i) = \vec{f}_\varphi e^{M_\varphi \tau} \vec{\rho}_\varphi^{\,i}(0), \tag{B.1}$$

where $\vec{\rho}_\varphi = (\rho_{eg}, \rho_{ge})$ is the vector representing the coherences of the density matrix. We then find

$$\delta\chi_\tau(\lambda, i|f) = \frac{1}{2}\cos(\Omega\tau)\,\sin\theta_i \sin\theta_f e^{-\Gamma_\varphi \tau}. \tag{B.2}$$

To calculate the change in the PDF, we need to perform a Fouriertransform. We then find

$$\begin{aligned}\delta\mathcal{P}_\tau(\epsilon, f|i) &= \frac{1}{2\pi}\int d\lambda e^{-i\lambda\epsilon}\delta\chi_\tau(\lambda, f|i) \\ &= \frac{1}{2}\cos(\Omega\tau)\,\sin\theta_i \sin\theta_f \frac{1}{2\pi}\int d\lambda e^{-i\lambda\epsilon} e^{-\Gamma_\varphi(\lambda)\tau}.\end{aligned} \tag{B.3}$$

It may be usefull to define the abbreviation

$$\Gamma_\varphi^0 = (\gamma^+(\Omega) + \gamma^-(-\Omega))/2 + \sin^2\theta(\gamma(\omega) + \gamma(-\omega))/4 \tag{B.4}$$

The integral of is of the form

$$\begin{aligned}\kappa\int_{-\infty}^{\infty} d\lambda e^{-i\lambda'\epsilon'} e^{-ate^{i\lambda'}} e^{-bte^{-i\lambda'}} &= \kappa\int d\lambda e^{-i\epsilon'\lambda'} \sum_{n,m=0}^{\infty} \frac{(-at)^n}{n!}\frac{(-bt)^m}{m!} e^{i\lambda'(n-m)} \\ &= 2\pi\kappa \sum_{n,m=0}^{\infty} \frac{(-at)^n}{n!}\frac{(-bt)^m}{m!}\delta(n-m-\epsilon') \\ &= 2\pi\kappa \sum_{n,m=0}^{\infty} \frac{(-at)^{m+\epsilon'}}{(m+\epsilon')!}\frac{(-bt)^m}{m!}\delta(n-m-\epsilon') \\ &= 2\pi\kappa \sum_{m=0}^{\infty}\sum_{n=-m}^{\infty} \frac{(-at)^{m+\epsilon'}}{(m+\epsilon')!}\frac{(-bt)^m}{m!}\delta(\epsilon'-n) \\ &= 2\pi\kappa \sum_{m=0}^{\infty}\sum_{n=-\infty}^{\infty} \frac{(-at)^{m+\epsilon'}}{(m+\epsilon')!}\frac{(-bt)^m}{m!}\delta(\epsilon'-n)\Theta(\epsilon'+m),\end{aligned} \tag{B.5}$$

where

$$\kappa = \frac{1}{2}\cos(\Omega\tau)\,\sin\theta_i \sin\theta_f \frac{1}{\omega 2\pi} e^{-\tau\Gamma_\varphi^0} \tag{B.6}$$

We now have to evaluate different regions of ϵ'. For $\epsilon' \geq 0$, the Heaviside function will always be one and we find

$$\delta\mathcal{P}_\tau^{>}(\epsilon, f|i) = \frac{1}{2}\cos(\Omega\tau)\,\sin\theta_i \sin\theta_f \times \sum_n \delta(\epsilon - n\omega)\left(\frac{i\gamma(\omega)^{1/2}}{\gamma(-\omega)^{1/2}}\right)^n J_n\left[i\eta\tau\right], \tag{B.7}$$

where we introduced $\eta = \sin^2(\theta)/2(\gamma(\omega)\gamma(-\omega))^{1/2}$ and $J_n[i\eta\tau]$ is the Bessel function of the first kind. In the region $\epsilon < 0$, at a first glance, we find some corrections. First we invoke another abbreviation

$$\Xi(m, \epsilon') = \frac{(-at)^{m+\epsilon'}}{(m+\epsilon')!}\frac{(-bt)^m}{m!}. \tag{B.8}$$

In the case of $\epsilon' < 0$, we find

$$\begin{aligned}\delta\mathcal{P}_\tau^<(\epsilon', f|i) &\propto \sum_{n=-\infty}^{\infty}\sum_{m=|\epsilon'|}^{\infty}\delta(\epsilon'-n)\Xi(m,\epsilon') \\ &= \sum_{n=-\infty}^{\infty}\delta(\epsilon'-n)\left(\sum_{m=0}^{\infty}\Xi(m,\epsilon') - \sum_{m=0}^{|\epsilon'|-1}\Xi(m,\epsilon')\right) \end{aligned} \tag{B.9}$$

We will now have a closer look at the second sum

$$\begin{aligned}\sum_{m=0}^{|\epsilon'|-1}\Xi(m,\epsilon') &= \sum_{m=0}^{|\epsilon'|-1}\frac{(-a)^{\epsilon'}(ab)^{2m}t^{2m+\epsilon'}}{(m+\epsilon')!\,m!} \\ &= \sum_{m=0}^{|\epsilon'|-1}\frac{(-a)^{\epsilon'}(ab)^{2m}t^{2m+\epsilon'}}{\Gamma(m+\epsilon'+1)\Gamma(m+1)}. \end{aligned} \tag{B.10}$$

As ϵ' is restricted to negative integers and the sum yields contributions from $m = 0$ to $|\epsilon'| - 1$, the first Gamma function in the denominator always diverges and thus the term vanishes. Hence the total quantum corrections are given by

$$\delta\mathcal{P}_\tau(\epsilon, f|i) = \frac{1}{2}\cos(\Omega\tau)\,\sin\theta_i\sin\theta_f \times \sum_n \delta(\epsilon - n\omega)\left(\frac{i\gamma(\omega)^{1/2}}{\gamma(-\omega)^{1/2}}\right)^n J_n\left[i\eta\tau\right]. \tag{B.11}$$

C. Calculations concerning the dissipative energy current $\hat{I}_\epsilon$

In this appendix we provide the calculation of the dissipative energy current $\hat{I}_\epsilon(t)$. We use the diagrammatic expansion and expand the current in the weak system-bath coupling. We restrict our calculations to the first order of non-vanishing contributions. Our calculation starts at Eq. (7.41)

$$\begin{aligned}\hat{I}_{\text{diss}}(t) &= -i\mathrm{Tr}_B\left[\int_0^\infty ds\; e^{-\mathcal{L}s}\hat{H}_I^I(s)\hat{I}_\epsilon^I(t)\rho_B + \int_{-\infty}^0 ds\;\hat{I}(t)\hat{H}_I^I(s)e^{\mathcal{L}s}\rho_B\right], \\ &\approx -i\mathrm{Tr}_B\left[\int_0^\infty ds\;\hat{H}_I^I(s)\hat{I}_\epsilon^I(t)\rho_B + \int_{-\infty}^0 ds\;\hat{I}(t)\hat{H}_I^I(s)\rho_B\right]. \end{aligned} \tag{C.1}$$

Explicitly we have

$$\hat{I}_\epsilon^I(t) = \tilde{A}(t)\hat{I}_B(t), \tag{C.2}$$

$$\hat{H}_I^I(t) = \tilde{A}(t)B(t), \tag{C.3}$$

where $\hat{I}_B = -i[\hat{H}_B, B]$ and

$$\tilde{A}(t) = a_z(t)\sigma_z + b(t)\sigma_+ + b^*(t)\sigma_-, \tag{C.4}$$

where

$$a_z(t) = -\cos\omega t\sin\theta \tag{C.5}$$

$$b(t) = e^{-i\Omega t}\left(\cos\theta\cos\omega t - i\sin\omega t\right). \tag{C.6}$$

With this we may rewrite Eq. (C.1) obtaining

$$\begin{aligned}\hat{I}_{\text{diss}}(t) = -i\int_0^\infty ds\;\Big(\tilde{A}(t+s)\tilde{A}(t) - \tilde{A}(t)\tilde{A}(t-s)\Big)\rho_S C_{BI}(s) \\ + i\int_{-\infty}^\infty ds\,\tilde{A}(t)\rho_S\tilde{A}(s+t)C_{BI}(s), \end{aligned} \tag{C.7}$$

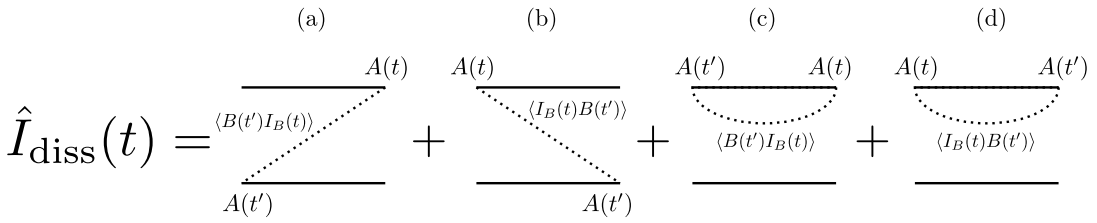

Figure C.1.: Lowest order diagrams contributing to the super operator $\hat{I}_{\rm diss}(t)$.

where the first line corresponds diagrams of type (c) and (d) and the second line corresponds diagrams of type (a) and (b) in Fig. C.1. It may be useful for further calculations to define

$$a_j(t,s) = \mathrm{Tr}\left[\sigma_j \tilde{A}(t)\tilde{A}(s)\right], \tag{C.8}$$

such that

$$\tilde{A}(t)\tilde{A}(s) = \frac{a_0(t,s) + \vec{a}(t,s)\vec{\sigma}}{2}. \tag{C.9}$$

The contributions of type (c) and (d) diagrams are easily obtained via

$$\alpha_j(t) = -i\int_0^\infty ds\, C_{BI}(s)\left(a_j(t+s,t) - a_j(t,t-s)\right), \tag{C.10}$$

$$\alpha_0(t) = -i\frac{\sin^2\theta\sin(2\omega t)}{2}\left(A_{BI}(\omega) - \frac{1}{2}\left(A^L_{BI}(\omega+\Omega) + A^L_{BI}(\omega-\Omega)\right)\right) \tag{C.11}$$

$$\begin{aligned}\alpha_x(t) = -i\cos\omega t\sin\theta\Bigg(&\frac{1}{2}\left(\cos\omega t\sin\Omega t + \cos\theta\cos\Omega t\sin\omega t\right)\left(-S^L_{BI}(\omega+\Omega) + S^L_{BI}(\omega-\Omega)\right)\\ &- \left(\cos\Omega t\sin\omega t + \cos\theta\cos\omega t\sin\Omega t\right)\left(-S^L_{BI}(\omega) + \frac{1}{2}\left(S^L_{BI}(\omega+\Omega) + S^L_{BI}(\omega-\Omega)\right)\right)\Bigg)\end{aligned} \tag{C.12}$$

$$\begin{aligned}\alpha_y(t) = i\cos\omega t\sin\theta\Bigg(&\cos\omega t\cos\Omega t\left(\cos\theta\left(S^L_{BI}(\omega) - \frac{1}{2}\left(S^L_{BI}(\omega+\Omega) + S^L_{BI}(\omega-\Omega)\right)\right)\right.\\ &\left.+\ \frac{1}{2}\left(S^L_{BI}(\omega-\Omega) - S^L_{BI}(\omega+\Omega)\right)\right)\\ &+ \sin\omega t\sin\Omega t\left(-\frac{\cos\theta}{2}\left(-S^L_{BI}(\omega+\Omega) + S^L_{BI}(\omega-\Omega)\right)\right.\\ &\left.+\ \left(-S^L_{BI}(\omega) + \frac{1}{2}\left(S^L_{BI}(\omega+\Omega) + S^L_{BI}(\omega-\Omega)\right)\right)\right)\Bigg)\end{aligned} \tag{C.13}$$

$$\alpha_z(t) = i\frac{1}{4}\sin^2\theta\sin 2\omega t\left(S^L_{BI}(\omega-\Omega) - S^L_{BI}(\omega+\Omega)\right). \tag{C.14}$$

From this, we can readily write down the contribution to the current by type (c) and (d) diagrams with contractions of bath operators on upper Keldysh contour, yielding

$$\hat{I}^{\rm same}_{\rm diss}(t) = \begin{pmatrix} I^{\rm div}_{gg\leftarrow gg} & 0 & I^{\rm div}_{gg\leftarrow eg} & 0\\ 0 & I^{\rm div}_{ee\leftarrow ee} & 0 & I^{\rm div}_{ee\leftarrow ge}\\ I^{\rm div}_{eg\leftarrow gg} & 0 & I^{\rm div}_{eg\leftarrow ge} & 0\\ 0 & I^{\rm div}_{ge\leftarrow ee} & 0 & I^{\rm div}_{ge\leftarrow ge}\end{pmatrix}, \tag{C.15}$$

where

$$I^{\text{div}}_{gg\leftarrow gg} = \alpha_0(t) + \alpha_z(t) \qquad I^{\text{div}}_{gg\leftarrow eg} = \alpha_x(t) - i\alpha_y(t) \tag{C.16}$$

$$I^{\text{div}}_{ee\leftarrow ee} = \alpha_0(t) - \alpha_z(t) \qquad I^{\text{div}}_{ee\leftarrow ge} = \alpha_x(t) + i\alpha_y(t) \tag{C.17}$$

$$I^{\text{div}}_{eg\leftarrow gg} = \alpha_x(t) + i\alpha_y(t) \qquad I^{\text{div}}_{eg\leftarrow eg} = \alpha_0(t) - \alpha_z(t) \tag{C.18}$$

$$I^{\text{div}}_{ge\leftarrow ee} = \alpha_x(t) - i\alpha_y(t) \qquad I^{\text{div}}_{ge\leftarrow ge} = \alpha_0(t) + \alpha_z(t) \tag{C.19}$$

The contribution to the current obtained by diagrams of type (a) and (b) where the contractions connecting bath operators on the lower and the upper Keldysh contour are obtained as

$$\hat{I}^{\text{cross}}_{\text{diss}}(t) = \begin{pmatrix} I^{\text{same}}_{gg\leftarrow gg}(t) & I^{\text{same}}_{gg\leftarrow ee}(t) & I^{\text{same}}_{gg\leftarrow eg}(t) & I^{\text{same}}_{gg\leftarrow ge}(t) \\ I^{\text{same}}_{ee\leftarrow gg}(t) & I^{\text{same}}_{ee\leftarrow ee}(t) & I^{\text{same}}_{ee\leftarrow eg}(t) & I^{\text{same}}_{ee\leftarrow ge}(t) \\ I^{\text{same}}_{eg\leftarrow gg}(t) & I^{\text{same}}_{eg\leftarrow ee}(t) & I^{\text{same}}_{eg\leftarrow eg}(t) & I^{\text{same}}_{eg\leftarrow ge}(t) \\ I^{\text{same}}_{ge\leftarrow gg}(t) & I^{\text{same}}_{ge\leftarrow ee}(t) & I^{\text{same}}_{ge\leftarrow eg}(t) & I^{\text{same}}_{ge\leftarrow ge}(t) \end{pmatrix}, \tag{C.20}$$

with the matrix elements

$$I^{\text{same}}_{gg\leftarrow gg}(t) = \int_{-\infty}^{\infty} ds\, a_z(s+t)a_z(t)C_{BI}(s) \qquad I^{\text{same}}_{gg\leftarrow ee}(t) = \int_{-\infty}^{\infty} ds\, b(t)b^*(t+s)C_{BI}(s) \tag{C.21}$$

$$I^{\text{same}}_{gg\leftarrow eg}(t) = \int_{-\infty}^{\infty} ds\, a_z(s+t)b^*(t)C_{BI}(s) \qquad I^{\text{same}}_{gg\leftarrow ge}(t) = \int_{-\infty}^{\infty} ds\, a_z(t)b(s+t)C_{BI}(s) \tag{C.22}$$

$$I^{\text{same}}_{ee\leftarrow gg}(t) = \int_{-\infty}^{\infty} ds\, b(s+t)b^*(t)C_{BI}(s) \qquad I^{\text{same}}_{ee\leftarrow ee}(t) = \int_{-\infty}^{\infty} ds\, a_z(s+t)a_z(t)C_{BI}(s) \tag{C.23}$$

$$I^{\text{same}}_{ee\leftarrow eg}(t) = -\int_{-\infty}^{\infty} ds\, b^*(s+t)a_z(t)C_{BI}(s) \qquad I^{\text{same}}_{ee\leftarrow ge}(t) = -\int_{-\infty}^{\infty} ds\, b(t)a_z(t+s)C_{BI}(s) \tag{C.24}$$

$$I^{\text{same}}_{eg\leftarrow gg}(t) = \int_{-\infty}^{\infty} ds\, b(t)a_z(s+t)C_{BI}(s) \qquad I^{\text{same}}_{eg\leftarrow ee}(t) = -\int_{-\infty}^{\infty} ds\, b(s+t)a_z(t)C_{BI}(s) \tag{C.25}$$

$$I^{\text{same}}_{eg\leftarrow eg}(t) = -\int_{-\infty}^{\infty} ds\, a_z(t)a_z(t+s)C_{BI}(s) \qquad I^{\text{same}}_{eg\leftarrow ge}(t) = \int_{-\infty}^{\infty} ds\, b^*(t)b^*(t+s)C_{BI}(s) \tag{C.26}$$

$$I^{\text{same}}_{ge\leftarrow gg}(t) = \int_{-\infty}^{\infty} ds\, a_z(t)b^*(s+t)C_{BI}(s) \qquad I^{\text{same}}_{ge\leftarrow ee}(t) = -\int_{-\infty}^{\infty} ds\, a_z(s+t)b^*(t)C_{BI}(s) \tag{C.27}$$

$$I^{\text{same}}_{ge\leftarrow eg}(t) = \int_{-\infty}^{\infty} ds\, b(s+t)b(t)C_{BI}(s) \qquad I^{\text{same}}_{ge\leftarrow ge}(t) = -\int_{-\infty}^{\infty} ds\, a_z(t)a_z(t+s)C_{BI}(s). \tag{C.28}$$

Finally, we obtain

$$\hat{I}_{\text{diss}}(t) = \hat{I}^{\text{same}}_{\text{diss}}(t) + \hat{I}^{\text{cross}}_{\text{diss}}(t), \tag{C.29}$$

which is the desired energy current operator of the problem.

C.1. Bath Correlation functions

In the above calculation, we introduced the bath correlation function $C_{BI}(t) = \langle B(s)\hat{I}_B\rangle$. In what follows we briefly discuss the properties of the bath correlation functions and their

Fourier- and Laplace-transforms,

$$\begin{aligned} L_{BI}(\omega) &= \int_0^\infty ds e^{i\omega s-\delta s} C_{BI}(s) = \int_0^\infty ds e^{i\omega s-\delta s} \int \frac{d\nu}{2\pi} C_{BI}(\nu) e^{-i\nu s} \\ &= i\int d\nu C_{BI}(\nu) \frac{1}{\omega-\nu+i\delta} \\ &= \frac{1}{2} C_{BI}(\omega) + E_{BI}(\omega), \end{aligned} \tag{C.30}$$

where

$$E_{BI}(\omega) = iP.V. \int \frac{d\nu}{2\pi} \frac{C_{BI}(\nu)}{\omega-\nu} \tag{C.31}$$

and we used

$$\frac{1}{\omega \pm i0} = P.V. \frac{1}{x} \mp i\pi\delta(\omega). \tag{C.32}$$

In the time domain, the correlation functions are given by

$$\begin{aligned} C_{BI}(s) &= \langle B(s) I_B \rangle \\ &= -i \sum_\alpha T_\alpha^2 \omega_\alpha \left(-e^{i\omega_\alpha s} n_B(\omega\alpha) + e^{i\omega_\alpha s} (n_B(\omega_\alpha)+1) \right), \end{aligned} \tag{C.33}$$

yielding

$$\begin{aligned} C_{BI}(\omega) &= -i \sum_\alpha \int ds e^{i\omega s} T_\alpha^2 \omega_\alpha \left(-e^{i\omega_\alpha s} n_B(\omega\alpha) + e^{i\omega_\alpha s} (n_B(\omega_\alpha)+1) \right) \\ &= -i \sum_\alpha T_\alpha^2 \omega \left(\frac{1}{e^{-\beta\omega}-1} \delta(\omega+\omega_\alpha) + \frac{e^{\beta\omega}}{e^{\beta\omega}-1} \delta(\omega-\omega_\alpha) \right). \end{aligned} \tag{C.34}$$

For $\omega > 0$ we have

$$C_{BI}(\omega) = -i\omega^2 \gamma_0 \frac{e^{\beta\omega}}{e^{\beta\omega}-1}, \tag{C.35}$$

The symmetrized and anti- symmetrized correlators are calculated as

$$S_{BI}(\omega) = C_{BI}(\omega) + C_{BI}(-\omega) = -i\gamma_0\omega^2 \tag{C.36}$$

$$A_{BI}(\omega) = C_{BI}(\omega) - C_{BI}(-\omega) = -i\gamma_0\omega^2 \coth\frac{\beta\omega}{2}. \tag{C.37}$$

Furthermore, we use the symmetrized versions of the Laplace-Transforms, i.e.

$$S_{BI}^L(\omega) = L_{BI}(\omega + L_{BI}(-\omega) \tag{C.38}$$

$$A_{BI}^L(\omega) = L_{BI}(\omega) - L_{BI}(-\omega). \tag{C.39}$$

C.2. Analysis of combinations of $S_{BI}(\omega)$ and $A_{BI}(\omega)$

In this section we investigate the combinations of

$$S_{BI}^E(\omega) = E_{BI}(\omega) + E_{BI}(-\omega) = iP.V. \int \frac{d\nu}{2\pi} C_{BI}(\nu) \frac{2\nu}{\omega^2-\nu^2}, \tag{C.40}$$

$$A_{BI}^E(\omega) = E_{BI}(\omega) - E_{BI}(-\omega) = iP.V. \int \frac{d\nu}{2\pi} C_{BI}(\nu) \frac{2\omega}{\omega^2-\nu^2}, \tag{C.41}$$

which occur in the matrix elements of the current $\hat{I}_{\rm diss}(t)$. We obtain combinations like

$$\begin{aligned}
&- S^E_{BI}(\omega) + \frac{1}{2}\left(S^E_{BI}(\omega+\Omega) + S^E_{BI}(\omega-\Omega)\right) \\
&= iP.V.\int \frac{d\nu}{2\pi}\nu C_{BI}(\nu)\left(-\frac{2}{\omega^2-\nu^2} + \frac{1}{(\omega+\Omega)^2-\nu^2} + \frac{1}{(\omega-\Omega)^2-\nu^2}\right) \\
&= iP.V.\int \frac{d\nu}{2\pi} C_{BI}(\nu)\nu \frac{2\Omega^2(\nu^2+3\omega^3-\Omega^2)}{(\omega^2-\nu^2)((\omega+\Omega)^2-\nu^2)(\omega-\Omega)^2-\nu^2)},
\end{aligned} \tag{C.42}$$

which turns out to be depending on an high frequency cutoff ω_c and hence cause contribution of the order of $\ln \omega_c/\omega$. Additionally we have

$$\begin{aligned}
S^E_{BI}(\omega-\Omega) - S^E_{BI}(\omega+\Omega) &= iP.V.\int \frac{d\nu}{2\pi} C_{BI}(\nu) 2\nu \left(\frac{1}{(\omega-\Omega)^2-\nu^2} - \frac{1}{(\omega+\Omega)^2-\nu^2}\right) \\
&= iP.V.\int \frac{d\nu}{2\pi} C_{BI}(\nu) \frac{-8\nu\omega\Omega}{((\omega-\Omega)^2-\nu^2)((\omega+\Omega)^2-\nu^2)},
\end{aligned} \tag{C.43}$$

which is also dominated by $\ln \omega_c/\omega$. Finally, we have

$$\begin{aligned}
&A^E_{BI}(\omega) - \frac{1}{2}\left(A^E_{BI}(\omega+\Omega) + A_{BI}(\omega-\Omega)\right) \\
&= iP.V.\int \frac{d\nu}{2\pi} C_{BI}(\nu)\left(\frac{2\omega}{\omega^2-\nu^2} - \frac{\omega+\Omega}{(\omega+\Omega)^2-\nu^2} - \frac{\omega-\Omega}{(\omega-\Omega)^2-\nu^2}\right) \\
&= iP.V.\int \frac{d\nu}{2\pi} \frac{-2C_{BI}(\nu)\omega\Omega^2\left(3\nu^2+\omega^2-\Omega^2\right)}{(\omega^2-\nu^2)((\omega+\Omega)^2-\nu^2)((\omega-\Omega)^2-\nu^2)},
\end{aligned} \tag{C.44}$$

which is non divergent, providing a smaller contribution than the above integrals.